Last Glacial to Holocene variability in the sea ice distribution in Fram Strait/Arctic Gateway

- A novel biomarker approach -

Kumulative Dissertation

zur Erlangung des akademischen Grades
eines Doktors der Naturwissenschaften

Dr. rer. nat.

an der Fakultät für Geowissenschaften
der Universität Bremen

vorgelegt von

Juliane Müller

Bremerhaven, 2011

Gutachter der Dissertation

Prof. Dr. Ruediger Stein

Prof. Dr. Rüdiger Henrich

Tag des Promotionskolloquiums: 21.Oktober 2011

Erklärung

Hiermit versichere ich an Eides statt, die vorliegende Arbeit, abgesehen von der Beratung durch meine akademischen Lehrer, selbständig und ohne Zuhilfenahme fremder als der hier angegebenen Quellen angefertigt zu haben.

Bremerhaven, 26.05.2011

Juliane Müller

When the game is over, the cards reshuffled, the parts dismantled
- membranes ruptured, shells dissolved, bones ground to dust -
a few of those organic molecules remain in the sediments and rocks,
bearing witness to the distant moments of their creation.

(Echoes of Life. Gaines, Eglinton, Rullkötter, 2009)

Abstract

The concern about the future development of Arctic sea ice also prompts a gaining interest in past variations of the ice extent in the Arctic Ocean. The important question as to whether the palaeo variability in sea ice coverage in this climate-sensitive area can be firstly identified, and secondly, linked to climatic fluctuations thus motivates to look for tools that permit the reliable reconstruction of palaeo sea ice conditions. The recently established sea ice proxy IP_{25} is considered to be such a tool though a proper evaluation of the applicability of this biomarker hitherto has not been available. Within this thesis the occurrence of IP_{25} and its capability to display a previous sea ice coverage has been investigated by means of sediment cores from the Fram Strait - the only deep-water passage between the Arctic and Atlantic Ocean.

Analyses of the biomarker composition of surface sediments revealed that the abundance of IP_{25} in these samples mirrors the recent, as derived from satellite and model data, sea ice distribution considerably well. It is found that the ice cover does not necessarily hamper but instead even may promote the phytoplankton productivity. This finding led to the establishment of a phytoplankton-IP_{25} (PIP_{25}) index that facilitates the identification of different sea surface conditions (no ice, less/variable ice, marginal ice, perennial ice cover). Correlation analyses of these PIP_{25}-based sea ice estimates with observed (and modelled) sea ice concentrations substantiate that this combinatory biomarker approach permits a more precise assessment of sea ice coverage than IP_{25} alone and could be used for quantitative (palaeo) sea ice reconstructions.

Further, the Holocene variability in IP_{25} and phytoplankton biomarker contents of sediment cores from the continental margin of West Spitsbergen and East Greenland was studied. Throughout the Middle to Late Holocene, the sea ice cover increased in eastern Fram Strait, whilst the sea ice export along the East Greenland coast continued and remained relatively unaffected by short-term variations in the oceanic circulation. Such fluctuations led to rapid sea ice oscillations along the West Spitsbergen margin during the Neoglacial that can be linked to abrupt changes in the advection of Atlantic water (possibly also due to shifts in the atmospheric NAO-like forcing).

In a third study, which also represents the first long-term application of IP_{25}, extreme variations in the sea ice cover during the last glacial-interglacial transition were reconstructed for northern Fram Strait. Permanent ice coverage is assumed for the Last Glacial Maximum

such that the productivity of ice algae and phytoplankton at the sea surface was inhibited. Abrupt short-term cooling and warming events (e.g. the Intra-Allerød cold period and the Bølling warm phase) were correlated convincingly with sea ice advances and retreats, respectively.

Within this thesis it is demonstrated that the approach to combine IP_{25} with phytoplankton-derived biomarkers occurs to be a promising and reliable method for palaeoceanographic sea ice reconstructions and which increases the significance of IP_{25}. The studies provide information about the usage and interpretation of IP_{25} and they give new insight into the evolution of the sea ice conditions in Fram Strait over the past 30,000 years. Future studies on the spatial and temporal distribution of IP_{25} will likely extend the approach to use this proxy for quantitative sea ice reconstructions and also to elucidate sea ice (and climate) conditions of ancient times.

Zusammenfassung

In der Diskussion über die zukünftige Entwicklung der arktischen Meereisbedeckung spielt auch das wachsende Interesse an vergangenen Schwankungen der Eisausdehnung im Arktischen Ozean eine große Rolle. Die grundlegende Frage, inwieweit die Paläovariabilität der Meereisbedeckung in dieser klimatisch empfindlichen Region erstens nachgewiesen und zweitens mit Klimaschwankungen in Verbindung gebracht werden kann, motiviert die Suche nach Indikatoren, die eine zuverlässige Rekonstruktion der Paläomeereisbedeckung ermöglichen. Der kürzlich entwickelte Meereisproxy IP_{25} wird als solch ein Anzeiger angesehen, obwohl es kaum Studien gibt, die die Verlässlichkeit dieses Biomarkers belegen. Im Rahmen dieser Arbeit wurde das Vorkommen von IP_{25} sowie sein Potential eine vergangene Meereisbedeckung anzuzeigen an Sedimentkernen aus der Framstraße, der einzigen Tiefwasserpassage zwischen dem Arktischen und Atlantischen Ozean, untersucht.

Analysen der Biomarkerverteilung in Oberflächensedimenten zeigen, dass der Gehalt an IP_{25} in diesen Proben die rezente, aus Satelliten- und Modelldaten abgeleitete Meereisverteilung recht gut widerspiegelt. Es zeigte sich, dass die Eisbedeckung die Produktivität von Phytoplankton nicht zwangsläufig reduziert sondern sogar begünstigen kann. Diese Beobachtung wurde genutzt, um einen Phytoplankton-IP_{25}-Index (PIP_{25}) zu erstellen, der es ermöglicht, zwischen unterschiedlichen Eisbedingungen (kein Eis, wenig/variable Eisbedeckung, stabile Eisrandlage, mehrjährige Eisbedeckung) zu differenzieren. Korrelationsanalysen dieser PIP_{25}-basierten Einschätzungen der Eisbedeckung mit gemessenen (und modellierten) Meereiskonzentrationen zeigen, dass dieser kombinierte Biomarkeransatz eine präzisere Beurteilung der Eisbedingungen erlaubt als IP_{25} allein und für quantitative (Paläo) Meereisrekonstruktionen genutzt werden könnte.

Des Weiteren wurde die holozäne Variabilität von IP_{25} und Phytoplankton-Biomarkern in Sedimentkernen von den Kontinentalhängen West-Spitzbergens und Ostgrönlands untersucht. Die Ergebnisse zeigen, dass im Mittleren und Späten Holozän die Meereisbedeckung in der östlichen Framstraße zunahm, während der Eisexport entlang der Ostgrönlandküste andauerte und relativ unbeeinflußt von kurzzeitigen Schwankungen der ozeanischen Zirkulation blieb. Im Neoglazial führten solche Schwankungen zu kurzfristigen Fluktuationen der Meereisbedeckung entlang des West-Spitzbergen Kontinentalhangs, die mit abrupten Änderungen des Zustroms von Atlantikwasser (möglicherweise aufgrund eines

wechselnden atmosphärischen (NAO-ähnlichen) Antriebs) in Zusammenhang stehen könnten.

In einer dritten Studie, die gleichzeitig die erste Anwendung des Meereisproxies IP_{25} über einen erdgeschichtlich längeren Zeitraum darstellt, wurde eine extrem variable Meereisbedeckung in der nördlichen Framstraße für den Übergang vom letzten Glazial bis in das heutige Interglazial rekonstruiert. Für das Letzte Glaziale Maximum wird eine permanente Eisbedeckung vermutet, wodurch die Produktivität von Eisalgen und Phytoplankton an der Meeresoberfläche unterdrückt wurde. Abrupte, kurzzeitige Abkühlungs- und Erwärmungsperioden (z.B. die Intra-Allerød-Kaltphase, oder die Bølling-Warmphase) konnten mit entsprechenden Vorstößen beziehungsweise Rückgängen des Meereises korreliert werden.

Mit dieser Arbeit wurde gezeigt, dass die Kombination von IP_{25} mit Phytoplankton-Biomarkern eine vielversprechende und zuverlässige Methode für paläozeanographische Meereisrekonstruktionen darstellt und die Aussagekraft von IP_{25} deutlich erhöht. Die Studien liefern Hinweise für die Anwendung und Interpretation von IP_{25} und sie geben Aufschluss über die Entwicklung der Meereisbedingungen in der Framstraße während der letzten 30.000 Jahre. Zukünftige Studien über die räumliche und zeitliche Verbreitung von IP_{25} werden den Ansatz, diesen Proxy für quantitative Meereisrekonstruktionen zu nutzen, sicherlich erweitern und zur Aufklärung der Meereis- (und Klima)bedingungen vergangener Zeiten beitragen.

Danksagung

An erster Stelle danke ich Prof. Dr. Ruediger Stein für die Anregung zu dieser spannenden Arbeit, das Vertrauen, das er in mich gesetzt hat, und seine mir viele Freiheiten gewährende Betreuung und ständige Bereitschaft zu Diskussionen, aus denen ich immer motiviert herausging.

Prof. Dr. Rüdiger Henrich danke ich für die Übernahme der Zweitbegutachtung.

Bei Kirsten Fahl bedanke ich mich ganz herzlich für ihre Hilfe in Sachen Chemie und wesentliche fachlich-kritische Auseinandersetzungen. Insbesondere danke ich ihr für die vielen sinnstiftenden und aufmunternden Gespräche aller anderen Art.

Jens Matthiessen sei für seinen Ansporn gedankt, gelegentlich auch einmal einen Blick über den organisch-geochemischen Tellerrand zu werfen.

Bei David Naafs, Walter Luttmer und Jens Hefter wiederum bedanke ich mich für eben jenen Biomarker Small-Talk und das entspannte Miteinander im Labor - auch wenn die Musik nicht immer mitspielte.

Für tatkräftige Unterstützung und die Einweisung in die unterschiedlichsten Laborgerätschaften und natürlich auch den ein oder anderen netten Plausch danke ich Susanne Wiebe, Rita Fröhlking, Ute Bock und Michael Seebeck. An dieser Stelle sei auch Adelina Manurung für ihre stets zuverlässige Arbeit in unseren Labors gedankt.

Ich danke Kirstin Werner dafür, dass sie zu jeder Zeit die Leiden und Freuden, die uns HOVAG bescherte, mit mir teilte. Auf unsere Treffen habe ich mich immer sehr gefreut - und natürlich auch auf "Onkel" Robert.

Ein ganz großes Dankeschön geht an den Bürokollegen Michael Schreck. Nicht nur weil er mir den Fensterplatz überließ, sondern weil er mir, wie auch Michelle Zarrieß, Corinna Kanzog, Normen Lochthofen, Nicole Händel, Corinna Borchard und Lars Möller, stets zur Seite stand. Ihr habt mir Halt gegeben, wenn ich mich in Bremerhaven verloren fühlte und ins Zweifeln geriet.

Meinen Eltern danke ich dafür, dass sie mich in die Sphären der Geowissenschaften abtauchen ließen und in den selbigen auch aktiv gefördert haben - nicht nur finanziell. Meine Schwester war so gut, mich daran zu erinnern, dass es auch ein Leben über Tage gibt. Ich danke dir!

Bei dir Silvio stehe ich wohl in der größten Dankesschuld. Du ließest mir die Freiheit nach Bremerhaven zu gehen und auch wenn die Entfernung spürbar zunahm, warst du mir stets die größte Motivation für diese Arbeit - insbesondere sie auch (beizeiten) abzuschließen.

Contents

1. Introduction

1.1 Arctic Ocean sea ice

The most prominent feature of the Arctic Ocean is its ice cover - yet. Consistent with its decline, the scientific (and also the public) interest in Artic sea ice increased continuously during the past decades. Among discussions about the fate of polar bears or the new accessibility of mineral and hydrocarbon resources in the high latitudes, the impact of sea ice loss on global climate attracts a great deal of attention (keyword IPCC; Solomon et al., 2007).

This "World of White" (Wadhams, 2000) experiences enormous (natural) seasonal changes in the ice distribution due to the pronounced difference in summer and winter insolation that accounts for ice-melt in summer and ice-growth during winter. The formation of sea ice is basically restricted to the autumn and winter months and depending on the sea surface conditions (calm vs. rough water) frazil or pancake ice is formed, which, after further congelation growth and consolidation, yield first-year ice (up to 0.5 m thick; Eicken, 2003; Wadhams, 2000). The sustained cooling and freezing of the sea surface waters results in a rejection of salt (brine formation) and thus initiates a densification and downward convection, which finally causes a stratification of the water column with cold (partly frozen) and less saline water on top and warm and dense water underneath (Dieckmann and Hellmer, 2003; Rudels and Quadfasel, 1991). This stratification is fundamentally supported by the huge input of riverine freshwater (e.g. from the rivers Yenisei and Lena) that enters the Arctic Ocean as low-density surface layer mainly via the broad Siberian shelves (Aagaard and Carmack, 1989; Macdonald et al., 2004). Within the subpolar North Atlantic, the temperature and density related overturn is a major driving mechanism of the thermohaline circulation - the engine of the so-called "Nordic Heat Pump" (see chapter 1.2; Broecker, 1992).

In contrast to the seasonally ice-free continental shelves (the birthplace of new sea ice), the central Arctic Ocean remains almost perennially covered with thicker (several metres) multi-year ice that withstands summer melt (Fig. 1). On average, an area of 6 Mio km^2 remains ice covered in summer whereas the winter ice cover (including first-year ice) extends to 15 Mio km^2 (NSIDC, http://nsidc.org/; accessed April 2011).

The recently observed decline in summer sea ice extent of 7.4 ± 2.4% per decade over the satellite period from 1979 to 2005 (Lemke, 2007) gives rise to the question of the contribution of natural climate variability on the one hand and the dimension of

anthropogenic influence on the other hand. However, not only the cause for the ice loss requires attention, also the effects of a decreasing ice cover demand consideration.

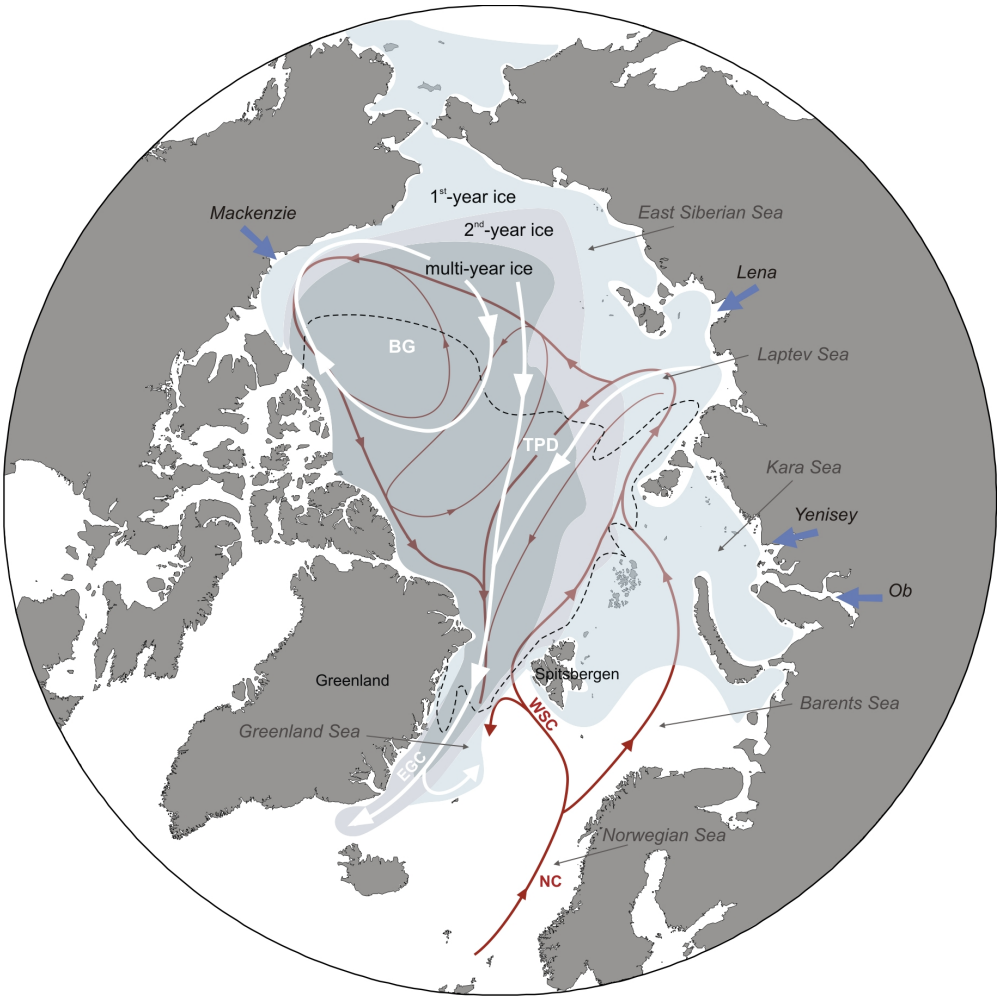

Fig. 1: Arctic Ocean sea ice coverage and ocean circulation (after Nørgaard-Pedersen et al., 2007; Macdonald et al., 2004; NSIDC, 2011). The average extent of multi-year, second-year, and first-year ice is indicated by the shaded areas. The black dotted line refers to the observed minimum summer sea ice extent in 2007. Red arrows indicate (subsurface) Atlantic water circulation following the basin bathymetry. White arrows denote ice circulation and transport within the Beaufort Gyre (BG), the Transpolar Drift (TPD), and the East Greenland Current (EGC) through Fram Strait. Major rivers contributing to freshwater supply are indicated.

Arctic sea ice is not only highly responsive to climate change; it also affects the world climate mainly through its interactions with the ocean and the atmosphere and also through its role as a buffer between these two elements (for a review see Aagaard and Carmack, 1994; Wadhams, 2000). Sea ice represents an effective insulator as it limits the exchange of heat and moisture between the ocean and the atmosphere, whilst it suppresses the wind mixing of the upper ocean layer and reduces evaporation. This affects the oceanic and atmospheric (near sea surface) heat-balance and also the intensity and pathways of atmospheric circulation patterns (Dieckmann and Hellmer, 2003; Untersteiner, 1982). The

ice controls the oceanic energy budget also through its high albedo, which reduces the solar heat uptake at the sea surface. Furthermore, the ice constitutes an enormous freshwater source that impacts on oceanic temperature and salinity profiles and thus alters circulation patterns (Aagaard and Carmack, 1989; Knies et al., 2007). This became particularly evident during an event in the 1970s known as the "Great Salinity Anomaly", when an enormous discharge of Arctic Ocean derived freshwater caused an anomalously low salinity sea surface layer that was circulated around the North Atlantic Ocean (Belkin et al., 1998; Dickson et al., 1988). This freshwater "cap" hampered the convective overturn (i.e. the thermohaline circulation) thus reducing the heat release from the ocean to the atmosphere, which finally caused a significant cooling in the North Atlantic (Dima and Lohmann, 2007; Kerr, 1992). Probably not the first theory on but a clear synopsis of the various feedback mechanisms between Arctic sea ice coverage, shifts in oceanic and atmospheric temperature and circulation patterns, and the importance of Arctic Ocean sea ice for glacial and interglacial climate cycles was already established 55 years ago by Ewing and Donn (1956). They considered that Pleistocene climate variability (i.e. shifts from glacial to interglacial stages) resulted from alternations of ice-covered and ice-free states of the Arctic Ocean. Soon after, fluctuations in earth's orbital geometry were identified as fundamental cause of large-scale changes in the Arctic's radiation budget to force the succession of ice ages during the Quaternary (e.g. Hays et al., 1976; Imbrie et al., 1992).

Another (more) environmental aspect of Arctic sea ice is its capacity as a habitat for ice associated (sympagic) organisms (Gosselin et al., 1997; Horner, 1985b). During the formation of ice in autumn, cells of ice algae (mainly diatoms) are incorporated and hibernate within the successively thickening ice (Gradinger and Ikävalko, 1998). During spring, brine drainage triggers a downward movement and enrichment of the cells at the bottom of the ice, where they grow and divide as soon as sufficient light becomes available (Horner, 1985a). Such bottom ice algae layers are a frequent spring phenomenon and clearly recognisable by their yellow-brownish colour (Horner and Alexander, 1972). These ice algae blooms provide the important base for a whole food web (from zooplankton over fish to mammals) and contribute significantly to the algal biomass and organic carbon release to the Arctic Ocean (Gosselin et al., 1997; Gradinger, 2009). Finally, these (spring/summer) brownish patches of sea ice algae colonies may even affect the micro climate (admittedly at a very local scale) as they reduce the reflectivity of the ice, which in turn promotes the melting of the ice floes (Light et al., 1998).

On account of the various scientific issues, Arctic sea ice research branches into different disciplines that contribute to our knowledge about the current, the past, and the future development of this sensitive region. With the onset of remote sensing (passive-microwave) sea ice imagery in the early 1970s a valuable instrument for the observation and documentation of the distribution of sea ice was established (Gloersen et al., 1992). The satellite-based quantitative assessment of the extent and the concentration (and to a minor degree also the thickness) of sea ice and its spatial and temporal variability largely improved the understanding of the short-term feedback between the ocean, the ice cover, and the atmosphere (Dickson, 2000; Spreen et al., 2006; Vinje, 2001a). Field studies (for a thorough overview of field techniques see Eicken et al., 2009), however, are a fundamental requirement as they provide detailed information about physical, chemical, and biological characteristics of the ice and thus facilitate the interpretation of ancient "sea ice signals" preserved within sediments.

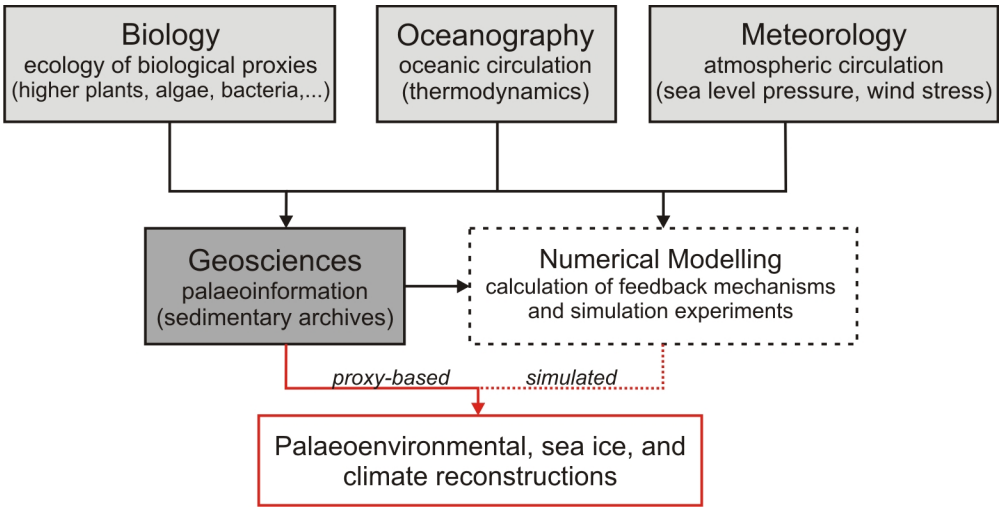

Fig. 2: Flow-chart summarising the contribution of biological, oceanographic and meteorological information to support environmental reconstructions on base of sediment archives and by means of numerical simulations.

With special regard to these palaeo sea ice studies the interdisciplinary collaboration of geoscientists, biologists, oceanographers, meteorologists, and (to an increasing degree) numerical modellers is of high importance to enable comprehensive examinations and reconstructions (Fig. 2). The evaluation of the processes that shaped palaeo climate conditions thus may help to answer the question to what extent the current climate warming can be attributed to natural variability or anthropogenic forcing.

1.2 Fram Strait - The major Arctic gateway

1.2.1 Oceanographic setting

With Fridtjof Nansen's *Fram* expedition (1893 - 1896) Henrik Mohn's theory of a transpolar ice drift from the East Siberian coast to the passage between Spitsbergen and Greenland has been proven (Frolov et al., 2005; Nansen, 1930). The *Fram*, which started its drift nearby the New Siberian Islands, where the vessel got (purposely) frozen in thick pack ice, ended its voyage three years later northwest of Spitsbergen. And though Nansen missed the North Pole, the idea of ocean and wind driven currents forcing ice across the Arctic Ocean towards the North Atlantic was verified (Frolov et al., 2005).

The Fram Strait, located between Greenland and Spitsbergen (Fig. 1), is with 2,600 m mean water depth the only deep-water connection between the Arctic Ocean and the World's Ocean. Further in and outlet systems are the Bering Strait, the Canadian Arctic Archipelago, and the Barents Sea with maximum water depths of 450 m, which do not provide for a comparable deep-water circulation. The huge discharge of sea ice from the Arctic Ocean (ca. 3,000 km^3 mean annual export between 1950 - 2000) through Fram Strait (Vinje, 2001b) is mainly confined to the western part of this passage, where the East Greenland Current (EGC) heads southward along the eastern continental margin of Greenland (Aagaard and Coachman, 1968; Rudels et al., 2002). The ice, which is transported by the EGC, basically originates from the shallow shelves of the distant Laptev or East Siberian Sea (30 - 50 m) from where it is circulated across the central Arctic Ocean with the Transpolar Drift until it finally exits through Fram Strait (Fig.1; Eicken et al., 1997; Vinje, 1982). Within Fram Strait a pronounced temperature (and salinity) gradient is observed that separates this narrow passage into a polar, ice-covered domain along the East Greenland continental margin and a warm, ice-free corridor along the continental margin of West Spitsbergen (Aagaard et al., 1987; Rudels et al., 2005). Here, Atlantic Ocean derived water is advected towards the north via the West Spitsbergen Current (WSC) and this supply with temperate and saline water causes dominantly ice-free conditions in eastern Fram Strait up to 80°N (Fig. 1; Aagaard et al., 1987; Gloersen et al., 1992). As these water masses become continuously cooler and thus denser (due to heat loss to the atmosphere and finally also due to mixing with polar water and ice coming from the north) a complex system of re-circulation, current branching, deep-water convection and formation is generated that drives the subpolar North Atlantic thermohaline circulation (Fig. 3; Rudels et al., 1999; Rudels and Quadfasel, 1991). Northwest of Spitsbergen part of this Atlantic water is carried further to the north and northeast where it enters the Arctic Ocean as a dense and saline subsurface

layer that can be traced to follow the ocean bathymetry cyclonically until it departs again through Fram Strait as intermediate and deep-water (Fig. 1; Aagaard, 1981; Rudels et al., 2002; Schauer et al., 2002).

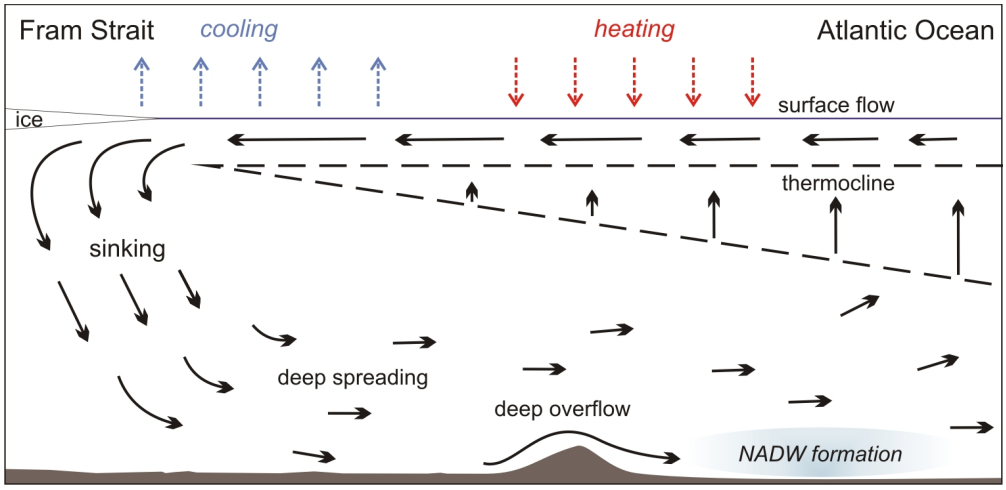

Fig. 3: Simplified scheme of the thermohaline circulation in the North Atlantic (after Wyrtki (1961)). Cooling and densification of northward flowing Atlantic surface water leads to convective overturn and the formation and export of North Atlantic Deep Water (NADW) towards the south, where the deep-water ascends through the thermocline into the surface layer.

The intensity of the large-scale overturning, the formation of deep-water within, and the additional export of Arctic deep-water through Fram Strait control the overflow of dense deep-water across the Greenland-Scotland Ridge into the North Atlantic (mainly via Denmark Strait) - the source of North Atlantic Deep Water (NADW; Rudels et al., 2002; Rudels and Quadfasel, 1991). It has been assumed previously that any changes in the strength of this "Nordic Heat Pump" directly affect the local climate of the subpolar North Atlantic and also that of remote areas (e.g. Aagaard and Carmack, 1994; Broecker, 1991; Broecker et al., 1985).

The impact of atmospheric forcing on the sea ice distribution in Fram Strait is mainly effected through variations in sea level pressure, wind strength and circulation patterns (depending on the respective mode of the North Atlantic Oscillation; NAO) that favour or inhibit the sea ice formation on the one hand and the export of sea ice via the EGC on the other hand (Dickson, 2000; Hurrell and Deser, 2009; Kwok et al., 2004; Vinje, 2001b; see chapter 5 for further discussion). Regarding the various oceanographic and atmospheric forcing parameters and the diverse feedback mechanisms that may impact on the North Atlantic thermohaline circulation, several approaches to assess its variability have been conducted by means of numerical simulation experiments (Delworth et al., 1993; Gregory et al., 2005; Saenko et al., 2004; Vellinga and Wood, 2008). With respect to palaeo conditions

and the respective modes of Atlantic and Arctic Ocean interaction, proxy-based reconstructions, however, provide the only source of information - also to equip palaeo-modelling experiments.

1.2.2 Palaeoceanographic overview

The connection between the Arctic and the Atlantic Ocean and thus the path for deep-water exchange was established with the opening of the Fram Strait during the Early Miocene (Fig. 4; for further discussion on the tectonic evolution of Fram Strait see Engen et al., 2008; Thiede et al., 1998; Vogt, 1986). With the launch of this deep-water circulation system the palaeoceanographic and climatic setting of the high northern latitudes became subjected to a fundamental redistribution of water masses (ventilation of the Arctic Ocean) and the production of NADW was initiated (Jakobsson et al., 2007; Thiede et al., 1998).

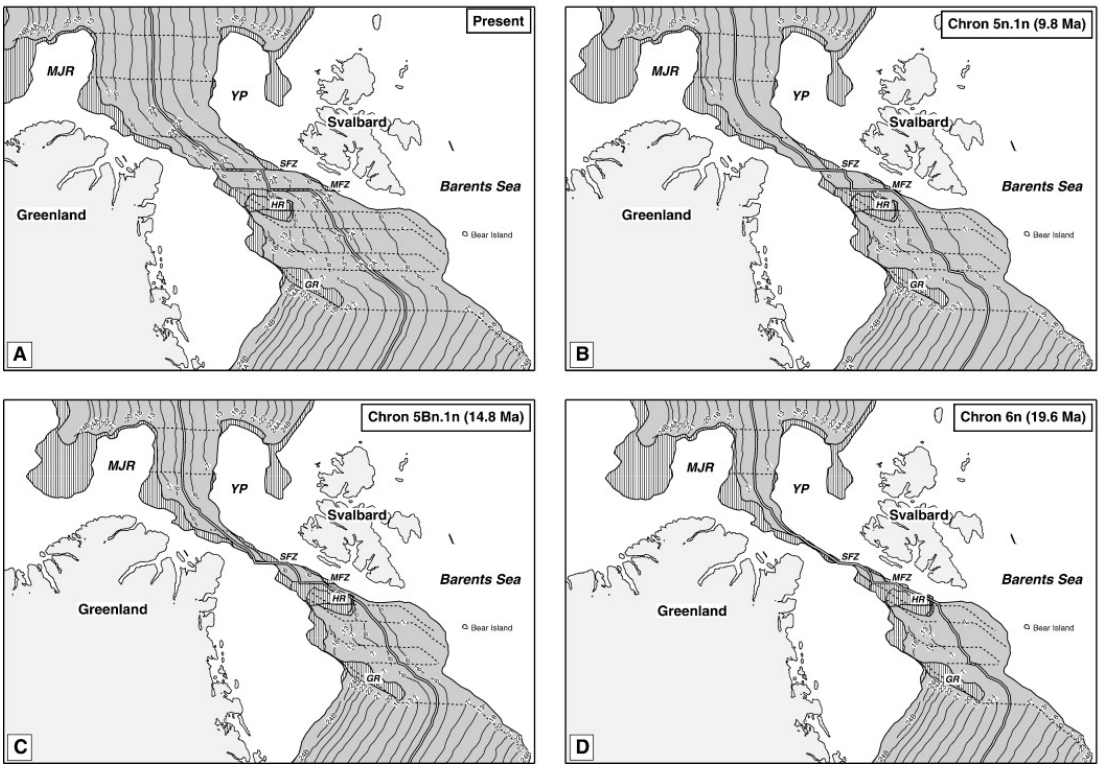

Fig. 4: Plate tectonic reconstruction of seafloor spreading and opening of the Fram Strait in the northern North Atlantic since the Miocene (Engen et al., 2008).

While the onset of a seasonal sea ice formation in the Arctic Ocean dates back to the Middle Eocene (Fig. 5; Stickley et al., 2009; St. John, 2008), a first perennial sea ice cover is suggested for the Middle Miocene by e.g. Clark (1982), Wolf and Thiede (1991), Darby (2008), and Krylov (2008) on base of ice rafted detritus (IRD) data. First IRD occurrences within the Fram Strait and the Nordic Seas are also documented for the Middle Miocene

and have been associated with the inception of northern hemisphere cooling (Knies and Gaina, 2008; Thiede et al., 1998; Wolf-Welling et al., 1996). Probably during the Late Miocene, the onset of the Denmark Strait overflow was initiated and during the Early Pliocene, at about 4 Ma, the first outflow of polar water to the North Atlantic (via a precursor of the East Greenland Current) occurred (Bohrmann et al., 1990).

An increased meridional circulation probably caused seasonal ice-free conditions in eastern and more severe sea ice coverage in western Fram Strait during the Middle Pliocene and thus supported ice sheet growth (due to higher evaporation and snow precipitation rates) in the Svalbard/Barents Sea area (Fig. 5; Knies et al., 2002; see Matthiessen et al., 2009 for recent review of the Pliocene palaeoceanographic development).

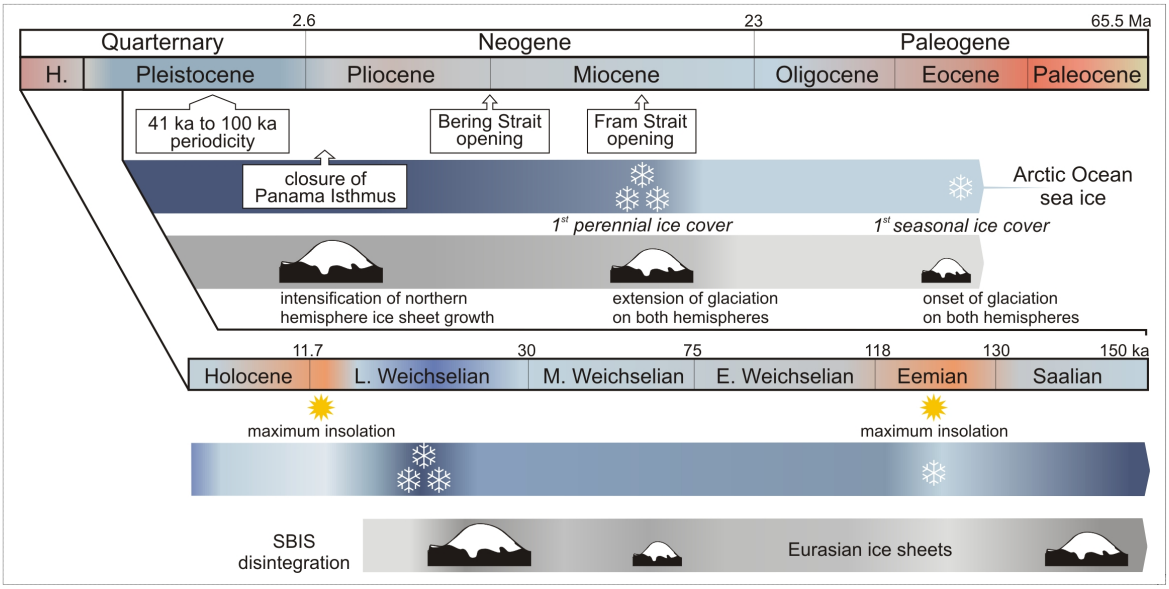

Fig. 5: Overview of the palaeoceanography of the Arctic Ocean during the Cenozoic. Major palaeoceanographic events (e.g. Arctic gateway openings, onset of sea ice formation) are indicated as well as glaciations and the Eurasian ice sheet history. SBIS = Svalbard-Barents Sea Ice Sheet; single white star = seasonal sea ice; triple white star = permanent sea ice.

Sustained and strengthened cooling promoted large-scale glacier growth and polar (ice-covered) sea surface conditions in the Fram Strait (Yermak Plateau) during the Plio- and Pleistocene transition (Jansen et al., 2000; Matthiessen and Brenner, 1996; Thiede et al., 1998), while the NADW production seemed to be reduced at 2.4 Ma (Raymo et al., 1992). Between 1.2 and 0.7 Ma, a transition from a 41 ka to a 100 ka periodicity in global ice volume occurred (Lisiecki and Raymo, 2005) - the reason for which is still under debate (for recent review and discussion see Miller et al., 2010b). This Middle Pleistocene climate shift is also traceable in the Nordic Seas by means of oxygen and carbon isotopic compositions, carbonate, foraminifer, and IRD records (Fronval and Jansen, 1996; Henrich et al., 2002; Jansen et al., 2000). A distinct glacial-interglacial cyclicity, however, characterised the past 1.1

Ma in the subpolar North Atlantic and was associated with variations in the advection of temperate Atlantic water, which finally caused a shift from a "siliceous" to a more "calcareous" setting in the Nordic Seas (and, with some delay, in the Fram Strait too) due to stronger Atlantic water input during interglacial stages (Baumannn et al., 1986; Henrich et al., 2002; Matthiessen and Brenner, 1996). On the base of biogenic carbonate records Baumann et al. (1986), for example, identify short-term interglacials with intensified deep-water production rates and strong Atlantic water intrusions, which also reached Fram Strait during the past 0.65 Ma years. These warm stages punctuated longer glacial episodes of pronounced input of IRD (Thiede et al., 1998). Frequent events of freshwater drainage from the Arctic Ocean through Fram Strait during the past 0.8 Ma years have been reconstructed and contextualised with perturbations of the Atlantic Meridional Overturning Circulation, thus strengthening the influence of Arctic versus North Atlantic water masses on deep-water circulation and formation (Knies et al., 2007). In a recent modelling study Green et al. (2011), for example, demonstrated that the collapse of the Barents Ice Sheet during MIS 6 and the associated mass input of freshwater considerably affected (reduced) the meridional overturning circulation and NADW formation in the Atlantic Ocean.

The last interglacial, the Eemian (MIS 5), was characterised by a maximum in solar radiation over the Arctic (Fig. 5; Berger, 1978), a notably increased Atlantic water advection through Fram Strait and shrinking ice sheets in the Northern Hemisphere (Bauch and Kandiano, 2007; Chapman et al., 2000; Matthiessen and Knies, 2001; Miller et al., 2010b; Spielhagen et al., 2004; Van Nieuwenhove et al., 2011). Furthermore, by means of planktic foraminifera Nørgaard-Pedersen et al. (2007) reconstruct that also the sea ice coverage in the Arctic Ocean must have been significantly reduced at that time (Fig. 5; Otto-Bliesner et al., 2006). Enhanced thermohaline circulation is assumed as being a main driver for a higher heat advection (via the North Atlantic and Norwegian Current) to the north, whilst it also provided for an important moisture source by causing ice-free conditions in the high latitudes and thus promoted renewed ice-sheet growth in the following stadial (McManus et al., 2002; Spielhagen et al., 2004).

The timing and the extent of the Weichselian glaciation in northern Eurasia has been frequently studied on the base of marine (mainly IRD) and on-shore (Spitsbergen) sedimentary records which point to three major advances of the Svalbard-Barents Sea Ice Sheet (Fig. 5; Elverhøi et al., 1995; Hebbeln, 1992; Mangerud et al., 1998; Svendsen et al., 2004). The rapid growth of this ice sheet during the Last Glacial Maximum (LGM) was associated with a lowered sea level and a higher precipitation due to temporarily open ocean

conditions in the subpolar North Atlantic during the Late Weichselian (Hebbeln et al., 1994; Jessen et al., 2010). These ice-free conditions were effected through periods of intensified Atlantic water advection through Fram Strait - the so-called Nordway Events (Hald et al., 2001; Hebbeln and Wefer, 1997). The maximum advance of the Svalbard-Barents Sea Ice Sheet beyond the shelf break west of Spitsbergen was accompanied by an organic carbon event that can be traced in a series of sediment cores from the Fram Strait (and adjacent areas) and has been interpreted to reflect a massive sediment discharge towards the sea (for further discussion see e.g. Andersen et al., 1996; Birgel and Stein, 2004; Jessen et al., 2010; Knies and Stein, 1998; Mangerud and Svendsen, 1992; Nørgaard-Pedersen et al., 2003; see also chapter 6). Contemporaneously, the Greenland Ice Sheet reached and covered the continental margin of East Greenland and perennial sea ice conditions established in western Fram Strait (Nam et al., 1995; Stein et al., 1996). The sea ice extent during the LGM remained highly controversial and estimates of the sea ice distribution in the subpolar North Atlantic accordingly ranged from perennially ice-covered to seasonally ice-free conditions (CLIMAP-Project-Members, 1981; Nørgaard-Pedersen et al., 2003; Sarnthein et al., 2003a).

The exact timing of the initial Svalbard-Barents Sea Ice Sheet disintegration is still under debate. By means of IRD data from the West Spitsbergen margin it has recently been proposed to initiate ca. 20,000 years BP, possibly supported by a reduced moisture supply due to increased Arctic sea ice cover (Jessen et al., 2010). Previous studies on base of (meltwater) $\delta^{18}O$ values had suggested a later onset of the deglaciation (Elverhøi et al., 1995; Jones and Keigwin, 1988). The last deglaciation was punctuated by several short-term climate reversals in the North Atlantic. Cold intervals such as the Intra-Allerød or the Younger Dryas have been linked to abrupt meltwater events (Teller et al., 2002; Thornalley et al., 2010; see also chapter 6).

The MIS2 - MIS1 transition, i.e. the shift towards Holocene climate conditions, is commonly placed at the abrupt rise in $\delta^{18}O$ values observed in the Greenland ice cores at the end of the Younger Dryas cold period (NGRIP-Members, 2004; Stuiver and Grootes, 2000). According to several studies that were conducted in the Fram Strait area the current interglacial can be roughly divided into (1) a warm Early Holocene characterised by a strong Atlantic water advection and reduced sea ice coverage (due to peak Northern Hemisphere insolation), (2) a gradually cooling Middle Holocene with gradually decreasing sea surface temperatures and increasing sea ice occurrences, and (3) a cold Late (Neoglacial) Holocene with a weakened Atlantic water inflow and a southward shift of the polar front (Andersen et al., 2004; Andrews et al., 2010; Jennings et al., 2011; Koç et al., 1993; Rasmussen et al., 2007;

Risebrobakken et al., 2010; Slubowska-Woldengen et al., 2007). According to Bauch et al. (2001) the modern-type circulation and the formation of distinct oceanic fronts (with steep east-west temperature gradients) in the Nordic Seas established during the Middle Holocene. Further description and discussion of the palaeoenvironmental (sea ice) development of the Fram Strait during the Holocene is given in chapter 5.

Terrestrial (and marine) proxy-based reconstructions of the climate development in the high northern latitudes document a shift to higher temperatures during the 20th to 21st century transition and thus reveal that the long-term cooling trend (associated with the decreasing summer insolation) became abruptly reversed (Kaufman et al., 2009; Spielhagen et al., 2011). With the recent retreat of Arctic sea ice, the role of the Fram Strait as the main gateway for Atlantic water inflow gained much attention. The observed increase in surface water temperature and salinity over a large area of the Arctic Ocean, for example, has frequently been attributed to a stronger advection of Atlantic water through Fram Strait due to an intensified atmospheric forcing during the 1990s (i.e. an unusual positive NAO; Hilmer and Jung, 2000; Serreze et al., 2007; Steele and Boyd, 1998; Zhang et al., 1998). The question if this intensified Atlantic water penetration is a temporary phenomenon or a permanent trend (triggering a chain reaction of Arctic amplification) hitherto remains unanswered and requires further understanding of oceanic-atmospheric feedback mechanisms and the role of increasing greenhouse gas concentrations driving global warming (Hurrell and Deser, 2010; Miller et al., 2010a; Zhang et al., 1998).

1.3 Sea ice reconstruction

1.3.1 Common tools for tracking palaeo sea ice occurrences

A variety of sedimentological, microfossil and geochemical parameters are commonly considered as indicators of a palaeo sea ice cover and hence used for sea ice and sea surface reconstructions within Arctic palaeoceanographic studies (Table 1; see also chapter 1.2.2). Among these parameters, ice rafted detritus is probably the most popular and frequent tool for the identification of a previous ice cover though the discrimination between sea ice and iceberg transport requires caution (Hebbeln, 2000; St. John, 2008). Mineralogical analyses of these particles, however, enable provenance assessments and thus the reconstruction of ice drift pathways (Darby and Bischof, 2004; Vogt et al., 2001). The entrainment of sediment particles (and also terrigenous organic matter) occurs mainly at the shallow shelves of the Arctic Ocean during suspension freezing or the reworking of coastal sediments by grounded ice or advancing glacier ice sheets (for a thorough review see Stein, 2008b and references therein). Terrigenous biomarker lipids have also been used and interpreted as being ice-rafted to refer to sea ice (or iceberg) coverage (e.g. Madureira et al., 1997). Further transport mechanisms for these vascular plant-derived molecules, for example aeolian or ocean current transport, substantially limit their significance as ice indicators (Fahl and Nöthig, 2007).

Parameter	Advantages	Limitations	Case studies
Ice rafted detritus - lithogenic particles (coarse > 500 μm and fine > 40 μm) - plant macrofossils	- direct signal for ice cover - provenance and ice drift estimates - summer & winter sea ice - high preservation potential	- ambiguous signal (sea ice or iceberg transport of fine-grained particles)	*- Hebbeln, 2000* *- Nürnberg et al., 1994* *- Knies et al., 2001* *- Jennings et al., 2011* *- Darby et al. 2009*
Microfossils - foraminifers - diatoms - dinoflagellate cysts - ostracods	- direct signal if ice-associated (sympagic) species - information on the ecological and environmental setting - primary productivity estimates	- unknown palaeoecology - limited preservation ($CaCO_3$, SiO_2 dissolution) - not indicative of winter sea ice	*- Sarnthein et al., 2003* *- Kohly 1998* *- Justwan & Koç, 2008* *- de Vernal et al., 2001* *- Cronin et al., 2010*
Stable isotopes - $\delta^{18}O$ of *N. pachyderma*	- information on sea ice foramtion rates	- indirect/ambiguous signal (affected by ocean salinity and/or temperature)	*- Hillaire-Marcel & de Vernal, 2008* *- Bauch et al., 1997*
Biomarkers - terrigenous long-chain *n*-alkanes, alcohols	- information on (distant) terrestrial vegetation setting - good preservation potential	- main transport occurs via ocean currents - (bio, O_2)degradable	*- Madureira et al., 1997* *- Schubert & Stein, 1996* *- Fahl & Nöthig, 2007*
Bulk proxies - TOC content - $CaCO_3$ content	- primary productivity estimates (ice cover limits productivity) - $CaCO_3$ to trace Atlantic water	- only indirect ice signals (argumentum e contrario)	*- Stein & Stax, 1991* *- Andrews et al., 2001* *- Henrich et al., 2002* *- Hebbeln et al., 1998*

Table 1: Overview of common proxies used for the identification and reconstruction of palaeo sea ice occurrences. Case studies are cited.

When using microfossils, such as sea ice associated foraminifers (and their $\delta^{18}O$ signature) and diatoms, which indeed may serve as excellent ice markers, carbonate and silica dissolution can reduce the applicability of these proxies (see also chapter 4.1). This does not account for organic-walled dinoflagellate cysts and hence makes them useful tracers of sea ice cover (e.g. de Vernal et al., 2005). Only indirect sea ice estimates can be derived from organic geochemical bulk parameters. Sedimentary contents of total organic carbon or carbonate (as assumed to be produced by phytoplankton thriving at the sea surface) occur to be reduced in areas that experience severe sea ice coverage, whereas high organic carbon and carbonate contents may point to favourable ice-free conditions (Andrews et al., 2001; Hebbeln and Berner, 1993; Henrich, 1998).

1.3.2 The novel sea ice proxy IP_{25}

In 2007, Simon T. Belt and co-authors presented an acyclic highly branched, monounsaturated C_{25} isoprenoid - a molecule with 25 carbon atoms and one double bond at the C_{23}-C_{24} carbon atoms (Fig. 6) - as new sea ice proxy IP_{25} (Belt et al., 2007). Highly branched isoprenoids (HBIs) are ubiquitous in marine sediments and phytoplankton (mainly diatoms) but normally occur with two or more double bonds within their molecule structure (Belt et al., 2000a; Grossi et al., 2004; Rowland and Robson, 1990; Volkman et al., 1994; Xu et al., 2006). As was demonstrated in culture experiments on the diatom *Haslea ostrearia*, the number of double bonds within haslenes (HBIs produced by diatoms of the genus *Haslea*) decreases with decreasing algal growth temperature thus indicating that the degree of unsaturation seems to be temperature dependent (Rowland et al., 2001). Belt et al. (2007) hence suggest that the IP_{25} monoene (with only one double bond) might be derived from diatoms that are restricted to sea ice. There is also evidence from compound specific ^{13}C isotope analyses of the IP_{25} hydrocarbon found in sea ice and sediment trap material from seasonally ice-covered sampling sites, that this molecule has its source within the Arctic sea ice (Belt et al., 2008). Hitherto the IP_{25} monoene could not be traced in marine sediments from the

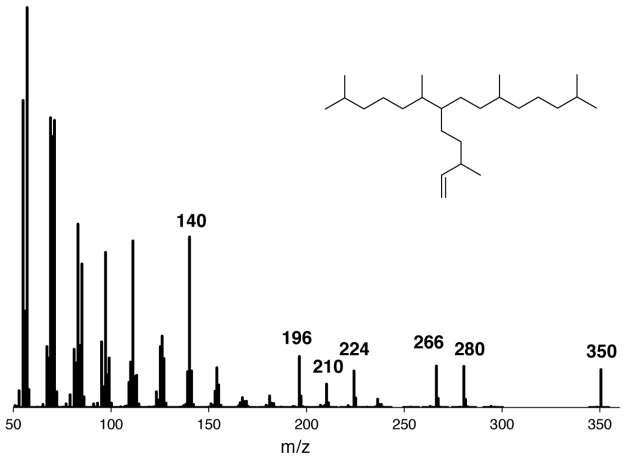

Fig. 6: Molecule structure of IP_{25} (2,6,10,14-tetramethyl-7-(3-methylpent-4-enyl)pentadecane) and characteristic mass fragmentation pattern (Belt et al., 2007).

Antarctic (personal communication Simon T. Belt, Guillaume Massé), which may indicate that the sea ice diatom that produces this molecule does not belong to a cosmopolitan species. In a recent study about the biomarker inventory of sea ice samples from the Canadian Beaufort Sea, Brown et al. (in press) substantiate that the main IP_{25} accumulation (90%) occurs coincident with sea ice algal blooms during spring (March to May). The finding of maximum IP_{25} contents in bottom ice sections with brine volume fractions characteristic for diatom colonisation and growth further strengthens the sea ice diatom origin for IP_{25} (Brown et al., in press). A real determination of the diatom species that synthesises this molecule hitherto has not been carried out.

The identification of IP_{25} in several sea ice and sediment samples from the Arctic, however, supports the consideration of IP_{25} as a direct sea ice marker (Belt et al., 2007; Brown et al., in press; Brown, 2011). The presence and variability of IP_{25} in down-core sediments thus has been interpreted as a direct hint for palaeo spring sea ice coverage and its change through time (Andrews, 2009; Belt et al., 2010; Gregory et al., 2010; Vare et al., 2010). Massé et al. (2008), for example, strengthen that the IP_{25} distribution in a sediment core from the North Iceland shelf correlates fairly well with historic data on sea ice occurrences during the past two millennia. Similarly, Vare et al. (2009) compare the IP_{25} variability in a sediment core from the Central Canadian Archipelago with other proxy data (e.g. foraminifera, IRD, bowhead whale remains) and convincingly relate fluctuating IP_{25} contents to changing sea ice conditions throughout the Holocene. However, Belt et al. (2007) point out that the absence of IP_{25} in marine (Arctic) sediments might reflect either the absence of sea ice or, in contrast, refer to a permanent ice cover (preventing any algal growth). This ambiguity seems to weaken the value of the novel proxy with regard to palaeo studies and requires notice. Another question addresses the temporal range of IP_{25}, i.e. the phylogenesis and distribution of the source sea ice diatoms. Studies on the chemical stability of HBIs (including IP_{25}) against photo-oxidation (in the upper water layer), biodegradation (at the sediment-water interface) or further chemical alteration processes (isomerisation, cyclisation reactions) demonstrate its comparatively good resistance to such transformations (Belt et al., 2000b; Robson and Rowland, 1988; Rontani et al., in press). Hence the identification of IP_{25} in respectively old sediments would serve as the best proof of its preservation potential as it is "axiomatic that the lipids found in ancient sediments are those which best resist chemical and biological degradation" (Volkman, 1986).

2. Analysis of organic matter in marine sediments

The study of organic geochemical bulk parameters and the biomarker composition of marine sediments from the Arctic realm enables a general characterisation of the organic material on the hand and a detailed identification of its origin and depositional history on the other hand. In the following, only a brief overview of the most common bulk proxies and biomarker molecules that were determined within the framework of this thesis is provided. Detailed background information and comprehensive, more explicit descriptions of further preparation and analyses techniques as well as assistance for the interpretation of these proxy data are given, for example, in Killops and Killops (2005), Romankevich (1984), Peters et al. (2005), Tissot and Welte (1984), Stein and Macdonald (2004b) and Stein (2008a).

2.1 Organic geochemical bulk proxies

Total organic carbon (TOC) contents are useful hints to estimate whether a sediment core site experienced a low or high marine primary productivity and/or terrestrial input - for the precise differentiation between marine and terrigenous derived organic matter, however, further analyses are indispensable. By means of TOC and Total Carbon (TC) contents the amount of carbonate ($CaCO_3$), which may also serve as an indicator for marine productivity (of calcareous-walled organisms), can be calculated according to the formula

$$CaCO_3 = (TC - TOC) \times 8.333, \quad (1)$$

where 8.333 is the stoichiometric calculation factor for $CaCO_3$ (assuming that all carbonate is present as calcite and not as dolomite).

The carbon/nitrogen ratio (C/N) accounts for the relative input of terrestrial (mainly higher landplant derived carbon) versus marine (mainly algae derived nitrogen) organic matter and thus enables a first, rough estimate of the primary source of the organic material preserved within the sediment. In general, C/N ratios <10 refer to marine organic matter, whereas values >15 point to a dominance of terrigenous organic material (Bordovskiy, 1965; Meyers, 1994). The clay mineralogy (biasing the nitrogen content) of the analysed sediment, however, requires special attention to avoid misleading interpretation (Hedges et al., 1986; Müller, 1977; Stevenson and Cheng, 1972).

Another means to determine the relative contribution of marine and terrestrial organic matter input is the Rock-Eval Pyrolysis, which has its origin in the source-rock evaluation within the petroleum industry (Espitalié et al., 1977). During the pyrolysis, hydrocarbons

(HC) and carbon dioxide (CO_2) are released (and partly generated) from the sediment sample. The amount of hydrocarbons, which mainly derive from lipid-rich marine organic matter (liptinite macerals), and the amount of CO_2, which refers to more humic (vitrinite) terrigenous material, are expressed as hydrogen (HI) and oxygen (OI) indices, respectively (Tissot and Welte, 1984). Within palaeoenvironmental studies, high HI values (>300 mg HC/g OC) are interpreted to reflect a marine organic matter composition, while a low HI (<100 mg HC/g OC) points to a significant input of terrigenous organic matter (this accounts for immature sediments; see also Stein et al., 2006; Stein and Macdonald, 2004a; Tissot and Welte, 1984). When using HI values for the characterisation of the organic material in marine sediments mineral-matrix effects and the content of refractory ("dead") carbon need to be considered as they affect the pyrolysis (Cornford et al., 1998; Dembicki Jr, 1992; Langford and Blanc-Valleron, 1990).

Within the framework of this thesis, sediment cores MSM5/5-712-2 and MSM5/5-723-2 from the West Spitsbergen continental slope (1490 m and 1350 m water depth, respectively) were subsampled each centimetre. Samples were freeze-dried and homogenised for further chemical treatment. Sedimentary total organic carbon (TOC) contents were determined by means of a carbon-sulphur analyser (CS-125, Leco) after the removal of carbonates by adding hydrochloric acid (500 µl). Total carbon (TC) contents measured by a CNS analyser (Elementar III, Vario) were used to calculate carbonate contents according to equation 1. Rock-Eval pyrolysis data were obtained on a Cristal 300, Rock-Eval 6 analyser (Vinci Technologies) following Espitalié (1977).

2.2 Biomarker composition of sediments

2.2.1 Biomarkers as palaeoenvironmental tracers

Molecular fossils or biomarkers, originally used for oil-source rock correlations for the petroleum exploration, are widely adopted for palaeoenvironmental and palaeoclimatic reconstructions and provide detailed information about the palaeoecology and biological productivity (for comprehensive reviews see e.g. Eglinton and Eglinton, 2008; Meyers, 1997; Stein, 2008a; Stein and Macdonald, 2004b; Volkman, 2006; Volkman et al., 1998). Biomarkers are organic compounds that originate from formerly living organisms and are preserved - alike macrofossils - within the sediment after the dead and decomposition of the organism in question. The identification of a biomarker within a sediment sample hence serves as a direct indication or as a fingerprint of the former occurrence of the respective source organism at the sampling site. Probably the first "markers […] in support of a

chlorophyll-based life as far back as 2.7 x 10^9 years ago" were phytane and pristane, the two molecular remnants of the hydrogenated and converted phytol side chain of the decomposed chlorophyll molecule (Eglinton, 1966). The high diversity of organic molecules that are synthesised by various organisms and are also preserved as biomarkers (Fig. 7) permits for a detailed reconstruction of palaeo ecosystems. And though biomarkers represent only a very small proportion of the original biomass, they enable an assessment of the relative contributions of the different source organisms (Killops and Killops, 2005). Main requirements of biomarkers are (1) their specificity with regard to their parent organic molecules (i.e. their biological precursors) and (2) the chemical stability of their principal molecular structure during sedimentation and digenesis (Peters et al., 2005).

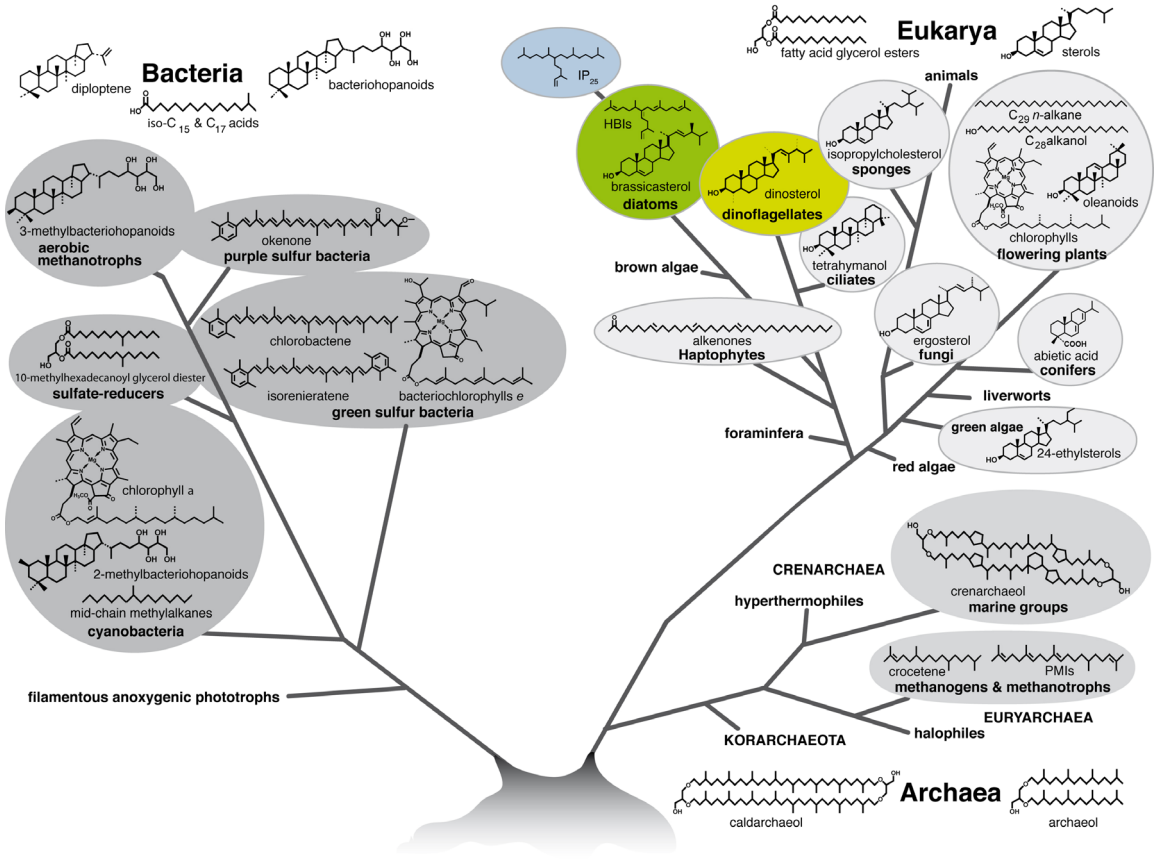

Fig. 7: A biomarker-centric tree of life with common names and (phylogenetic) groupings of organisms and respective biomarkers (Gaines et al., 2009; graphic kindly provided by Florian Rommerskirchen, MARUM, Bremen). Key biomarkers that were in the focus of this thesis are highlighted (the IP_{25} molecule is not included in the original graphic).

Regarding the interpretation of sedimentary biomarker data it should be considered that different chemical and physical alteration processes, such as oxidation and transport or mixing (e.g. through turbidites or bioturbation), may affect the biomarker composition particularly of marine sediments (Wakeham and Canuel, 2006; Zonneveld et al., 2010).

Many compounds that are frequently targeted within palaeoenvironmental biomarker studies can be grouped according to their distinct biological affiliation (Fig. 7). Odd-numbered long-chain *n*-alkanes and even-numbered alkanols, for example, are main lipid components of higher landplant leaf waxes (Eglinton and Hamilton, 1967) and thus serve as indicators for a terrestrial vegetation and, if identified in marine sediments, point to an allochthonous (aeolian, riverine, ice-rafted) transport towards the core site (Fahl and Stein, 1997; Yunker et al., 2005). Likewise, landplant specific sterols such as b-sitosterol or campesterol (Huang and Meinschein, 1979; Pryce, 1971) are used as terrigenous biomarkers. A wide band of biomarkers used to reconstruct sea-surface primary productivity or sea surface temperatures is mainly derived from phytoplankton algae belonging to the classes haptophyceae, bacillariophyceae, or dinophyceae (e.g. Blumer et al., 1971; Boon et al., 1979; Eglinton and Eglinton, 2008; Volkman, 2006; Volkman et al., 1998). Brassicasterol and dinosterol, for example, are widely acknowledged as being produced by diatoms and dinoflagellates (Fig. 7), though it has also been shown that these molecules may have other algal sources (Goad and Withers, 1982; Kanazawa et al., 1971; Volkman et al., 1993). Short-chain *n*-alkanes, however, are also considered to reflect marine phytoplankton productivity (Blumer et al., 1971; Youngblood and Blumer, 1973).

The organic geochemical treatment of sediments to obtain biomarker lipids is commonly based on the extraction of the soluble (bituminous) organic matter from the sediment by means of specific solvents. Purification and chromatographic fractionation of this extract finally allows separating polar and neutral compounds, which basically enables or at least facilitates the further instrumental examination. Identification and quantification of these compounds are carried out mainly via gas chromatography (GC) and gas chromatography-mass spectrometry (GC-MS) analyses.

2.2.2 Biomarker studies

Since the use of the novel sea ice proxy IP_{25} (see chapter 1.3.2) was a main objective of this PhD project, the analytical procedure to obtain and identify this trace compound in marine sediments was acquired during a stay at the University of Plymouth (UK) under the supervision of Guillaume Massé and Simon T. Belt. This method was adopted and - owing to the different instrumental facilities at the AWI in Bremerhaven and also to extend the analysis of the biomarker composition (including sterols) - modified. The original "Plymouth" preparation pathway is described in chapter 6.2.

For the lipid biomarker analyses at home laboratories ca. 1 - 4 g of freeze-dried and homogenised sediment were extracted with an Accelerated Solvent Extractor (DIONEX, ASE 200; 100°C, 5 min, 1000 psi) using a dichloromethane:methanol mixture (2:1 v/v; 20 ml in total). Prior to this step, 7-hexylnonadecane, squalane and cholesterol-d6 (cholest-5-en-3β-ol-D6) were added as internal standards for quantification purposes. Total extracts were esterified with 1 ml 3 N methanolic hydrochloric acid (12 hrs, 50°C) to enable the separation of fatty acids during further column chromatography. After adding 3 ml *n*-hexane to the derivatised extract, the upper organic phase was collected and dried using Na_2SO_4 - this step was repeated twice (with 2 ml *n*-hexane). Finally, hydrocarbons, fatty acids and sterols were separated via open column chromatography (SiO_2) using *n*-hexane (5 ml), dichloromethane:*n*-hexane (1:1 v/v; 6 ml) and methylacetate:*n*-hexane (20:80 v/v; 6 ml), respectively. Sterols were silylated with 500 µl BSTFA (60°C, 2 h) prior to instrumental analysis.

GC-MS compound analyses of hydrocarbon and sterol fractions were performed using an Agilent 6850 GC (30 m HP-5ms column, 0.25 mm inner diameter, 0.25 µm film thickness) coupled to an Agilent 5975 C VL mass selective detector. The GC oven was heated from 60°C to 150°C at 15°C min^{-1}, and then at 10°C min^{-1} to 320°C (held 15 min) for the analysis of hydrocarbons and at 3°C min^{-1} to 320°C (held 20 min) for sterols, respectively. Helium was used as carrier gas. Operating conditions for the mass spectrometer were 70 eV and 230 °C (ion source). Hydrocarbon fractions were analysed in full scan mode and also in selected ion monitoring (SIM) mode (m/z 350, 348, 346, 266) to facilitate the detection of the trace compound IP_{25} (m/z 350) at very low concentrations. Further m/z 348 and m/z 346 served for monitoring the diene and triene C_{25} HBI isomers, whilst m/z 266 refers to the abundant fragment ion of 7-hexylonadecane.

Individual compound identification was based on comparisons of their retention times with that of reference compounds (applies to sterols and *n*-alkanes) and on comparisons of their mass spectra with published data (Belt et al., 2007; Boon et al., 1979; Johns et al., 1999; Volkman, 1986). A sediment sample from the Lancaster Sound (PS72/287-2; obtained during ARK-XXIII/3) with a very high, known concentration of IP_{25} was repeatedly prepared and analysed together with samples of unknown IP_{25} content to provide for laboratory and instrumental quality control. In figure 8, the chromatogram and mass spectrum of this "control" sediment sample is shown and compared with results obtained on surface sediments from the East Greenland shelf. This Lancaster Sound sediment was

used to establish IP_{25} calibration curves to obtain conversion factors, which were used for the further IP_{25} quantification (Fig. 9).

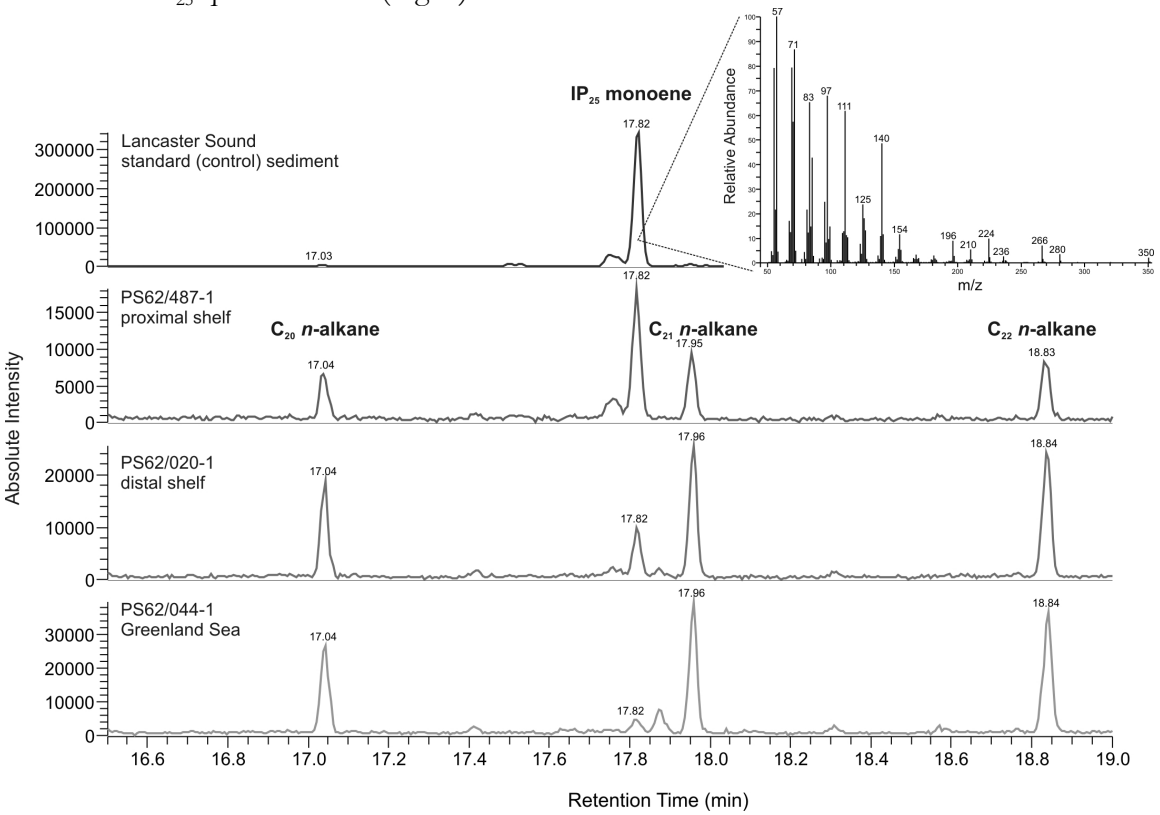

Fig. 8: Comparison of partial GC-MS chromatograms (m/z 140) obtained from the alkane fraction of the "control" sediment from Lancaster Sound (with mass spectrum) and surface sediments from the continental margin of East Greenland. IP_{25} elutes shortly before the C_{21} *n*-alkane.

In general, biomarker concentrations were calculated on the basis of their individual GC-MS ion responses compared with those of respective internal standards (to account for analytical inconsistencies) using the formula:

(2) $$\text{Compound [µg/g sed]} = (\text{µg IStd} / A_{IStd} \times A_{compund}) / \text{g sediment},$$

with µg IStd referring to the amount of internal standard added to the sediment prior to extraction and A_{IStd}, $A_{compound}$ referring to integrated peak areas of the internal standard and the target compound. Thus calculated IP_{25} concentrations were finally multiplied with the calibration factor obtained from the respective calibration curve (those were generated whenever the GC-MS instrumental settings were changed). The quantification is based on the assumption that the ion yield is nearly identical for the analytes and the internal standards. All correlations of the monitoring ions for internal standards versus TIC (Total Ion Current) and versus concentration were highly satisfactory (R^2 = 0.987 - 1). IP_{25} was quantified using its molecular ion *m/z* 350 in relation to the abundant fragment ion *m/z* 266

of 7-hexylnonadecane. Brassicasterol (24-methylcholesta-5,22E-dien-3β-ol) and dinosterol (4a,23,24-trimethyl-5α-cholest-22E-en-3β-ol) were quantified as trimethylsilyl ethers using the molecular ions *m/z* 470 and *m/z* 500, respectively, and *m/z* 464 for cholesterol-d6. Fragment ion *m/z* 57 was used to quantify the short-chain *n*-alkanes (*n*-C_{15}, *n*-C_{17}, *n*-C_{19}) via squalane. Sterol concentrations and the calibration curve for quantifying IP_{25} have been verified by GC measurements.

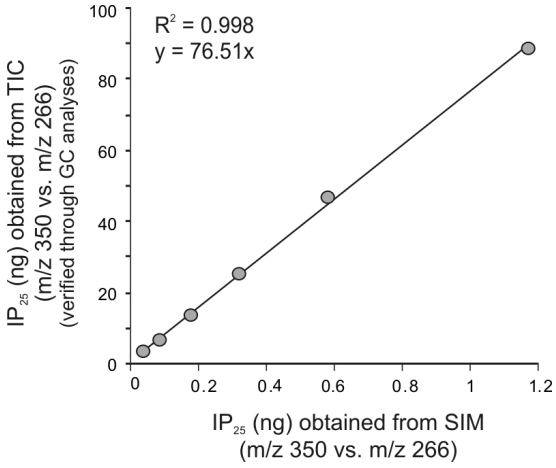

Fig. 9: Calibration curve for the quantification of IP_{25} via selected ion monitoring (SIM). Different IP_{25} concentrations determined from total ion current (TIC) GC-MS analyses are shown against respective results determined by selected ion monitoring (m/z 350 for IP_{25} and m/z 266 for 7-hexylnonadecane) GC-MS analyses. The calibration factor is thus obtained from the regression line and accounts for the different percentages of the 350 and 266 ions in the TIC and SIM measurements.

For this thesis, sediment samples were studied, which were already analysed for some of the organic geochemical bulk proxies and biomarker contents - these data are published and available via the PANGAEA data repository. This accounts for the TOC and brassicasterol data from the Kastenlot core PS2837-5 (Yermak Plateau) and the TOC contents of the surface sediments from the continental shelves of West Spitsbergen and East Greenland. The use of these data is appropriately indicated and cited within the respective studies (chapter 4 and 6).

3. Rationale and objectives of individual studies

The importance of sea ice for local and also global climate is widely acknowledged and thus the approaches to reconstruct and link its palaeo variability with respective climate conditions are manifold. Various studies about the palaeoceanographic and climatic development in the Fram Strait and adjacent areas strengthen a distinct interdependence between Atlantic water advection, deep-water circulation, and sea ice coverage (see chapter 1.2). The reconstruction of palaeo sea ice conditions in this climate sensitive area hence also supports the assessment of the other two variables. The novel sea ice biomarker IP_{25} constitutes a promising tool to identify and track palaeo sea ice coverage in the Artic realm. With regard to new invented parameters, such as IP_{25}, it is highly necessary that their utility, their temporal distribution, and also their limitations are evaluated thoroughly - in part to demonstrate their potential to the scientific community. The Fram Strait provides an excellent study area to examine the reliability of IP_{25} since the sea ice conditions are highly variable (in space and time) due to the complex ocean circulation system that characterises this passage. The IP_{25} studies presented herein accordingly contribute to the evaluation of the applicability of IP_{25} and its palaeoenvironmental significance and they give insight into the sea ice history of the Fram Strait.

The specific objectives of the three studies that constitute this thesis were:

1) The examination of the applicability of IP_{25} in Fram Strait.
To depict sea surface conditions at the West Spitsbergen and East Greenland continental margin in more detail phytoplankton-derived biomarkers were studied as well. Thus a suite of surface sediments was analysed to answer the following questions:

> *Does the sedimentary IP_{25} content mirror the recent spring sea ice extent in the study area?*
> *Do high/low IP_{25} contents refer to qualitatively (or even quantitatively) more/less sea ice cover?*
> *How does the ice cover affect phytoplankton productivity?*
> *How can the ambiguity of the absence of IP_{25} be dealt with?*

2) The reconstruction of Holocene sea ice conditions in the Fram Strait using the combinatory biomarker approach presented in the first study.
Sediment cores from the West Spitsbergen continental slope and the East Greenland shelf were studied to capture the spatial and temporal development of sea surface conditions

within these two in and outlet pathways for Atlantic and Arctic water (and sea ice) exchange to answer the following questions:

> *(How) did the sea ice cover respond to Holocene climate change?*
> *How did changes in the sea ice cover relate to the palaeoceanographic evolution?*
> *Was the development in eastern and western Fram Strait comparable?*
> *Can the approach of a quantitative sea ice reconstruction be applied?*

3) The reconstruction of sea ice conditions in northern Fram Strait during the last glacial-interglacial transition.
The examination of an already well-studied sediment core from the Yermak Plateau for its IP_{25} content provided for a first long-term application of IP_{25} and aimed to answer the following questions:

> *Is it possible to trace IP_{25} in pre-Holocene sediments?*
> *What was the sea ice extent before, during, and after the Last Glacial Maximum?*
> *How (fast) did the sea cover change throughout this period of distinct climate change?*
> *How did changes in the sea ice cover relate to the palaeoceanographic evolution?*

4. Towards quantitative sea ice reconstructions in the Northern North Atlantic: A combined biomarker and numerical modelling approach

Juliane Müller [a], Axel Wagner [a,b], Kirsten Fahl [a], Ruediger Stein [a], Matthias Prange [b,c], Gerrit Lohmann [a,b]

[a] Alfred Wegener Institute for Polar and Marine Research, 27568 Bremerhaven,Germany
[b] University of Bremen, 28359 Bremen, Germany
[c] MARUM Center for Marine Environmental Sciences, 28359 Bremen, Germany

Published in Earth and Planetary Science Letters (June 2011).

Abstract

Organic geochemical analyses of marine surface sediments from the continental margins of East Greenland and West Spitsbergen provide for a biomarker-based estimate of recent sea ice conditions in the northern North Atlantic. By means of the sea ice proxy IP_{25} and phytoplankton derived biomarkers (e.g. brassicasterol and dinosterol) we reconstruct sea ice and sea surface conditions, respectively. The combination of IP_{25} with a phytoplankton marker (in terms of a phytoplankton marker-IP_{25} index; PIP_{25}) proves highly valuable to properly interpret the sea ice proxy signal as an under- or overestimation of sea ice coverage can be circumvented. A comparison of this biomarker-based assessment of the sea ice distribution in the study area with (1) modern remote sensing data and (2) numerical modelling results reveals a good agreement between organic geochemical, satellite and modelling observations. The reasonable simulation of modern sea ice conditions by means of a regional ocean-sea ice model demonstrates the feasibility to effectively integrate the complex atmospheric and oceanic circulation features as they prevail in the study area. The good correlation between modelled sea ice parameters and the biomarker-based estimate of sea ice coverage substantiates that linking proxy and model data occurs to be a promising concept in terms of a cross-evaluation. This combinatory approach may provide a first step towards quantitative sea ice reconstructions by means of IP_{25}. Future IP_{25} studies on marine surface sediments from the Arctic realm, however, are recommended to extend and validate this new attempt of using IP_{25} in combination with a phytoplankton marker as a quantitative measure for sea ice reconstructions.

4.1 Introduction

Arctic sea ice is a pivotal element of the global climate as it influences the heat and moisture exchange between the ocean and the atmosphere. Furthermore it significantly affects the oceanic heat transfer and salinity regulation between southern and northern latitudes, thus impacting on the thermohaline circulation in the northern North Atlantic (e.g. Dieckmann and Hellmer, 2003; Rudels, 1996).

Information on modern Arctic sea ice conditions derive mainly from remote sensing data (e.g. Gloersen et al., 1992; Spreen et al., 2008) and research vessel observations (for instance, sediment trap and buoy data; e.g. Bauerfeind et al., 2005; Fahl and Nöthig, 2007; Perovich et al., 2009; see Eicken et al., 2009 for further field techniques) and allow for the monitoring of the most recent development of sea ice coverage in higher latitudes. Besides the concern about its future development, the currently observed retreat of Arctic sea ice, however, also prompts a gaining interest in past (natural) variations of the sea ice extent in the Arctic Ocean.

Most studies on the palaeodistribution of sea ice are commonly based on sedimentological data (Knies et al., 2001; Spielhagen et al., 2004) and microfossils (e.g. Carstens and Wefer, 1992; Koç et al., 1993; Matthiessen et al., 2001; Polyak et al., 2010; for a recent review see Stein, 2008a). In particular, sea ice associated (sympagic) organisms (e.g. pennate ice diatoms; Horner, 1985a) which contribute remarkably to the primary production in the marine Arctic ice environment (Gosselin et al., 1997; Gradinger, 2009), are frequently used for reconstructing sea ice conditions (Abelmann, 1992; Justwan and Koç, 2008; Koç et al., 1993; Kohly, 1998). However, it has also been shown previously that the preservation of fragile siliceous diatom frustules can be relatively poor in surface sediments from the Arctic realm and the same is also true (if not worse) for calcareous-walled microfossils, thus limiting their application potential (Kohly, 1998; Matthiessen et al., 2001; Schlüter and Sauter, 2000; Steinsund and Hald, 1994).

In recent decades, the organic geochemical investigation of marine sediments for specific molecular tracers (biomarkers), which are indicative of the type of organic matter they are derived from, has become a valuable tool for assessing palaeoenvironmental conditions (e.g. Eglinton and Eglinton, 2008; Meyers, 1997; Stein and Macdonald, 2004b; Volkman, 2006). The novel sea ice proxy IP_{25} (Belt et al., 2007), a monounsaturated highly branched isoprenoid lipid associated with diatoms that are restricted to sea ice, has been successfully used as a direct proxy for sea ice coverage. The identification of this molecule in marine

sediment cores from the Canadian Arctic Archipelago, the shelf north off Iceland and from northern Fram Strait, thus enabled reconstructions of the ancient sea ice variability in these regions (Belt et al., 2010; Massé et al., 2008; Müller et al., 2009; Vare et al., 2009). We recently demonstrated that the additional use of the phytoplankton-derived biomarker brassicasterol (e.g. Goad and Withers, 1982; Kanazawa et al., 1971; Volkman, 2006) as an indicator for open-water conditions notably facilitates the environmental reconstruction as ambiguous IP_{25} signals (i.e. its absence, which may refer to either a lack of sea ice or, in contrast, a permanent and thick ice cover limiting any algal growth) can be circumvented (Müller et al., 2009).

Along with these proxy-based sea ice reconstructions, physically based numerical ocean-sea ice models provide a complementary tool as they consider thermodynamic and dynamic key elements that shape sea surface and sea ice conditions. A particularly beneficial feature of these models is the possibility to reproduce sea ice thickness. The instrumental assessment of ice thickness (e.g. by means of ice-floe drilling, upward-looking sonar, ground-based/airborne EM; see Haas and Druckenmiller, 2009 for review) is still a spatially limited method, especially when compared to the relatively straightforward determination of the extent or concentration of sea ice by remote sensing. Ocean-sea ice models therefore provide a valuable source of ice thickness estimates that may be potentially useful within palaeo sea ice studies. However, the assessment of a model's accuracy (in representing sea ice conditions) reasonably builds on comparisons with observational (mainly satellite) or proxy data. With particular regard to palaeo-modelling studies, a calibration of proxy- and model-based assumptions of sea ice conditions would certainly improve forthcoming climate/sea ice reconstructions.

As the major discharge of Arctic sea ice to the northern North Atlantic occurs through Fram Strait (Fig. 10; Aagaard and Coachman, 1968; Rudels et al., 2005) marine sediments from this region may serve as ideal climate archives and provide useful information about the dynamics of this sea ice export system. With the organic geochemical analyses of surface sediments from the continental margins of East Greenland and West Spitsbergen, we herein give insight into the modern environmental situation of these areas. In addition to relatively common phytoplankton derived biomarkers (short-chain *n*-alkanes, certain sterols) we mainly focus on the sea ice proxy IP_{25} to estimate (spring/summer) sea ice conditions and to evaluate the applicability of this relatively novel ice proxy in an area of highly variable (seasonal) ice cover and strong ocean surface currents. With the incorporation of numerically modelled modern (spring) sea ice concentrations and thicknesses, we finally aim

at a cross-evaluation of proxy and model data, which may give direction towards a quantitative assessment of sea ice conditions in the past with implications for predictions of the future.

4.2 Regional Setting

The oceanographic setting in Fram Strait is characterised by two opposing current systems separating the passage into a comparatively temperate eastern region and a polar western domain. Warm Atlantic water enters the Nordic Seas via the northward heading Norwegian Current (NC) and, to a minor extent, via the Irminger Current (IC) west of Iceland (Fig. 10; after Rudels et al., 2005). In eastern Fram Strait the warm Atlantic water enters the Arctic Ocean via the West Spitsbergen Current (WSC). In western Fram Strait, polar water from the Arctic Ocean is transported southwards by the East Greenland Current (EGC) along the East Greenland continental margin (Aagaard and Coachman, 1968).

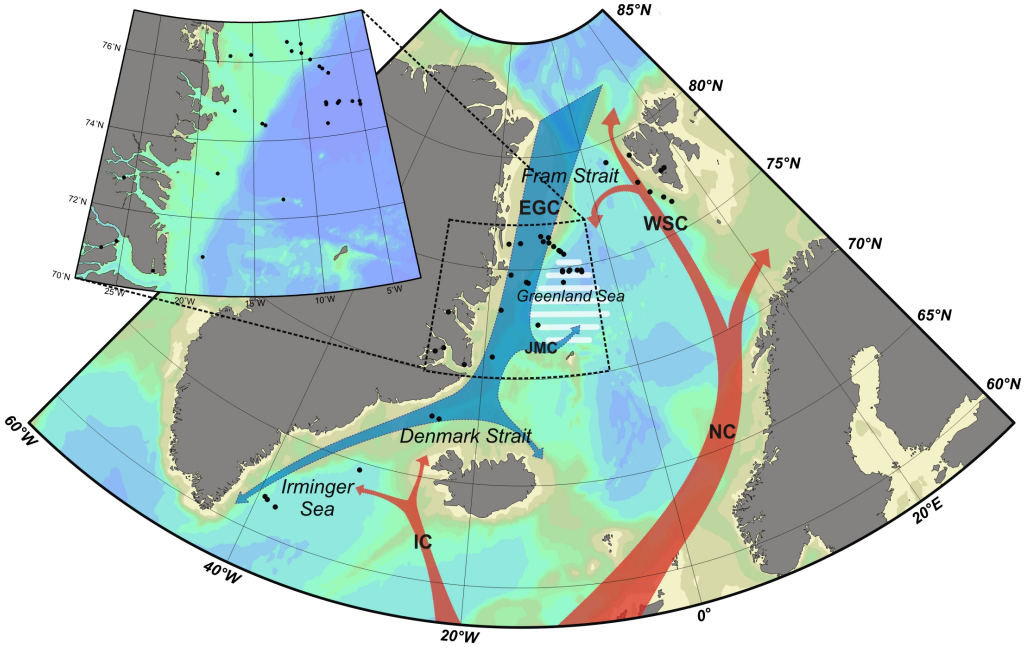

Fig. 10: Oceanographic setting in the study area (after Rudels et al., 2005) and locations of sampling sites (black dots). Red arrows refer to Atlantic Ocean derived warm surface waters: NC = Norwegian Current, WSC = West Spitsbergen Current, IC = Irminger Current. Blue arrows indicate Arctic Ocean derived cold surface waters: EGC = East Greenland Current, JMC = Jan Mayen Current. White bars denote area of Odden ice tongue development.

Sea ice conditions in the study area are hence subjected to (1) a massive seasonal discharge of old/multi-year sea ice and icebergs via the EGC and (2) the formation of new sea ice during autumn and winter. In general, the ice cover is more extensive in duration and concentration in coastal and proximal shelf areas of the East Greenland continental margin

with a pronounced southward sea-ice drift parallel to the coast (e.g. Gloersen et al., 1992; Martin and Wadhams, 1999). A frequent and prominent winter sea ice feature is the development of the Odden ice tongue (lasting until early spring), which covers the catchment area of the cold Jan Mayen Current in the central Greenland Sea (72° - 74°N; Fig. 10; Comiso et al., 2001; Wadhams et al., 1996).

As the WSC supplies eastern Fram Strait with warm Atlantic water, sea ice conditions at the West Spitsbergen continental margin are less severe. Winter sea ice formation is confined largely to near-shore areas and the fjords with the latter remaining covered in fast ice until early summer (Wiktor, 1999). Furthermore, ice conditions are subjected to the northward advection of sea ice that originates from the Barents Sea (Boyd and D'Asaro, 1994; Haugan, 1999).

4.3 Materials and Methods

4.3.1 Sediment samples

The surface sediment samples (0 - 1 cm; n = 44) studied herein were obtained during RV *Polarstern* cruises ARK-X/2 (Hubberten, 1995), ARK-XVI/1-2 (Krause and Schauer, 2001), ARK-XVIII/1 (Lemke, 2003) and ARK-XIX/4 (Jokat, 2004) by means of box- and multicoring equipment. Sediments were collected along the East Greenland continental margin (including the continental slope and adjacent deep-sea) and the continental margin of West Spitsbergen (Fig. 10; see Appendix A1 for coordinates of sampling locations). All samples were stored in clean brown glass vials at -30°C until further treatment.

For lipid biomarker analyses, the freeze-dried and homogenised sediments were extracted with an Accelerated Solvent Extractor (DIONEX, ASE 200; 100°C, 5 min, 1000 psi) using a dichloromethane:methanol mixture (2:1 v/v). Prior to this step, 7-hexylnonadecane (0.1064 µg/sample), squalane (0.6 µg/sample) and cholesterol-d6 (cholest-5-en-3b-ol-D6; 1.455 µg/sample) were added as internal standards for quantification purposes. Hydrocarbons and sterols were separated via open column chromatography (SiO_2) using *n*-hexane and methylacetate:*n*-hexane (20:80 v/v), respectively. Sterols were silylated with 500 µl BSTFA (60°C, 2 h) prior to analysis. Gas chromatography-mass spectrometry (GC-MS) compound analyses of both fractions were performed using an Agilent 6850 GC (30 m HP-5MS column, 0.25 mm inner diameter, 0.25 µm film thickness) coupled to an Agilent 5975 C VL mass selective detector. The GC oven was heated from 60°C to 150°C at 15°C min^{-1}, and then at 10°C min^{-1} to 320°C (held 15 min) for the analysis of hydrocarbons and at 3°C min^{-1} to 320°C (held 20 min) for sterols, respectively. Helium was used as carrier gas. Individual

compound identification was based on comparisons of their retention times with that of reference compounds (applies to brassicasterol and *n*-alkanes) and on comparisons of their mass spectra with published data (Belt et al., 2007; Boon et al., 1979; Volkman, 1986). Biomarker concentrations were calculated on the basis of their individual GC-MS ion responses compared with those of respective internal standards. The quantification is based on the assumption that the ion yield is nearly identical for the analytes and the internal standards. All correlations of the monitoring ions for internal standards versus TIC (Total Ion Current) and versus concentration are highly satisfactory (R^2 = 0.987 - 1). IP_{25} was quantified using its molecular ion m/z 350 in relation to the abundant fragment ion m/z 266 of 7-hexylnonadecane and by means of an external calibration curve (R^2 = 0.9989). Brassicasterol and dinosterol were quantified as trimethylsilyl ethers using the molecular ions m/z 470 and m/z 500, respectively, and m/z 464 for cholesterol-d6. Fragment ion m/z 57 was used to quantify the short-chain *n*-alkanes (*n*-C_{15}, *n*-C_{17}, *n*-C_{19}) via squalane.

With respect to individual sedimentary (facies) regimes within the study area, absolute biomarker concentrations have been normalised to total organic carbon contents (TOC; data from Birgel and Stein, 2004; Kierdorf, 2006) to compensate for different depositional and burial efficiencies. Sedimentation rates within fjords or at continental margins, for example, are two to three times higher than in the deep-sea (Dowdeswell and Cofaigh, 2002), which may cause a dilution of the biomarker content. Presenting biomarker concentrations per gram sediment hence could result in an underestimation of the biomarker content of the respective sediments. The pronounced concentration difference between phytoplankton markers and IP_{25} is likely attributable to the variety of source organisms that are known to synthesise short-chain *n*-alkanes, brassicasterol, and dinosterol (e.g. Blumer et al., 1971; Volkman et al., 1998; Volkman et al., 1993). In contrast, IP_{25} seems to be exclusively produced by one distinct sea ice diatom species (Belt et al., 2007), which would explain for the comparatively low abundance of this trace compound.

4.3.2 Numerical model - experimental design

In order integrate sea ice within climate modelling, a dynamical downscaling from a coarse-resolution climate model (3.8° x 3.8° horizontal resolution) to a high-resolved regional ocean-sea ice model (0.25° horizontal resolution) has been specifically designed for palaeo-modelling studies. The coarse-resolution (T31L19) climate model simulations have been performed for present and Holocene conditions (Lorenz and Lohmann, 2004). The coarse-resolved SST and sea ice fields of Lorenz and Lohmann (2004) have been bilinearly

interpolated to a finer resolved 1.1° x 1.1° matrix and applied to a high-resolution version (T106L31) of the atmospheric circulation model ECHAM5 (Roeckner et al., 2006). Each high-resolution simulation covers 50 integration years, where the last 40 years are used as forcing for the regional North Atlantic/Arctic Ocean-Sea Ice Model (NAOSIM). NAOSIM has been developed to simulate present sea ice variability, circulation, and hydrography in the North Atlantic/Arctic realm (Gerdes et al., 2003; Karcher et al., 2003). The model domain of NAOSIM encompasses the Arctic Ocean and adjacent North Atlantic seas. Our employed model experiments have been carried out at a horizontal grid resolution of 0.25 degrees and 30 vertical levels. Following Kauker et al. (2003), lateral ocean boundaries (volume flux, temperature, salinity) have been set to present observations at 50°N in the North Atlantic and at 65°N in the Bering Strait. In order to get a realistic halocline in the Arctic Ocean, the ocean surface salinity is weakly restored (time-scale of 6 months) to the monthly sea surface salinity climatology (Steele et al., 2001). The modern and Middle Holocene NAOSIM runs are integrated over 100 model years, where the last 30 years are analysed in terms of sea ice coverage and thickness.
A detailed analysis of the Middle Holocene will be the subject of a forthcoming study.

4.4 Results and discussion

4.4.1 Biomarker data: autochthonous versus allochthonous signal

With reference to the particular ice drift and dynamic current system in the study area, input of allochthonous matter and lateral advection of organic material demand consideration as they potentially affect the accumulation and composition of the biomarker assemblages investigated herein. For example, the allochthonous input of lithogenic and organic particles entrained in sea ice, which may originate from the shallow shelves of the Laptev Sea (Eicken et al., 1997; Nürnberg et al., 1994; for a recent review see Stein, 2008a), probably impacts on the biomarker content of sediments from the East Greenland shelf. In terms of absolute IP_{25} concentrations, we thus suggest that a blend of in-situ produced and allochthonous IP_{25} should be considered. Nonetheless, the occurrence of IP_{25} in these sediments strongly indicates the former presence (and melt) of (drift) sea ice.

As we notice that no correlation exists between phytoplankton biomarker and sea ice concentrations (Fig. 11), we assume that the allochthonous input of brassicasterol, dinosterol, and short-chain *n*-alkanes via sea ice seems to be of less importance in the study area. Sedimentary biomarker contents also depend on the fate of the sea surface derived organic material (1) on its way towards and (2) at the sea floor as, for instance, lateral

advection by subsurface currents, biodegradation or the physical/chemical alteration of organic matter may imprint on the preservation of biomarker lipids (see Zonneveld et al., 2010 and references therein).

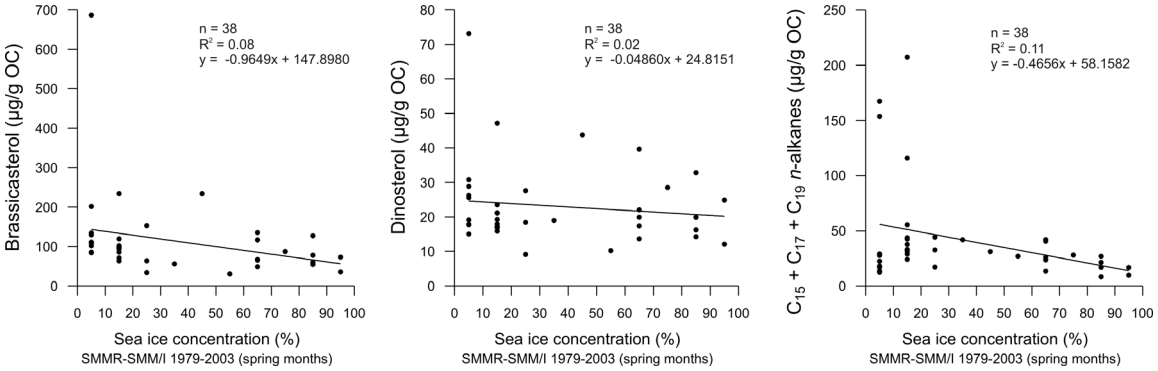

Fig. 11: Concentrations of individual phytoplankton biomarkers show no correlation with satellite derived (spring) sea ice concentrations. The allochthonous input of phytoplankton-derived biomarkers via sea ice hence seems to be negligible in the study area.

However, given that we do not observe a distinct correlation between the water depth at the individual sampling sites and their biomarker contents (Fig. 12) and that the distribution of IP_{25} and the phytoplankton markers display the modern sea surface conditions reasonably well (see section 4.4.4), we suggest that the organic matter is effectively transported through the water column.

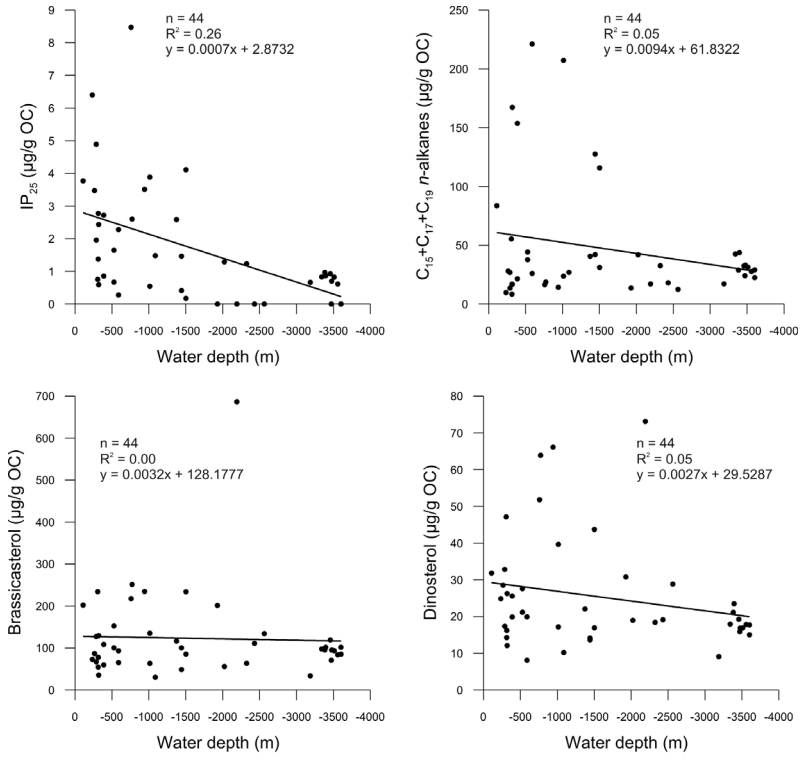

Fig. 12: Correlation of biomarker contents of sediment samples with water depth. Regression lines and coefficients of determination (R^2) are provided for each correlation chart.

The (concurrent) release of fine-grained lithogenic material during the ice melt in the study area supports the formation of organic-mineral aggregates (and zooplankton faecal pellets; Bauerfeind et al., 2005), which notably accelerates the downward transport of organic matter towards the seafloor. This provides for a rapid sedimentation of the biomarker lipids and reduces their residence time at the sediment-water interface, where degradation takes place (Bauerfeind et al., 2005; Knies, 2005; Stein, 1990). Finally, besides indicating a lack of sea ice coverage, the absence of IP_{25} in surface sediments from the Irminger Sea - the major discharge area for Denmark Strait Overflow Water (Rudels et al., 2005) - substantiates that relocation of biomarker signals by (sub)surface currents seems to be negligible - at least in this part of the study area. Thus, we interpret our biomarker data as direct proxies for sea ice cover and surface water productivity.

4.4.2 Biomarker distribution: sea ice conditions and sea surface primary productivity

Concentrations of IP_{25} and phytoplankton specific biomarker lipids (short-chain *n*-alkanes, brassicasterol and dinosterol; for review see Volkman (2006)) determined on surface sediments from the continental margins of East Greenland and West Spitsbergen are visualised by means of the Ocean Data View Software 4.2.1 (Fig. 13a-d; Schlitzer, 2009; for biomarker concentrations see also Appendix A1).

Highest IP_{25} concentrations are found in sediments from the East Greenland fjords (3.5 - 8.5 μg/g OC), along the proximal shelf of north-east Greenland (2.3 - 6.4 μg/g OC) and in the two samples from Denmark Strait (ca. 4 μg/g OC; Fig. 13a) and likely refer to an extended (lasting throughout spring and early summer) sea ice cover at these sites. Furthermore, these elevated IP_{25} concentrations align well with microfossil data from Matthiessen et al. (2001) and Andersen et al. (2004), who report on the dominance of polar dinoflagellate cysts and sea ice diatom assemblages in sediments underlying the ice-covered polar water masses along the East Greenland shelf. North of 75°N this sea ice lasts until summer (Gloersen et al., 1992) and hence hampers phytoplankton productivity, which explains for the minimum concentrations of short-chain *n*-alkanes (< 30 μg/g OC), brassicasterol (< 60 μg/g OC), and dinosterol (< 20 μg/g OC) in these sediments (Fig. 13b-d).

Gradually reduced IP_{25} contents in samples from the distal East Greenland shelf (2 - 3.5 μg/g OC) and the continental slope (1.2 - 2.6 μg/g OC) suggest less intense or variable ice conditions towards the east. This is consistent with findings of Koç Karpuz and Schrader (1990) who observed an eastward shift in the geographic distribution of a sea ice diatom

assemblage (dominant at the shelf) towards an Arctic water diatom assemblage (dominant along the continental margin). Similarly, Pflaumann et al. (1996) found an eastward decrease in the abundance of the polar planktic foraminifer *Neogloboquadrina pachyderma*.

A north-south gradient of generally low IP_{25} concentrations in sediments from eastern Fram Strait (0.2 - 0.8 µg/g OC; Fig. 13a) likely reflects the influence of warm Atlantic water carried by the WSC along the West Spitsbergen shelf towards the north.

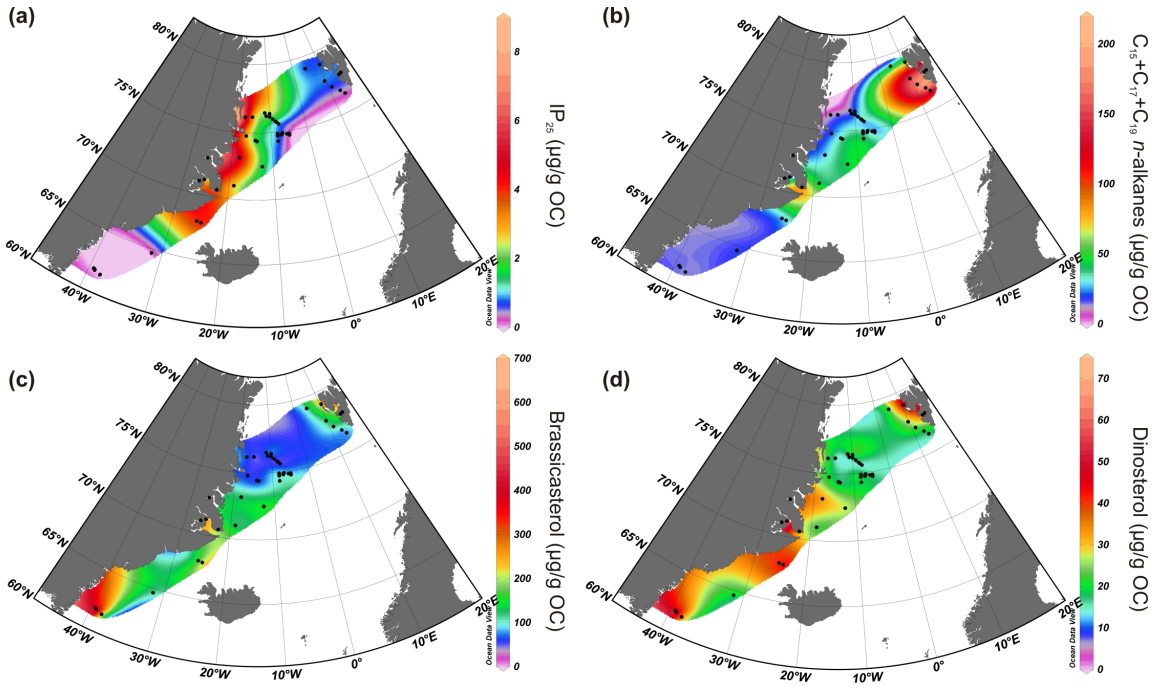

Fig. 13: Concentrations of the sea ice proxy IP_{25} (a) and phytoplankton-derived biomarkers (short-chain *n*-alkanes (b), brassicasterol (c), and dinosterol (d)) in surface sediments from the continental margins of East Greenland and West Spitsbergen. Maps are generated with the Diva Gridding Algorithm supplied by the Ocean Data View software package (Schlitzer, 2009). Note that on concentration scales absolute values are given equidistantly while colours are automatically adjusted to accentuate concentration gradients.

Minimum IP_{25} concentrations at the southern part of the West Spitsbergen shelf thus point to minor sea ice occurrences. At these sites, the still remarkable heat content of the Atlantic water reduces the formation of sea ice during autumn and accelerates its melt during spring/summer. The growth of phytoplankton consequently benefits from these mainly ice-free conditions and is reflected in significantly elevated contents of short-chain *n*-alkanes (40 - 220 µg/g OC), dinosterol (20 - 50 µg/g OC), and - to a lower extent - brassicasterol (90 - 230 µg/g OC; Fig. 13b-d). Likewise, elevated TOC values determined on surface sediments from western Fram Strait are related to a higher surface water productivity caused by warm WSC waters (Birgel et al., 2004; Hebbeln and Berner, 1993).

Diminished concentrations of both IP_{25} (< 1 μg/g OC) and phytoplankton biomarkers in sediments from the northern Greenland Sea (off the East Greenland continental margin; ca. 75°N), however, are possibly attributable to unsuitable environmental conditions. The (spring) sea ice cover in the Odden ice tongue area mainly consists of newly formed frazil and pancake ice (Comiso et al., 2001), which, in comparison to multiyear sea ice, presumably does not accommodate high amounts of sea ice diatoms (synthesising IP_{25}). Furthermore, the highly variable ice conditions with a rapidly (within days) oscillating ice-edge position and high salinity fluxes that result from brine expulsion (Comiso et al., 2001; Gloersen et al., 1992) may negatively impact on the spring primary productivity. Limited nutrient availability due to the gyre-like surface circulation within the Greenland Sea and thus isolation from external supply of nutrients as suggested by Rey et al. (2000), may also account for reduced phytoplankton biomarker abundances.

In contrast, the co-occurrence of increased IP_{25} and phytoplankton biomarker contents along the distal shelf of East Greenland (< 74°N) and at Denmark Strait indicates favourable living conditions for both ice algae and open-water phytoplankton. We thus conclude that these areas confine a more or less stable (i.e. lasting from spring to summer) ice-margin regime as an advantageous living habitat for both algal species. This is consistent with the findings of Smith (1987) and Sakshaug (2004) who demonstrated previously that marine primary productivity is enhanced at the ice-edge due to a stabilisation of the water column and increased nutrient release from melting sea ice (for "marginal ice zone" carbon fluxes see also Wassmann et al., 2004). Further studies in the Greenland Sea highlighted maximum phytoplankton biomass and chlorophyll-*a* concentrations in the vicinity of the ice edge (Richardson et al., 2005; Smith et al., 1985). Higher sedimentary TOC values and elevated fluxes of particulate organic carbon and biogenic silica are also described by Kierdorf (2006), Ramseier et al. (1999) and Peinert et al. (2001) from the marginal ice zone along the continental margin of East Greenland, which supports our assumption of a "high productive" ice-edge corridor along the outer shelf.

No IP_{25} could be detected in the sediments from the Irminger Sea (< 65°N; Fig. 13a). Since brassicasterol and dinosterol are enriched in these samples (130 - 680 μg/g OC and 30 - 73 μg/g OC, respectively), thus suggesting a satisfactory environmental setting for open-water phytoplankton (i.e. diatoms, coccoliths, and dinoflagellates as main source organisms of brassicasterol and dinosterol; Volkman, 1986 and references therein; Volkman et al., 1993), we conclude that the absence of IP_{25} results from a considerably reduced formation and/or advection of sea ice at these sites (Lisitzin, 2002; Ramseier, 2001). The generally low

concentrations of short-chain *n*-alkanes in these surface sediments, however, may refer to less favourable ecological conditions (nutrient depletion, grazing pressure) for the respective short-chain *n*-alkane synthesising algae (mainly brown-, red-, green-algae; Blumer et al., 1971; Gelpi et al., 1970).

4.4.3 Phytoplankton-IP$_{25}$ Index

Including a phytoplankton component to assess sea ice conditions occurs reasonable since sea ice evidently acts not only as a limiting factor for phytoplankton growth (as demonstrated for the marginal ice zone along the continental margin of East Greenland). The risk to overestimate sea ice coverage purely on the base of high IP_{25} concentrations thus can be reduced. Similarly, an underestimate of sea ice coverage deduced from the absence of IP_{25}, which in fact may also result from a permanent ice cover (Belt et al., 2007; Müller et al., 2009), can be circumvented, when the content of phytoplankton markers is known (for a first application of this combinatory approach within a palaeo sea ice study see Müller et al., 2009). Figure 14 provides a generalised overview about sea ice conditions and the corresponding productivity of sea ice algae and phytoplankton at the sea surface; respective biomarker fluxes towards the sea floor are indicated too.

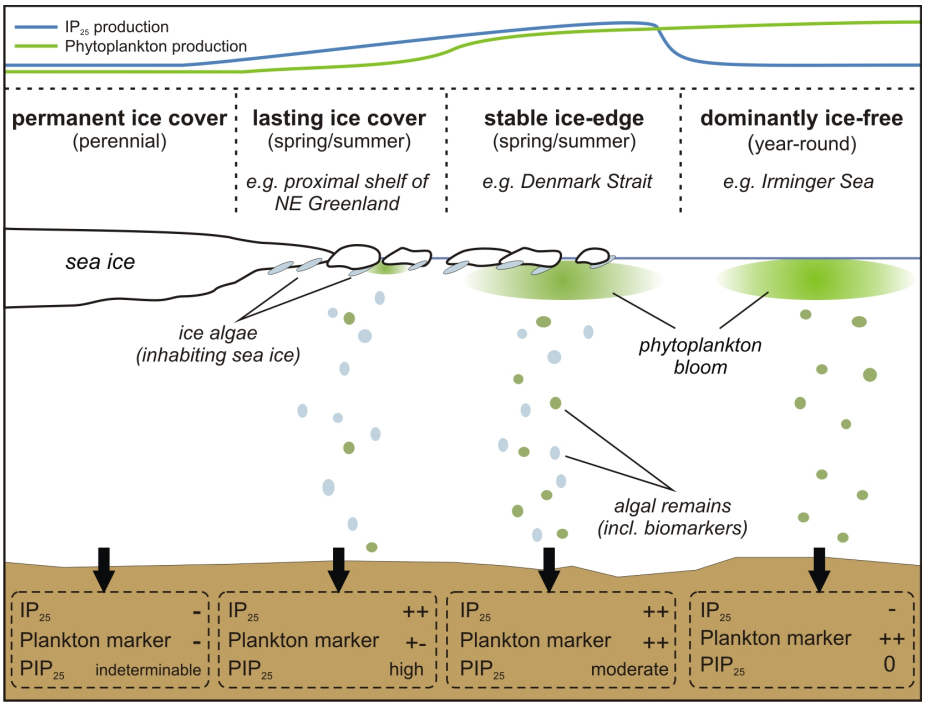

Fig. 14: Generalised scheme illustrating distinct sea surface conditions and respective (spring/summer) productivities of ice algae and phytoplankton. Overview sedimentary contents of IP_{25} and the phytoplankton-derived biomarkers and resulting PIP_{25} indices are indicated for each setting.

By means of the sedimentary biomarker contents a phytoplankton-IP_{25} index (PIP_{25}) can be calculated, which gives the fraction of IP_{25} to the combined IP_{25} and phytoplankton marker content. Since we herein observed a significant concentration difference between IP_{25} and phytoplankton derived biomarkers, and as we assume that this may also account for other marine environments in the Arctic, we propose that a concentration balance factor (c) needs to be considered for the calculation of this PIP_{25} index:

(3) $PIP_{25} = IP_{25} / (IP_{25} + (\text{phytoplankton marker} \times c))$ with

(4) c = mean IP_{25} concentration / mean phytoplankton biomarker concentration.

The PIP_{25} index accounts for the (spring/summer) algal activity beneath the sea ice (mainly ice algae), at the ice-edge (ice and phytoplankton algae), and in ice-free areas (phytoplankton) and thus allows a rough estimate of the spatial and temporal extent of the sea ice cover (Fig. 14). High PIP_{25} values accordingly refer to high sea ice cover, while low values point to a reduced sea ice cover. With respect to the variety of phytoplankton biomarkers we propose that this PIP_{25} index should be appropriately specified through indices, for example as P_BIP_{25} or P_DIP_{25} when using brassicasterol or dinosterol. The use of such an index to distinguish between different sea ice conditions, however, requires essential awareness of the individual biomarker concentrations to avoid misleading interpretations. For instance, coevally high amounts of both biomarkers (suggesting ice-edge conditions) as well as coevally low contents (suggesting permanent-like ice conditions) would give the same PIP_{25} value.

A correlation of IP_{25} versus brassicasterol and dinosterol concentrations in sediments from the study area is given in figure 15, where we also denote different zones of sea ice conditions with corresponding P_BIP_{25} and P_DIP_{25} values determined for the surface samples.

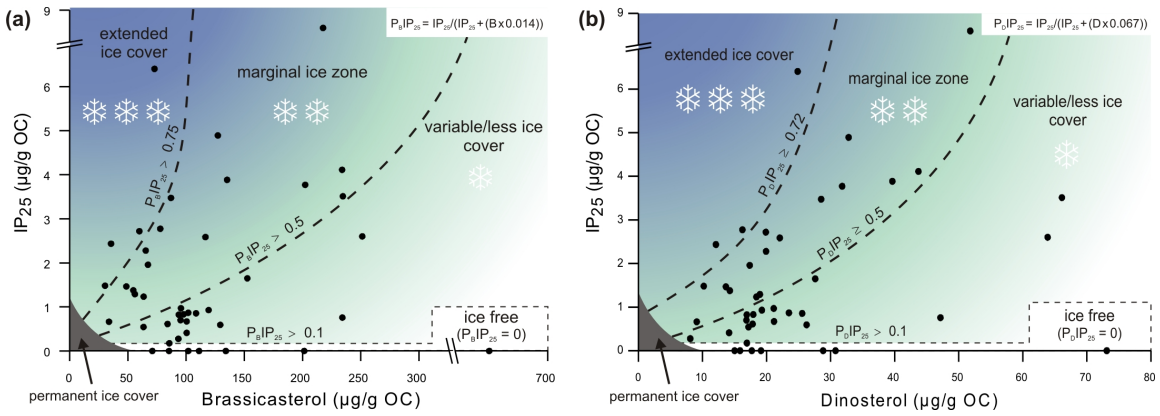

Fig. 15: Correlation of IP_{25} versus brassicasterol (a) and dinosterol concentrations (b) and corresponding P_BIP_{25} and P_DIP_{25} indices calculated for sediments from the study area by means of respective equations (upper right corner within each panel). The light-green to blue shaded background fields and snow symbols indicate the transition from minimum to maximum sea ice coverage. Note that permanent ice cover (dark grey field) is not observed herein.

Conveniently, such an index also facilitates the graphic representation of the environmental information carried by the ice proxy and the phytoplankton marker as shown for the P_BIP_{25} values (Fig. 16a). Maximum P_BIP_{25} values (dark blue contour lines in Fig. 16a; $P_BIP_{25} \pm 0.85$) indicate pronounced ice coverage throughout the spring and summer season as found along the proximal shelf of NE Greenland, whereas an index of 0 (no IP_{25}; pale yellow contours in Fig. 16a) suggests pre-dominantly ice-free conditions as, for example, at the sampling sites in the Irminger Sea. Accommodating living conditions for ice algae and open-water phytoplankton characterise the marginal ice zone (with a relatively stable ice edge lasting from spring to summer) along the distal shelf of East Greenland towards Denmark Strait (dark-green contours; $P_BIP_{25} \pm 0.65$). Light-green contours ($P_BIP_{25} \pm 0.25$) finally denote a short-lasting maximum sea ice extent with notably lowered ice concentrations in the north-eastern Greenland Sea (at ca. 75°N) and along the West Spitsbergen margin (Fig. 16a).

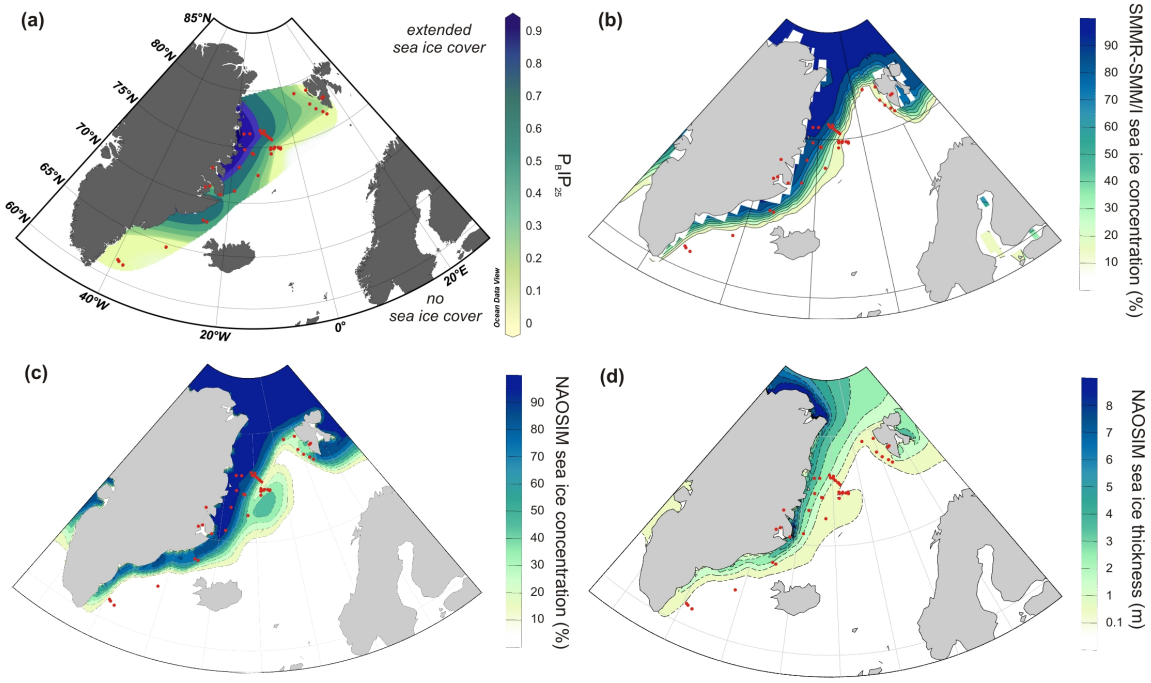

Fig. 16: Comparison of the (a) biomarker-based estimate of sea ice coverage using the P_BIP_{25} index with (b) SMMR-SSM/I satellite derived mean spring sea ice concentrations, (c) NAOSIM modelled spring sea ice concentrations, and (d) sea ice thicknesses. Both satellite and NAOSIM-based sea ice data are averaged over the period from 1979 to 2003. Red dots denote sites of sediment samples.

We point out that using dinosterol or short-chain *n*-alkane contents (instead of brassicasterol) for the calculation of respective P_DIP_{25} and $P_{Alk}IP_{25}$ indices yields basically similar results (Fig. 17; see also Appendix A2). That means that these biomarker ratios could be used to qualitatively estimate sea ice coverage as well, though we note that the $P_{Alk}IP_{25}$ index seems to somewhat overestimate the sea ice coverage, for example, in the Denmark

Strait. Since the P_BIP_{25} values show a slightly higher correlation with sea ice concentrations determined by satellite imagery than the P_DIP_{25} index we herein used the P_BIP_{25} index for reconstructions of sea ice conditions in the study area.

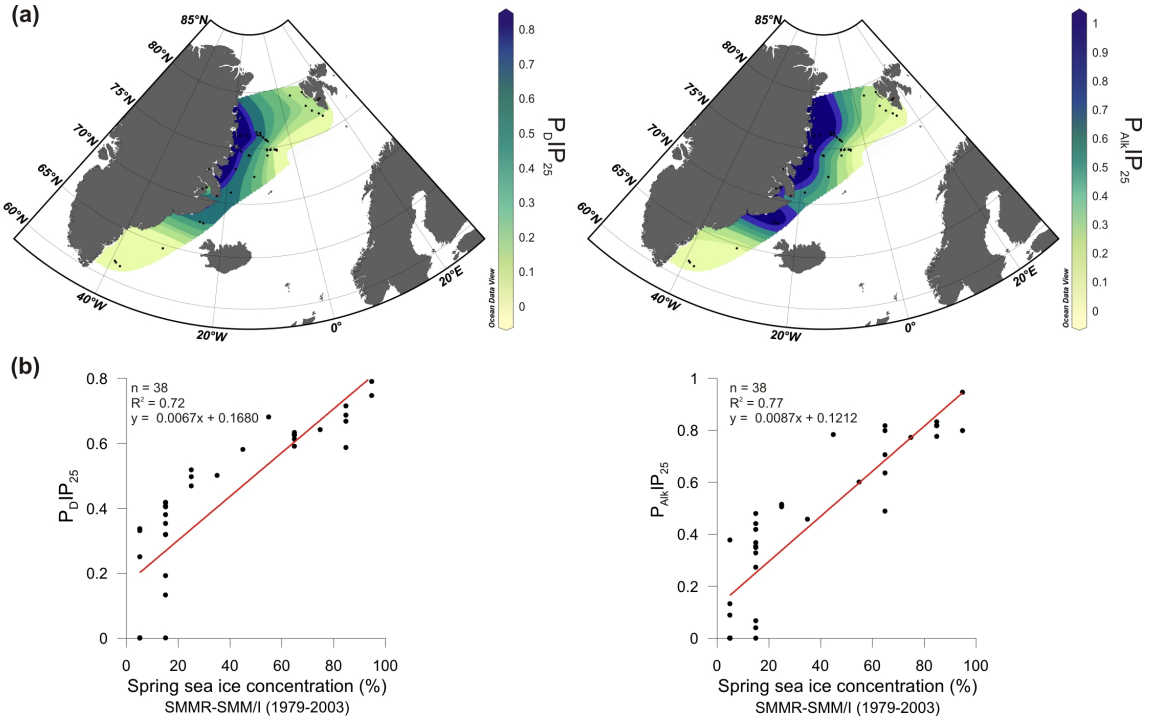

Fig. 17: (a) Sea ice estimates as derived from the P_DIP_{25} index (using dinosterol) and the $P_{Alk}IP_{25}$ index (using short-chain *n*-alkanes). For the calculation of the indices concentration balance factors (0.067 for P_DIP_{25} and 0.036 for $P_{Alk}IP_{25}$) have been considered. Using dinosterol instead of brassicasterol yields a largely similar distributional pattern of sea ice. The use of *n*-alkanes seems to result in an overestimate of the sea ice cover at Denmark Strait. (b) Correlation analyses of these ratios with satellite derived (spring) sea ice concentrations (1979 - 2003) with respective coefficients of determination.

4.4.4 Comparison of biomarker and satellite sea ice data

The SMMR (NIMBUS-7 satellite) and SSM/I (DMSP satellites) based sea ice map (Fig. 16b) shows mean (spring) sea ice concentrations derived from the AMSR-E Bootstrap Algorithm (Comiso, 1999 (updated 2008)). Monthly (March-April-May) mean sea ice concentrations have been averaged for the period from 1979 to 2003. Certainly, a one-to-one comparison of sea ice conditions obtained from satellite observations (displaying a 25 years mean) with estimates based on sediment data is flawed by the different time frames that are captured by both methods. Depending on sedimentation rates, surface sediments from the study area may easily represent a much longer time interval (decades to centuries) - this needs to be kept in mind. The problematic age control is also common to other "modern analogue" geochemical or microfossil studies (de Vernal et al., 2001; Müller et al., 1998) and can partly be solved by ^{14}C age determinations of the respective sediments only (Pflaumann et al.,

2003).

Remote sensing imagery indicates highest sea ice concentrations (about 100%) at the northernmost and western part of Fram Strait along the EGC affected continental margin of Greenland (Fig. 16b). This aligns with maximum IP_{25} concentrations in the respective sediments. A gradual eastward decline in sea ice concentrations (from highest to lowest values) is observed along the polar front paralleling the continental slope of East Greenland, which is also reflected in the biomarker data. Minimum to zero ice concentrations within the Greenland Sea could explain for the general low contents of IP_{25} and also its absence in some of these surface sediments (Fig. 13a). Similarly, sampling sites south of Denmark Strait (in the Irminger Sea) are located in virtually ice-free waters (Fig. 16b), which is also reflected in the absence of IP_{25}.

For a more quantitative comparison of the biomarker and satellite data we used the sea ice concentrations as they are displayed for the individual sediment sampling sites (Fig. 16b; see Appendix A3). As expected, IP_{25} concentrations correlate positively with ice coverage (Fig. 18a; $R^2 = 0.67$). This correlation, however, may importantly highlight the fundamental ambiguity of the sea ice proxy, as, for example, relatively low IP_{25} contents are observed not only for minimum but also maximum ice coverage (Fig. 18a).

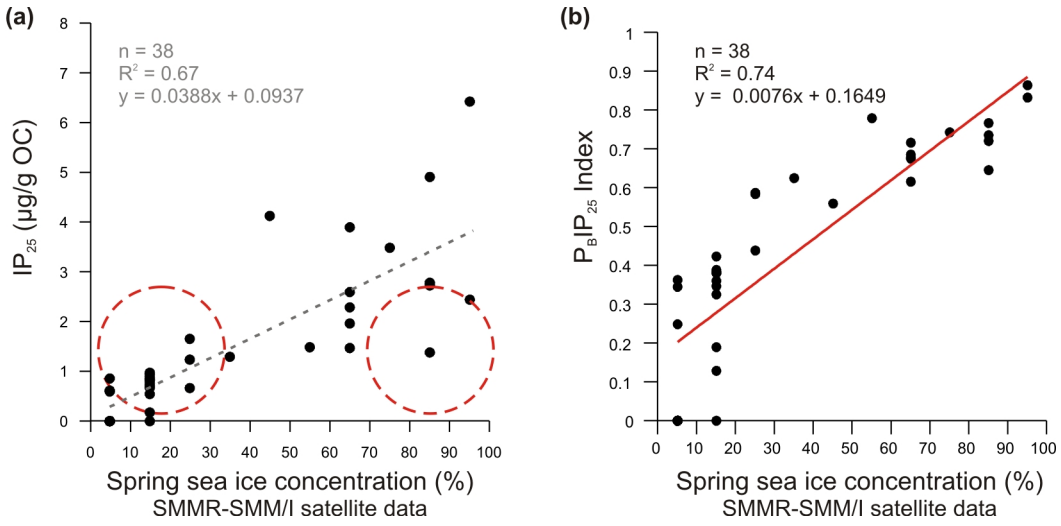

Fig. 18: Correlation of spring sea ice concentrations (± 5%) derived from satellite data (SMMR-SSM/I; 1979 - 2003) with (a) IP_{25} concentrations and (b) P_BIP_{25} values. Coefficients of determination (R^2) are given for the respective regression lines. Red dashed circles highlight low IP_{25} concentrations, which misleadingly may be interpreted as indicative of low sea ice concentrations though they result from severe sea ice coverage limiting ice algae growth at the bottom of the ice.

Sedimentary IP_{25} contents hence should not be used as a direct measure for sea ice concentrations. This and also the higher correlation of P_BIP_{25} values with sea ice

concentrations (Fig. 18b; $R^2 = 0.74$) strengthens that the coupling of IP_{25} with a plankton marker (e.g. brassicasterol) proves to be a valuable and more reliable approach for realistic sea ice reconstructions.

4.4.5 Modelled sea ice distribution

The NAOSIM (spring) sea ice concentrations and thicknesses in the study area have been simulated for modern (1979 - 2003; Fig. 16c, d) and Middle Holocene conditions.

Modelled sea ice cover and satellite-derived data yield largely consistent regional patterns. North of Fram Strait, Greenland, and Spitsbergen, the ice cover occurs to be almost 100% everywhere. Within the Fram Strait area, NAOSIM sea ice concentrations reveal a positive westward gradient with maximum concentrations of up to 100% at the East Greenland coast (Fig. 16c). These maximum sea ice concentrations are in good agreement with the development of extensive landfast ice over the shelf of NE Greenland (Hughes et al., 2011). As also observed via satellite, ice concentrations are reduced to 10% at the lowest at the western coastline of Spitsbergen. Along the proximal shelf of East Greenland, the model reproduces a band of high sea ice concentrations (approximately 90% to 100%) extending far to the south (70°N), thus mirroring the path of the EGC. South of 70°N, ice concentrations near the Greenland shoreline are still in the range of 60% to 80%, however, with a steeper decreasing gradient towards the south. The model depicts a gradual eastward decrease in sea ice concentrations (from 100% to 10%) to parallel the continental shelf break of East Greenland, as is also observed via satellite (Fig. 16b). To the east of the EGC affected shelf, between 70° and 76°N, an exposed patch of sea ice coverage (10% to 40% ice concentration) successfully represents the Odden ice tongue that results from the anticlockwise ocean gyre circulation of the Jan Mayen Current within the Greenland Sea (Wadhams et al., 1996). In the satellite image (Fig. 16b) this tongue-shaped protrusion of Odden ice, however, appears less pronounced with regard to its extent and also concentration-wise (0% - 20%) than calculated by the model. The NAOSIM also tends to slightly overestimate the sea ice concentration north of Iceland and along the continental margin of West Spitsbergen by ca. 10%. Correlation analysis of satellite-based and modelled sea ice concentrations as they prevail at 38 of the 44 sediment-sampling sites (both satellite and model do not resolve conditions within fjords), however, reveals that the two data sets are in good agreement ($R^2 = 0.89$; Fig. 19).

Modelled ice thicknesses (Fig. 16d) pinpoint highest values of 7 to 9 m at the northern coast of Greenland (> 80°N), consistent with the local accumulation of very thick multiyear

sea ice and the formation of pressure ridges enforced by the wind-driven surface circulation in this area (Haas et al., 2006; Wadhams, 1990). In contrast, significantly lowered ice thicknesses in the eastern Fram Strait (0.5 - 1 m) likely reflect the impact of warm Atlantic water carried northwards by the WSC. Moderate ice thicknesses of about 3 to 4 m parallel the coast and proximal shelf of East Greenland (between 80° and 70°N) and are gradually reduced in a south-eastward direction (Fig. 16d). This general reduction in ice thicknesses is in good agreement with the findings of Wadhams (1997 and 1992), who reported a continuous decline in the mean ice thicknesses with decreasing latitude from the northern Fram Strait (up to 4 m ice draft) towards the Greenland Sea (less than 1 m ice draft). Modelled ice thicknesses also align with observations from upward looking sonars located at 79°N, 5°W in the Fram Strait, which document mean spring sea ice thicknesses of 2.8 to 3.2 m for the period 1990-1994 (Vinje et al., 1998). Across the Greenland Sea, a patch of sea ice thickness of around 0.1 to 1 m is detached from the nearshore sea ice field. This pattern is consistent with the recognised field of sea ice concentrations in Fig. 16c.

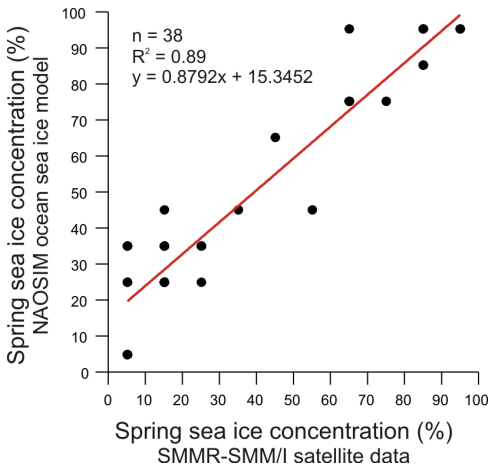

Fig. 19: Correlation of spring sea ice concentrations derived from satellite (SMMR-SSM/I) data and NAOSIM. Data points reflect sea ice concentrations (± 5%) as determined at sediment sampling sites.

Simulations of the palaeo modelling experiment (Fig. 20) suggest that (spring) sea ice concentrations and thicknesses in the study area were basically lower during the Middle Holocene than during modern times (Fig. 20). Particularly in eastern Fram Strait, sea ice concentrations were significantly reduced, which may point to an intensified Atlantic water inflow at this time. A detailed analysis of the Middle Holocene, however, is beyond the scope of this study, though a comparison of modelled and reconstructed sea ice parameters for past climates like the Middle Holocene would be a logical next step.

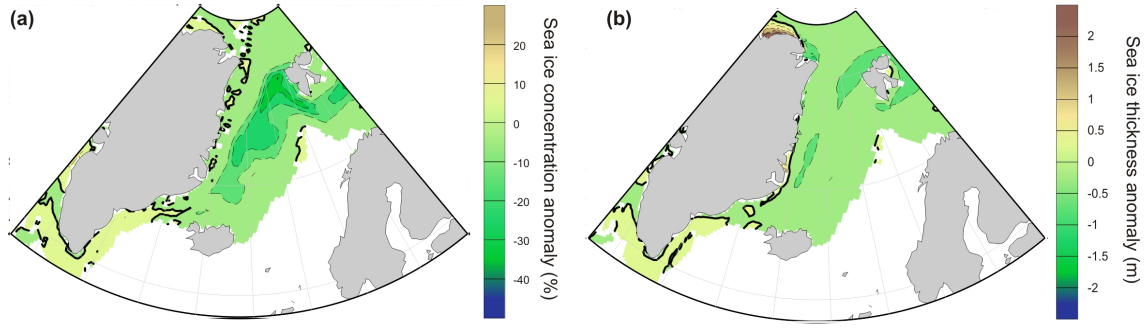

Fig. 20: NAOSIM modelled spring sea ice concentration (a) and thickness (b) anomalies for Middle Holocene relative to pre-industrial times. Positive (negative) values relate to higher (lower) sea ice concentrations or thicknesses during the Middle Holocene compared to pre-industrial times.

4.4.6 Proxy and model data: qualitative and quantitative comparisons

A rough qualitative comparison of the biomarker-based estimate of sea ice coverage (Fig. 16a) with model results exhibits a comparable pattern of the sea ice distribution in the study area with maximum sea ice cover along the proximal shelf of East Greenland, reduced sea ice cover along the West Spitsbergen continental slope and ice free conditions in the Irminger Sea. However, we also identify some inconsistencies between the modelled and proxy-based sea ice reconstruction. Unlike the model, which reproduces low to medium sea ice concentrations in the Odden ice tongue area, the P_BIP_{25} index seems to be less suitable to reflect the distribution of newly formed sea ice. Furthermore, maximum ice thicknesses at the outlet of the Scoresby Sund fjord system (East Greenland) are not supported by the biomarker data. According to the model, this sampling site experienced severe ice cover with more than 5 m ice thickness. But, instead of a hampered primary productivity (due to the limited light availability below the thick ice cover), we find enhanced contents of phytoplankton markers and IP_{25} in the respective sediment sample, indicating stable ice-edge conditions. Apparently, the ice cover was not completely closed at the fjord's mouth.

With regard to the general need of linking proxy and model approaches for palaeo reconstructions we herein provide a quantitative cross-evaluation of our biomarker and model results. Modelled sea ice concentrations correspond moderately with IP_{25} contents (Fig. 21a; $R^2 = 0.65$) and slightly stronger with P_BIP_{25} values (Fig. 21b; $R^2 = 0.67$), which again supports the assumption that this ratio reflects sea ice coverage more properly than the IP_{25} signal alone. In contrast, IP_{25} concentrations correlate more clearly with modelled ice thicknesses than the P_BIP_{25} values (Fig. 22).

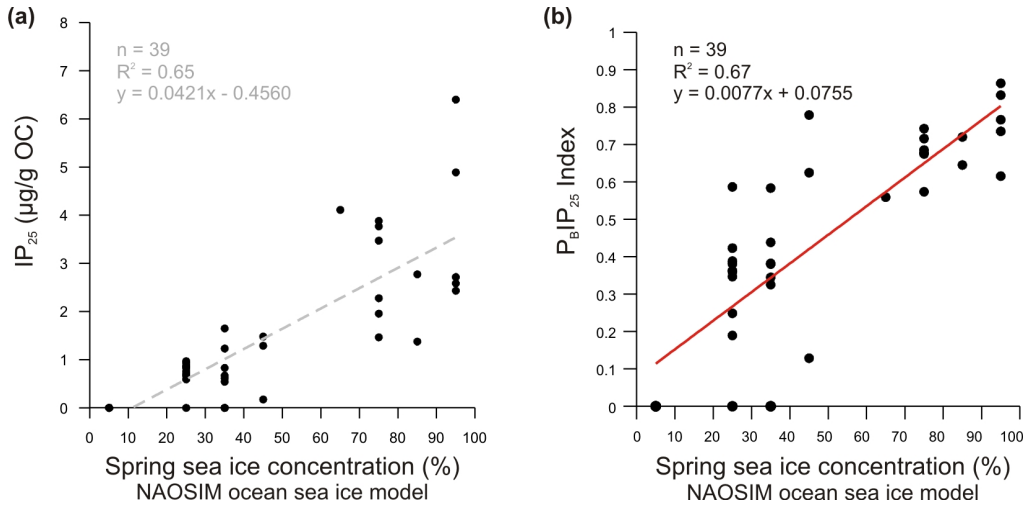

Fig. 21: Correlation of NAOSIM modelled spring sea ice concentrations (± 5%) with IP_{25} contents (a) and P_BIP_{25} values (b). Coefficients of determination (R^2) are given for the respective regression lines.

We assume that this indicates a non-linear response of (lower) phytoplankton activity to increasing ice thickness. The higher correlation between IP_{25} contents and ice thickness is probably due to the allochthonous transport of IP_{25} within thicker multi-year sea ice.

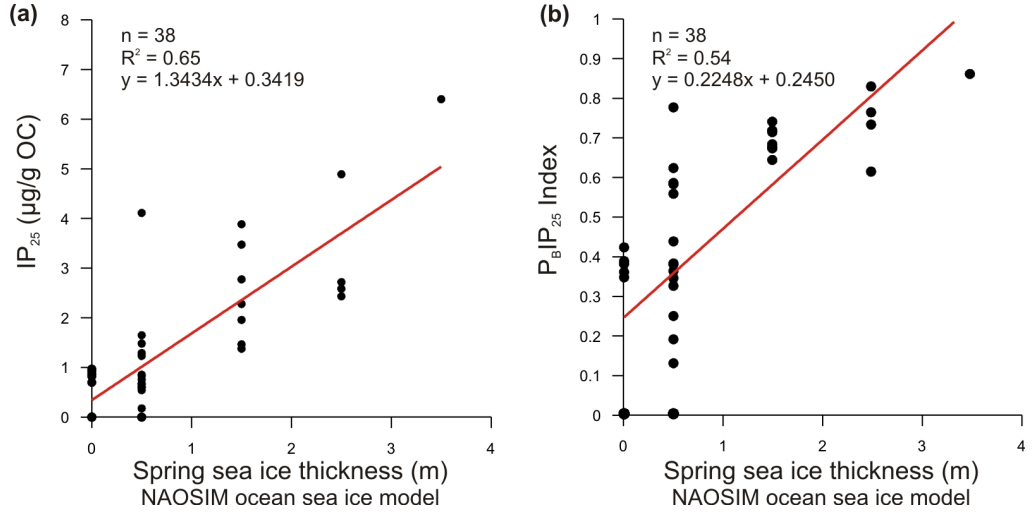

Fig. 22: Correlation of NAOSIM modelled spring sea ice thicknesses (± 0.5 m) with (a) IP_{25} concentrations and (b) P_BIP_{25} values. Coefficients of determination (R^2) are given for the respective regression lines. From this correlation we excluded one outlying data point, which derives from the sediment sample located at the outlet of the Scoresby Sund fjord system.

The largely good correlations of NAOSIM modelled sea ice concentrations with P_BIP_{25} values, however, occur rather enticing with regard to a quantitative proxy-model calibration. And though we surely acknowledge the utility of such a "sea-ice formula", i.e. the possibility to calculate absolute sea ice concentrations or thicknesses on base of biomarker data, we herein recognise few points that (hitherto) give concern about the applicability of this calibration. These are (1) the highly dynamic drift-ice component and hence the hardly assessable allochthonous input of organic matter (a transfer function based on the herein observed biomarker distribution, presumably would not be applicable to other Arctic sea ice environments); (2) the unknown age of the herein analysed sediments (do they reflect sea ice conditions of the past decades or centuries?); and (3) the relatively poor data base (n = 39) and the scatter of data points within correlation charts, which entails a notable degree of uncertainty. We thus suggest that such a proxy-model calibration requires a larger biomarker dataset with a higher spatial distribution of sediment samples (ideally covering the whole Arctic Ocean). More IP_{25} studies on marine surface (and down-core) sediments from the Arctic realm will firstly provide for a validation of the P_BIP_{25} index and secondly provide for a valuable database to support (palaeo) model experiments. This would finally allow for a comparison of the herein included Middle Holocene sea ice model results (Fig. 20) with the respective Holocene sediment data. Once the reliability of this biomarker approach has been

verified through further investigations it may enable for a quantitative assessment of sea ice concentrations and thicknesses.

Nonetheless, we consider this direct (and first) intercomparison of proxy- and model-based sea ice estimates an encouraging attempt that provides a new perspective on the use of a PIP_{25} index as quantitative means for sea ice reconstructions.

4.5 Conclusions

With the consideration of the sea ice proxy IP_{25} and biomarkers derived from open-water phytoplankton (i.e., brassicasterol, dinosterol, and short-chain *n*-alkanes) we gain useful information about the occurrence, the spatial and lateral extent, and the environmental impact of sea ice (e.g. where primary productivity is either stimulated or lowered due to the ice cover) in the northern North Atlantic. The coupling of IP_{25} with phytoplankton biomarkers such as brassicasterol (P_BIP_{25} index) proves to be a viable approach to determine (spring/summer) sea ice conditions as is demonstrated by the good alignment of the P_BIP_{25}-based estimate of the recent sea ice coverage with satellite observations. Modern sea ice concentrations as derived from the high-resolution ocean-sea ice model are in good agreement with the satellite data as well. The capability of the IP_{25} proxy (in combination with a phytoplankton marker) on the one hand and the NAOSIM model on the other hand to satisfactorily trace and reproduce sea ice conditions encourages a cross-evaluation of both approaches. As we observe good correlations between P_BIP_{25} values and model data, the establishment of a proxy-model calibration (in terms of transfer functions) appears feasible. More extensive IP_{25} data, however, are a needed prerequisite to verify this approach towards a quantitative sea ice assessment. Putting IP_{25} on the agenda of further biomarker studies hence will provide for a valuable database and support model experiments to describe past and, probably even more demanded, also future sea ice variations in the Arctic realm.

Biomarker data are available at doi:10.1594/PANGAEA.759566.

Acknowledgments

Kai Mangelsdorf and Cornelia Karger (GFZ-Potsdam, Germany) are kindly acknowledged for auxiliary GC-MS analyses. Special thanks go to Silvio Engelmann (TU-Berlin, Germany) for help on GIS-data processing and to Frank Kauker and Michael Karcher (AWI-Bremerhaven, Germany) for support in the set up of NAOSIM. Financial support was provided by the Deutsche Forschungsgemeinschaft, through SPP INTERDYNAMIK (STE 412/24-1, LO 895/13-1 and PR 1050/3-1). We also thank the anonymous reviewers for their constructive comments on the manuscript.

5. Holocene cooling culminates in Neoglacial sea ice oscillations in Fram Strait

Juliane Müller [a], Kirstin Werner [b], Ruediger Stein [a], Kirsten Fahl [a], Matthias Moros [c], Eystein Jansen [d]

[a] Alfred Wegener Institute for Polar and Marine Research, 27568 Bremerhaven,Germany
[b] IfM-GEOMAR, 24148 Kiel, Germany
[c] Leibniz Institute for Baltic Sea Research, IOW, 18119 Rostock, Germany
[d] Bjerknes Centre for Climate Research, University of Bergen, Norway

Under review with Quaternary Science Reviews (since September 2011).

Abstract

A reconstruction of Holocene sea ice conditions in the Fram Strait provides insight into the palaeoenvironmental and palaeoceanographic development of this climate sensitive area during the past 8,500 years BP. Organic geochemical analyses of sediment cores from eastern and western Fram Strait enable the identification of variations in the ice coverage that can be linked to changes in the oceanic (and atmospheric) circulation system. By means of the sea ice proxy IP_{25}, phytoplankton derived biomarkers and ice rafted detritus (IRD) increasing sea ice occurrences are traced along the western continental margin of Spitsbergen throughout the Holocene, which supports previous palaeoenvironmental reconstructions that document a general cooling. A further significant ice advance during the Neoglacial is accompanied by distinct sea ice fluctuations, which point to short-term perturbations in either the Atlantic Water advection or Arctic Water outflow at this site. At the continental shelf of East Greenland, the general Holocene cooling, however, seems to be less pronounced and sea ice conditions remained rather stable. Here, a major Neoglacial increase in sea ice coverage did not occur before 1,000 years BP. Phytoplankton-IP_{25} indices ("PIP_{25}-Index") are used for more explicit sea ice estimates and display a Mid Holocene shift from a minor sea ice coverage to stable ice margin conditions in eastern Fram Strait, while the inner East Greenland shelf experienced less severe to marginal sea ice occurrences throughout the entire Holocene.

5.1 Introduction

The extent of sea ice coverage in Fram Strait, the major gateway connecting the Arctic with the Atlantic Ocean, is intrinsically tied to the advection of warm Atlantic Water along the

continental margin of West Spitsbergen. As these temperate waters head to the north, they encounter polar water (and air) and sea ice from the Arctic Ocean, which causes cooling, brine rejection and subsequent descent of Atlantic Water into the Nordic Sea's deep sea basins via the Greenland Sea Gyre (Fig. 23; Aagaard, 1982; Rudels and Quadfasel, 1991; Watson et al., 1999). These processes are of crucial importance for the so-called Nordic heat pump, which bestows a comparatively temperate climate upon Europe (e.g. Broecker, 1992). The finding of past variations in the sea ice distribution in Fram Strait thus supports the identification of palaeo-fluctuations in the intensity of Atlantic Water inflow and may reveal periods of a strengthened or weakened thermohaline circulation and/or atmospheric (North Atlantic Oscillation; NAO-like) forcing. The influence of the NAO on climate and sea ice conditions in the (sub)Arctic realm frequently has been appraised as fundamental, though hardly assessable or predictable due to its highly variable temporal evolution (e.g. Dickson, 2000; Hurrell and Deser, 2010). In short, positive NAO phases are accompanied by stronger westerlies carrying moist air over Europe and Siberia, an increased Atlantic Water inflow through Fram Strait, and warmer temperatures in the Arctic, which lead to a reduction in sea ice formation. During intervals of a negative NAO these phenomena occur to be reversed (Dickson, 2000; Hurrell and Deser, 2010; Kwok, 2000).

Though Northern Hemisphere climate (boundary) conditions throughout the Holocene are generally considered as fairly stable (Grootes and Stuiver, 1997), variations in sea surface temperatures, glacier growth or terrestrial vegetation communities are increasingly substantiated within marine and terrestrial Arctic palaeoclimate studies (Andersen et al., 2004; Birks, 1991; Svendsen and Mangerud, 1997; for recent review see Miller et al., 2010). Changes in sea ice conditions, however, have been deduced mainly indirectly from microfossil or geochemical data (Andrews et al., 2001; Bonnet et al., 2010; Jennings et al., 2002). In 2009, Vare et al. and Müller et al. presented reconstructions of Holocene sea ice conditions for the central Canadian Archipelago and northern Fram Strait, respectively, based on the molecular sea ice proxy IP_{25} - a highly branched isoprenoid associated with sea ice diatoms (Belt et al., 2007; Brown et al., in press). Both studies suggest gradually increasing (spring) sea ice occurrences from the Mid to the Late Holocene, presumably as a response to the Neoglacial cooling (Müller et al., 2009), but do not provide an in-depth analysis of the palaeoenvironmental and palaeoceanographic setting. Main object of this study hence is to estimate to what extent this Holocene cooling affected the sea ice distribution in the subpolar North Atlantic. For this purpose, organic geochemical and IRD analyses were performed on sediment cores from the western continental margin of

Spitsbergen and the continental shelf of East Greenland. This provides for a reconstruction of the spatial and temporal evolution of the sea ice coverage within the two most important oceanic (in and outlet) pathways that characterise the Fram Strait and influence the Arctic Ocean heat budget. The findings are compared and contextualised with previous palaeoenvironmental reconstructions for the study area.

5.2 Regional Setting

The environmental setting in Fram Strait is controlled by a dynamic ocean current system and, owing to the high latitude, a distinct seasonality.

Warm and saline Atlantic is directed towards northern Fram Strait by the Norwegian Current (NC) and the West Spitsbergen Current (WSC), thus constituting the northernmost area of open (ice-free) water in the Arctic during winter (Fig. 23; Aagaard, 1982; Vinje, 1977). South of Spitsbergen these temperate waters encounter cold water and sea ice, which is carried by the minor Sørkapp Current (SC) from the Barents Sea along the southern tip and west coast of Spitsbergen (Swerpel, 1985).

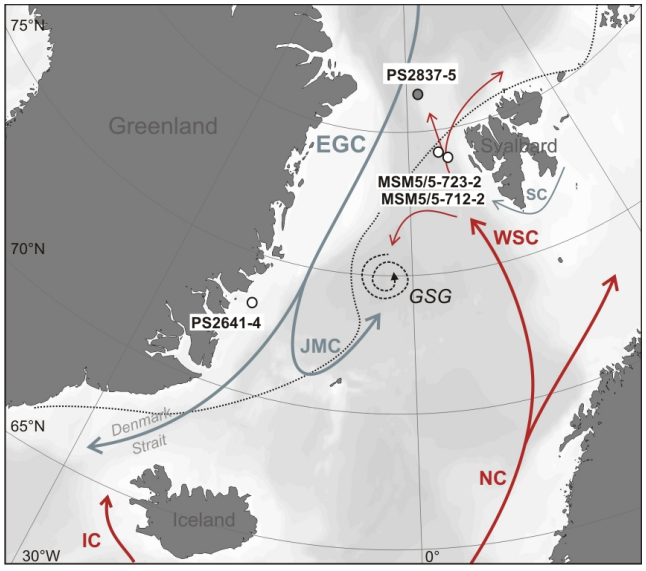

Fig. 23: Oceanographic setting and location of core sites in the study area. Red arrows refer to warm Atlantic water carried by the Norwegian Current (NC), the Irminger Current (IC), and the West Spitsbergen Current (WSC). Blue arrows refer to polar water and sea ice carried by the East Greenland Current (EGC), the Jan Mayen Current (JMC) and the minor Sørkapp Current (SC). The Greenland Sea Gyre (GSG) and the modern winter sea ice margin (dotted line) are indicated as well.

Further to the north at about 79°N, the WSC splits in two current systems, with an eastern (Svalbard) branch flowing along the northeastern shelf of Spitsbergen and a western (Yermak) branch following the western flank of the Yermak Plateau where it is partly recirculated southward (Fig. 23; Bourke et al., 1988).

The western part of Fram Strait experiences a huge discharge of polar water and sea ice that originates from the Arctic Ocean (i.e. predominantly from the East Siberian and the Laptev Sea) and is exported along the continental shelf of East Greenland by the East Greenland Current (EGC; Aagaard and Coachman, 1968; Rudels et al., 1999). Currently,

only the proximal (inner) shelf of East Greenland and northern Fram Strait remain ice-covered until early summer (NSIDC, Boulder, USA). During periods of extreme cold winter (and spring) months with severe temperature and sea ice conditions in the Arctic, the ice flux may extend towards the east (and south), such that also the eastern part of Fram Strait experiences an intensified (drift) sea ice coverage (for association with NAO variability see Dickson, 2000; Vinje, 2001a). This is also substantiated through IRD studies of sediment trap material from the continental slope of West Spitsbergen by Hebbeln (2000), who shows that fine-grained lithic material may be released from sea ice originating not only from Spitsbergen but also from the north (i.e. the Arctic Ocean).

5.3 Sediment material and methodology

The sediment cores MSM5/5-712-2 and MSM5/5-723-2 were obtained from the western continental margin of Spitsbergen (at 78°54.94 N, 6°46.03 E; 1487 m water depth, and at 79°09.66 N, 5°20.27 E; 1349 m water depth, respectively) during a *Maria S. Merian* cruise in 2007 (Budéus, 2007). The core sites are both located in close vicinity to the modern winter sea ice margin (Fig. 23). Sediment cores were stored at -30°C until further treatment. For organic geochemical analyses subsamples were taken each cm, freeze-dried and homogenized. Sedimentary total organic carbon (TOC) contents were determined by means of a carbon-sulfur determinator (CS-125, Leco) after the removal of carbonates by adding hydrochloric acid. Total carbon (TC) contents measured by a CNS analyser (Elementar III, Vario) were used to calculate carbonate contents ($CaCO_3$ = (TC-TOC) x 8.333). Core MSM5/5-712-2 was further studied for ice rafted detritus (IRD). Lithic grains of freeze-dried subsamples were counted on a representative split (> 100 grains) in the 150-250 μm size fraction.

Sediment core PS2641-4 from the East Greenland shelf (73°9.3 N, 19°28.9 W; 469 m water depth) was obtained during *Polarstern* cruise ARK-X-/2 (Hubberten, 1995). TC and TOC (and thus also carbonate) contents of freeze-dried and homogenised subsamples (5 to 10 cm sampling intervals) from this core were determined by means of a Heraeus CHN-O-Rapid Elementar Analyser. We note that the freeze-dried sediment material was stored at room temperature for ca. 15 years before it was analysed for its biomarker composition. This probably promoted some chemical alteration of the organic matter, which needs to be considered when looking at the absolute concentration profiles of the biomarkers.

For lipid biomarker analyses ca. 1 - 4 g of sediment were extracted by an Accelerated Solvent Extractor (DIONEX, ASE 200; 100°C, 5 min, 1000 psi) using

dichloromethane:methanol (2:1 v/v). Prior to this step, 7-hexylnonadecane, squalane and cholesterol-d6 (cholest-5-en-3β-ol-D6) were added as internal standards for quantification purposes. Further separation of alkanes and sterols was carried out via open-column chromatography using SiO_2 as stationary phase. Hydrocarbons were eluted with *n*-hexane (5 ml) and sterols with methylacetate:*n*-hexane (20:80 v/v; 6 ml). The latter were silylated with 500 µl BSTFA (60 °C, 2 hrs). Compound analyses of both fractions were carried out on an Agilent 6850 GC (30 m HP-5MS column, 0.25 mm i.d., 0.25 µm film thickness) coupled to an Agilent 5975 C VL mass selective detector. The GC oven was heated from 60 °C to 150 °C at 15 °C min^{-1}, and then at 10 °C min^{-1} to 320 °C (held 15 min) for the analysis of alkanes and at 3 °C min^{-1} to 320 °C (held 20 min) for sterols, respectively. Operating conditions for the mass spectrometer were 70 eV and 230 °C (ion source). Helium was used as carrier gas. The identification of individual biomarkers is based upon comparison of their retention times and mass spectra with published data (Belt et al., 2007; Boon et al., 1979; Volkman, 1986). Biomarker concentrations were calculated on the basis of their individual GC-MS ion responses compared with those of respective internal standards. For the quantification of IP_{25} a calibration factor was considered that was obtained from calibration experiments using a sediment with known IP_{25} concentration (for further details see Müller et al., 2011). Within this study hydrocarbon fractions from sediment core PS2837-5 (Müller et al., 2009) were re-analysed and their IP_{25} contents accordingly calibrated, which eases the comparison with the results obtained from core PS2641-4 and the *Maria S. Merian* cores.

5.4 Core chronologies

The chronology of the sediment cores MSM5/5-712-2 and MSM5/5-723-2 is based upon AMS ^{14}C ages obtained from tests of the polar planktic foraminifer *Neogloboquadrina pachyderma* (sin.), whereas the age model of the sediment core PS2641-4 is based upon AMS ^{14}C ages that were obtained from tests of benthic foraminifera. Additionally, AMS ^{14}C ages were derived from shells of the bivalve *Bathyarca glacialis* (Evans et al., 2002). For the *Maria S. Merian* cores a marine reservoir correction of 408 years has been assumed to convert radiocarbon ages into calibrated calendar years before present (cal. years BP) using the calibration software CALIB 6 (see table 2; Stuiver and Reimer, 1993; Stuiver et al., 1998; updated to CALIB 6.0 by Stuiver et al., 2005; see CALIB at http://calib.qub.ac.uk/). A reservoir age of 550 years has been assumed for the correction of radiocarbon ages of the PS2641-4 core according to Hjort (1973). For the age model of this core we omitted one ^{14}C

age at 90.5 cm (1705 ± 110 = 1091 cal. years BP) because this sample contained only a very little amount of carbon (0.06 mg).

Sediment core	Lab reference	Core depth (cm)	AMS ^{14}C age	Calibrated age BP (2 σ)
MSM5/5-712-2	KIA 45217[1]	11	815 ± 25	459 ± 49.5
	KIA 41024[1]	21	1570 ± 25	1130 ± 82.5
	KIA 45218[1]	28	1985 ± 25	1544 ± 96.5
	KIA 45219[1]	41	2565 ± 25	2242 ± 83
	SacA 19113[2]	60.5	3365 ± 30	3240 ± 97.5
	SacA 19114[2]	94.5	4915 ± 30	5256 ± 104
	SacA 19115[2]	139	6440 ± 30	6927 ± 106.7
	KIA 38080[1]	169	7305 ± 35	7767 ± 93.5
	KIA 41025[1]	192	7815 ± 45	8285 ± 97
MSM5/5-723-2	KIA 38738[3]	11.5	675 ± 25	319 ± 68
	KIA 38700[3]	51.5	2125 ± 25	1714 ± 93
	KIA 43851[3]	102.5	3820 ± 30	3769 ± 99
	KIA 38739[3]	131.5	4950 ± 35	5294 ± 119
	KIA 43853[3]	181	6120 ± 40	6545 ± 108
	KIA 38740[3]	231.5	7290 ± 40	7752 ± 98
PS2641-4	LuS 8471	20	995 ± 60	451 ± 139
	LuS 9500	43	1240 ± 90	644 ± 182
	LuS 8469	58	1645 ± 60	1033 ± 176.5
	LuS 9124	90.5	1705 ± 110	1091 ± 247
	LuS 9125	128	2835 ± 100	2382 ± 296.5
	LuS 9502	181.5	3775 ± 150	3519 ± 407
	LuS 8468	230	4625 ± 60	4640 ± 198
	LuS 8470	261.5	5400 ± 60	5598 ± 192
	AAR-2422*	375	6980 ± 130	7327 ± 278.5
	AAR-2688*	413	7600 ± 70	7893 ± 196
	LuS 8467	461.5	8415 ± 80	8783 ± 256.5

Table 2: AMS radiocarbon ages for *Maria S. Merian* cores obtained from tests of the planktic foraminifer *Neogloboquadrina pachyderma* sin. For these dates a marine reservoir age of 408 years has been assumed according to Hughen et al. (2004). AMS radiocarbon ages for the *Polarstern* core were obtained from tests of mixed benthic foraminifera. In addition, two AMS ^{14}C dates (labelled with a star) determined in shells of the bivalve *Bathyarca glacialis* (Evans et al., 2002) were used. For radiocarbon ages of this core a reservoir age of 550 years has been assumed according to Hjort (1973). The age obtained from benthic foraminifera at 90.5 cm sediment depth in PS2641-4 has been ignored for the calculation of the age model. Superscript numbers in the lab reference indicate ^{14}C dates provided by Robert Spielhagen (1), Jacques Giraudeau (2), and Christian Hass (3).

Furthermore, this dating would imply an enormous sedimentation rate (> 500 cm/1,000 years) compared to the adjacent intervals (< 50 cm/1,000 years). Such an "event" of extreme sediment deposition, however, cannot be identified in the sediment structures of the respective core section. Anticipating linear sedimentation rates at the core sites, ages of sediment intervals between ^{14}C-dated horizons are based on linear interpolation (Fig. 24). Mass accumulation rates (g/cm^2/1,000 years) were calculated on the base of these sedimentation rates, density and porosity data (Evans, 2000), and were finally used to convert absolute sedimentary biomarker contents into flux rates.

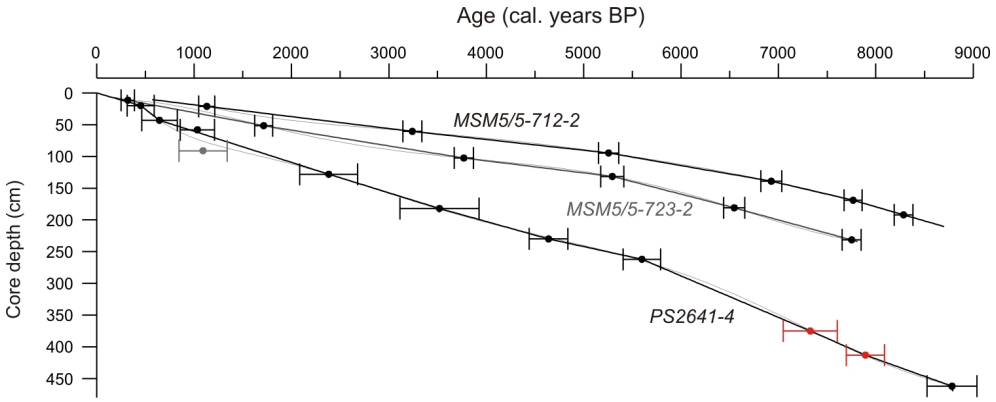

Fig. 24: Age model for sediment cores MSM5/5-712-2, MSM5/5-723-2, and PS2641-4 (thin grey lines refer to 5- and 7-point polynomial fits, respectively). Reservoir corrected and calibrated ^{14}C ages with respective error bars are indicated for each age-depth correlation. Red ^{14}C ages were determined on shells of the bivalve *Bathyarca glacialis* (Evans et al., 2002). ^{14}C age at 90.5 cm core depth is not included in the age model of PS2641-4.

5.5 Results

5.5.1 West Spitsbergen continental margin (cores MSM5/5-712-2 and MSM5/5-723-2)

On the base of our organic-geochemical and IRD records the sedimentary sequence of core MSM5/5-712-2 can be separated into three intervals covering the past 8,500 years BP (Fig. 25). Results obtained on core *MSM5/5-723-2* cover the past 7,000 years BP (Fig. 26).

In core MSM5/5-712-2 the late Early Holocene (8,500 - 7,000 years BP) is characterised by lowest IRD counts (< 20 grains per gram sediment), reduced TOC (0.8 - 1 wt.%) and moderate to maximum $CaCO_3$ contents (10 - 16 wt.%). Accumulation of phytoplankton-derived biomarkers (dinosterol and brassicasterol; Boon et al., 1979; Volkman et al., 1998) is at its maximum during this interval, whilst the accumulation of the sea ice proxy IP_{25} becomes significantly reduced after 8,300 years BP (Fig. 25). Within this period, at about 8,200 years BP, a short-term increase in the IRD content coincides with minimum TOC values and lowered phytoplankton biomarker flux rates. Meanwhile, an abrupt decline in previously high IP_{25} values is observed between 8,300 and 8,100 years BP. Further short-term lows in brassicasterol and dinosterol accumulation rates at 7,600 and at 7,100 years BP are not reflected in the IRD, TOC, or IP_{25} data (Fig. 25). Maximum $CaCO_3$ contents peak at about 7,400 years BP.

During the Mid Holocene (7,000 - 3,000 years BP), TOC contents of both *Maria S. Merian* cores reach slightly elevated values (ca. 1 wt.% in MSM-5/5-712-2; ca. 1.2 wt.% in MSM5/5-723-2) between 6,400 and 5,800 years BP and between 4,200 and 3,400 years BP (Figs. 25 and 26). $CaCO_3$ contents of both cores decrease and maintain at minimum values (8 - 12 wt.%). Continuously decreasing accumulation rates of phytoplankton biomarkers in

core MSM5/5-712-2, however, are associated with consistently rising IP_{25} and IRD contents throughout this period (Fig. 25). Considerable dinosterol minima occur at about 5,000 and 3,200 years BP. The IP_{25} record of core MSM5/5-723-2 shows that a period of slightly higher IP_{25} flux rates between ca. 6,200 and 5,200 years BP is followed by an IP_{25} minimum at about 5,000 years BP (Fig. 26). Thereafter, a gradual increase in the accumulation of IP_{25} is observed for the Mid Holocene.

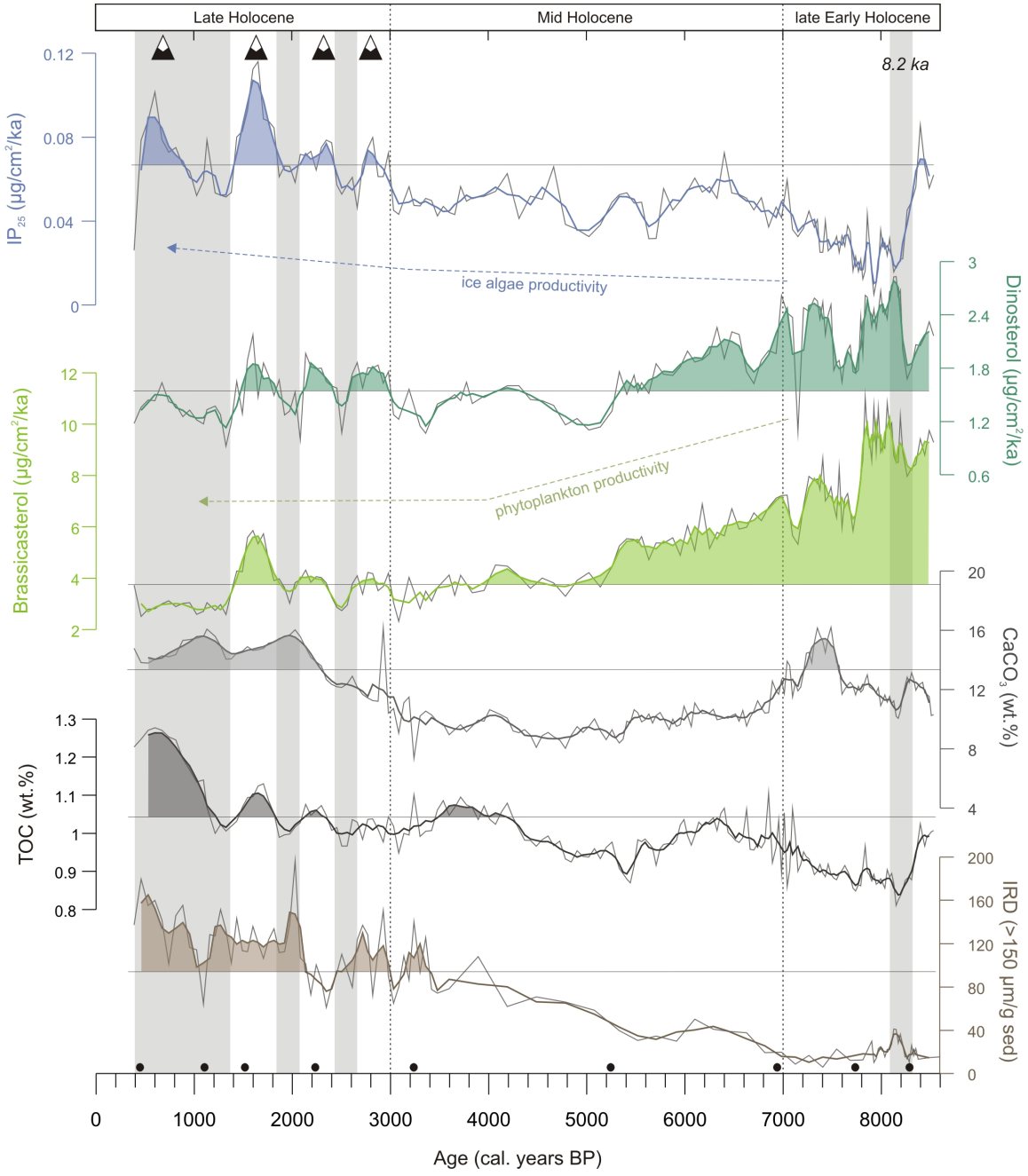

Fig. 25: IRD, TOC, and $CaCO_3$ contents and biomarker accumulation rates of sediment core MSM5/5-712-2. Bold curves represent 5-point smoothed averages. Curve fillings highlight maximum values (thresholds are chosen arbitrarily). Grey vertical bars indicate cooling intervals. Black-white triangles denote glacier advances on Spitsbergen (Svendsen and Mangerud, 1997). Black dots refer to AMS datings.

The Late Holocene (3,000 - 300 years BP) is marked by further increasing TOC and $CaCO_3$ contents in both sediment cores (Figs. 25 and 26). The IRD content in core MSM5/5-712-2 increases as well and reaches maximum values at ca. 500 years BP (> 160 grains per gram sediment; Fig. 25). We note that the accumulation of biomarkers in this core is highly variable throughout the past 3,000 years (Fig. 25), whereas the increase in IP_{25} at core site MSM5/5-723-2 occurs to be rather gradual and maximum values are reached at about 300 years BP (Fig. 26). In core MSM5/5-712-2 we observe that during intervals of an elevated IP_{25} accumulation at ca. 2,800, 2,300 and 1,600 years BP, the flux rates of brassicasterol and dinosterol and also the TOC contents are increased as well (Fig. 25). Vice versa, intermediate periods of lowered IP_{25} accumulation correspond to periods of reduced phytoplankton marker contents. Divergent from these in-phase fluctuations, we find minimum phytoplankton marker flux rates that coincide with the youngest IP_{25} peak at about 500 years BP (Fig. 25). The TOC content, however, reaches maximum values at this time.

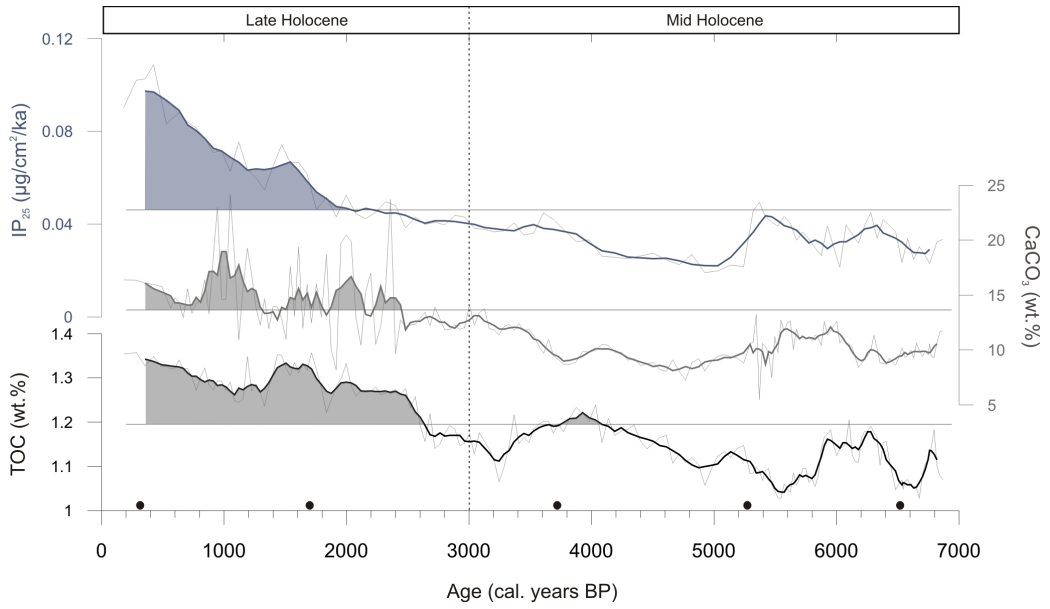

Fig. 26: TOC and $CaCO_3$ contents and IP_{25} accumulation rates of sediment core MSM5/5-723-2. Bold curves represent 5-point smoothed averages. Curve fillings highlight maximum values (thresholds are chosen arbitrarily). Black dots refer to AMS datings.

5.5.2 Inner East Greenland shelf (core PS2641-4)

In comparison with the data from core MSM5/5-712-2, we obtained rather monotonous TOC and $CaCO_3$ records from the Holocene section of core PS2641-4 (Fig. 27). TOC contents of 0.8 to 1.3 wt.% remain relatively stable and only a slight long-term increase is observed during the Mid to Late Holocene. Notably low $CaCO_3$ contents (0.3 - 1.6 wt.%) contrast those of the sediment cores from the West Spitsbergen slope, and refer to the shift

from an Atlantic Water influenced to an EGC dominated sea surface within Fram Strait (Hebbeln and Berner, 1993; Henrich, 1998; Huber et al., 2000). We note that the accumulation rates of biomarkers (in particular of IP_{25}) are significantly higher at core site PS2641-4 than at the West Spitsbergen margin, which probably can be attributed to the basically higher mass accumulation at the East Greenland shelf due to ice rafting.

The late Early Holocene (8,500 - 7,000 years BP) is characterised by highest $CaCO_3$ contents and elevated phytoplankton marker flux rates, whereas the accumulation of IP_{25} fluctuates from minimum to moderate values (Fig. 27). The most remarkable feature of the biomarker distribution of this core is a lack of dinosterol and brassicasterol between 7,900 and 7,400 years BP. This interval seems to interrupt the late Early Holocene section of relatively high phytoplankton marker contents (Fig. 27).

During the Mid Holocene (7,000 - 3,000 years BP), the accumulation of phytoplankton biomarkers decreases until ca. 5,300 years BP and thereafter increases again. Meanwhile, the IP_{25} flux rate first peaks at about 6,000 years BP, then decreases and maintains relatively low values between 5,200 and 2,300 years BP.

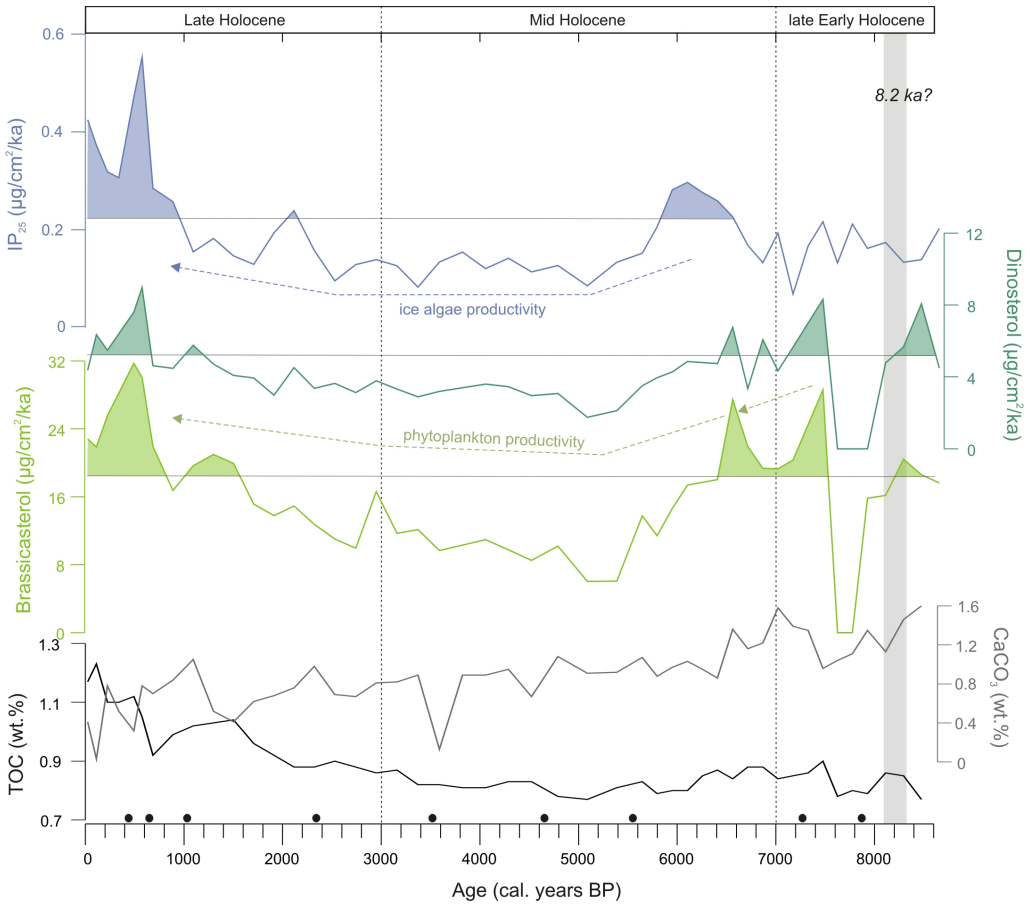

Fig. 27: TOC and $CaCO_3$ contents and biomarker accumulation rates of sediment core PS2641-4. Curve fillings highlight maximum values (thresholds are chosen arbitrarily). Black dots refer to AMS dating points.

For the Late Holocene, we note an increasing accumulation of brassicasterol, dinosterol, and particularly of IP_{25} since ca. 3,000 years BP (Fig. 27). The phytoplankton markers even reach highest values alike during the late Early and early Mid Holocene. Considerable maxima in all biomarker records and also TOC contents are observed for the past 1,000 years BP. $CaCO_3$ contents, in contrast, become successively reduced during the past 1,000 years BP.

5.6 Discussion

With the identification of the sea ice biomarker IP_{25} in the sediment cores MSM5/5-712-2, MSM5/5-723-2, and PS2641-4 we yield novel and direct information about the development of the sea ice conditions along the West Spitsbergen continental margin and the continental shelf of East Greenland throughout the Holocene (Fig. 28).

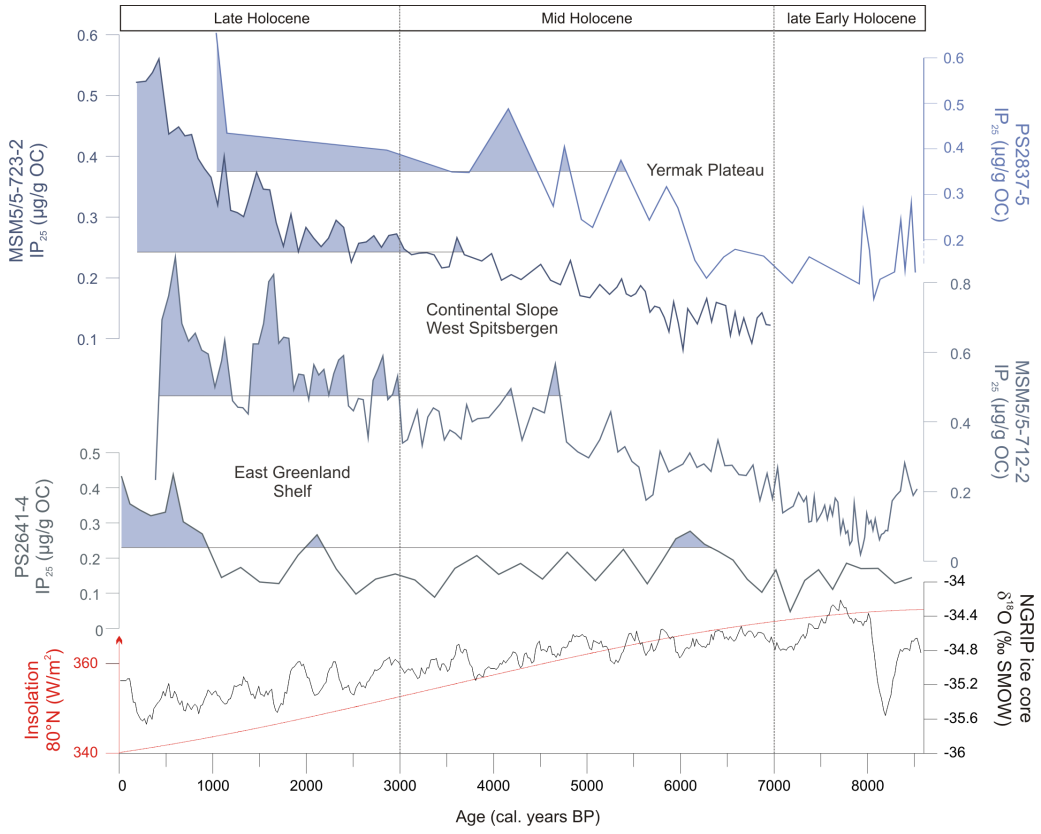

Fig. 28: Comparison of IP_{25} concentrations of sediment cores from northern, eastern, and western Fram Strait. Summer insolation for 80°N (red curve) taken from Laskar et al., 2004 and $\delta^{18}O$ values from the NGRIP ice core (NGRIP Members, 2004) strengthen a Holocene cooling.

In agreement with the sustained cooling, which is inferred from decreasing $\delta^{18}O$ values in the NGRIP Greenland ice core (NGRIP-Members, 2004) and a decline in Northern Hemisphere insolation (Laskar et al., 2004), a gradual increase in IP_{25} concentrations is

observed in the *Maria S. Merian* cores and also in core PS2837-5 located on the Yermak Plateau close to the modern summer sea ice margin (Müller et al., 2009). This points to a successive (spatial and temporal) extension of the spring sea ice coverage in eastern Fram Strait - possibly due to a lowered sea surface temperature (SST). IP_{25} concentrations in core PS2641-4 remain, within a certain range of variability, relatively constant throughout the Holocene and a notable increase did not occur before 1,000 years BP (Fig. 28). We thus suggest that the export of Arctic sea ice towards this core site possibly continued throughout the Holocene but did not experience significant changes that could be traced in sediments from the inner shelf of East Greenland.

5.6.1 The late Early Holocene (8,500 - 7,000 years BP)

Based on the high phytoplankton biomarker and minimum IP_{25} flux rates in core MSM5/5-712-2 comparatively warm sea surface conditions along the West Spitsbergen shelf can be assumed for the late Early Holocene (Fig. 25). This is also supported by the relatively high (even maximum) $CaCO_3$ contents reflecting a higher productivity of calcareous walled organisms (e.g. foraminifers, coccoliths). We suggest that this interval represents the latest phase of the Holocene Climate Optimum in eastern Fram Strait and consider that in addition to higher insolation values an intensified Atlantic Water inflow likely supported phytoplankton growth, whereas the (spring) sea ice margin was located further northward (i.e., the core site experienced only minor sea ice occurrences during the late winter/early spring months). This aligns with maximum SSTs reconstructed for the western continental margin of the Barents Sea by Sarnthein et al. (2003) and findings of Salvigsen et al. (1992), who report optimum climate conditions for thermophilous molluscs on western Svalbard for the period between 8,700 to 7,700 years BP. Likewise, foraminifer-based reconstructions of ocean circulation changes along the West Spitsbergen shelf by Slubowska-Woldengen et al. (2008) reveal a strengthened inflow of Atlantic Water at that time.

The abrupt reductions in the phytoplankton marker contents of core MSM5/5-712-2 at about 8,300, 7,600 and 7,100 years BP that punctuate the late Early Holocene probably point to short-term deteriorations of the sea surface conditions. Since the decline at ca. 8,200 years BP - a prominent cooling event in the High Latitudes (Alley et al., 1997; Clarke et al., 2004; Kleiven et al., 2008) - coincides with a (somewhat retarded) minor short-term increase in IRD and a rapid decrease of previously high IP_{25} contents, we assume that the core site was affected by a massive ice discharge that reduced not only the growth of phytoplankton but also that of ice algae. This agrees with significantly reduced SSTs along the Barents Sea margin for this period (Sarnthein et al., 2003). Similarly, Müller et al. (2009)

interpreted minimum fluxes of IP_{25} and brassicasterol as indicative for a near-perennial sea ice cover in northern Fram Strait at about 8,200 years BP.

Relatively warm conditions probably also prevailed in western Fram Strait during the late Early Holocene since at core site PS2641-4 accumulation rates are relatively high for dinosterol and brassicasterol, and only moderate for IP_{25} (Fig. 27), which may point to a reduced (not absent) ice cover at the East Greenland shelf. Similarly, e.g. Bauch et al. (2001) and Andersen et al. (2004) reconstruct rather warm sea surface conditions in the central Nordic Seas and at the East Greenland shelf for the late Early Holocene by means of foraminifer and diatom assemblages. This period likely corresponds to the recession of the Greenland ice sheet from the inner shelf as is reconstructed by Evans et al. (2002) on base of sediment lithology and $\delta^{18}O$ data from core PS2641-4. The sudden lack of the phytoplankton markers between 7,900 and 7,600 years BP could point to a short-term deterioration in sea surface conditions, which is not reflected in the IP_{25} contents (Fig. 27). Increased meltwater discharge from the adjacent Kejser Franz Joseph Fjord could have caused a strong stratification of the upper water layer, thus reducing the ventilation and availability of nutrients required for phytoplankton growth.

5.6.2 The Middle Holocene (7,000 - 3,000 years BP)

Lowered $CaCO_3$ contents, continuously decreasing accumulation rates of phytoplankton markers and the sustained increase in IRD and IP_{25} contents in sediment core MSM5/5-712-2 (and MSM5/5-723-2) point to a gradually reduced phytoplankton productivity due to a cooling of the sea surface and a successive growth and extension of (winter/spring) sea ice at the continental slope of West Spitsbergen during the Mid Holocene. This is in well accordance with a concurrent increase in IRD contents of sediment cores along the West Spitsbergen continental shelf and margin documented by Jessen et al. (2010) and Slubowska-Woldengen (2007), who assume a Mid Holocene ice advance. Decreasing SSTs off and enhanced glaciation on West Spitsbergen (Hald et al., 2004) support this interpretation. To what extent this Holocene cooling trend observed in the subpolar North Atlantic domain (e.g. Andersen et al., 2004; Hald et al., 2007; Miller et al., 2010) may be related to the lowered Northern Hemisphere insolation and/or a reduced Atlantic Water advection and/or changes in the atmospheric circulation remains disputable. A general recovery of the Arctic's sea ice after its significant recession during the Holocene Climate Optimum (see e.g. Polyak et al., 2010 for review), however, occurs as a plausible and natural response to the mitigation of orbital forcing. Sustained oceanic surface cooling that stimulated the sea ice

formation during winter and retarded its retreat/melt during the late spring and early summer months is also supported by e.g. Rasmussen et al. (2007) and Jennings et al. (2002) who reconstruct increasingly cooler conditions along the West Spitsbergen shelf and an increased sea ice export through Fram Strait by means of benthic and planktic foraminifera and IRD records. Furthermore, on base of e.g. increasing $\delta^{18}O$ values, increasing abundances of *N. pachyderma* (sin.) and diatom data, Rasmussen et al. (2007), Bauch et al. (2001) and Koç et al. (1993) strengthen that the southwestern continental margin of Spitsbergen and the Nordic Seas experienced an intensified water mass exchange with the Arctic Ocean for the period after 7,000 years BP and continuous surface cooling (in-step with the lowered insolation) since ca. 6,000 years BP. Reduced winter SSTs are also reconstructed for the western continental margin of the Barents Sea and have been related to a weakened heat input with the WSC and a strengthened East Spitsbergen (Sørkapp) Current leading to periods of extended sea ice coverage (Sarnthein et al., 2003).

Successively reduced phytoplankton marker contents in core PS2641-4 indicate that also the East Greenland shelf became gradually cooled since ca. 6,600 years BP (Fig. 27). A higher accumulation of IP_{25} around 6,000 years BP may point to a stronger discharge of sea ice via the EGC at this time. Similarly, Ran et al. (2006) interpret higher abundances of Arctic diatom taxa in a sediment core from the northern shelf of Iceland as indicative of a strengthening of the EGC between 6,800 and 5,500 years BP. The subsequent relatively low and uniform (i.e. with some minor fluctuations) IP_{25} and phytoplankton marker flux rates, however, suggest that largely constant sea ice conditions prevailed at the East Greenland shelf since 5,000 years BP. Recent reconstructions by Jennings et al. (2011) document that an intensified Irminger Current carried more warm Atlantic Water to Denmark Strait between 6,800 and 3,500 years BP. This could be related to a weakening of the EGC during this period, but is not reflected in the IP_{25} or phytoplankton marker data at our core site. Moros et al. (2006), in turn, observe a long-term trend of increasing drift ice export via the EGC towards the North Atlantic since the past 5,000 years. With respect to our biomarker data, we suggest that Mid Holocene variations in the strength or extent of the EGC, however, did not automatically alter the sea ice cover (and the IP_{25} sedimentation) at the inner shelf but rather could be traced at the outer shelf of East Greenland.

5.6.3 The Late Holocene (the past 3,000 years BP)

Maximum IRD release and a sustained increase in the accumulation of IP_{25} during the past 3,000 years - a period that is widely acknowledged as Neoglacial cooling phase (for recent

review see Miller et al., 2010) - point to intensified sea ice occurrences at the West Spitsbergen continental margin. Forwick and Vorren (2009) and Forwick et al. (2010) assume an enhanced formation of shore-fast sea ice and/or a permanent sea ice cover along the West Spitsbergen coast that trapped IRD laden icebergs within the Isfjorden system during the past ca. 4,000 years BP. Thus, the elevated IRD contents at core site MSM5/5-712-2 may suggest a transport of lithic grains by sea ice rather than by icebergs originating from Spitsbergen glaciers. Further reconstructions of gradually cooled sea surface temperatures, lowered productivity, and a higher polar water ouflow to the Nordic Seas during the past 3,000 years BP, however, support this general increase in sea ice coverage (Andersen et al., 2004; Andrews et al., 2001; Calvo et al., 2002; Jennings et al., 2011; Jennings et al., 2002; Koç et al., 1993).

We suggest that the in-phase fluctuations of IP_{25} and phytoplankton marker contents in core MSM5/5-712-2 (Fig. 25) can be attributed to periods of a rapidly advancing and retreating sea ice margin at this core site until ca. 1,200 years BP. Accordingly, the less variable though steadily rising accumulation of IP_{25} at core site MSM5/5-723-2 - ca. 40 km further to the north of core site MSM5/5-712-2 - relates to a continuously increasing ice coverage during the past 3,000 years BP. As marine primary productivity is demonstrably stimulated in the marginal ice zone (release of nutrients from the melting sea ice triggers the bloom of the phytoplankton algae in the proximity of the ice edge; Hebbeln and Wefer, 1991; Ramseier et al., 1999; Sakshaug, 2004; Smith et al., 1987), we conclude that the periods of peak IP_{25} and phytoplankton marker contents in core MSM5/5-712-2 at about 2,800, 2,300 and 1,600 years BP reflect beneficial living conditions at the ice edge for both sea ice algae and plankton thriving in open water (Müller et al., 2009; Müller et al., 2011). Interestingly, Svendsen and Mangerud (1997) report concurrent (with minor temporal shifts) periods of abrupt glacier advances on West Spitsbergen. Since glacier growth requires a higher winter precipitation (and the main moisture source for the Svalbard archipelago is the subpolar North Atlantic; Dickson, 2000; Humlum, 2005), we hence assume that these intervals of glacier advance (and ice edge conditions at the core site) may have been triggered by a temporarily strengthened WSC and/or changes in the atmospheric circulation pattern, which caused these recurrent northward retreats of the sea ice cover (Fig. 29). This is also supported by findings of Sarnthein et al. (2003) who identify two intervals of warmer SSTs at the western continental margin of the Barents Sea at about 2,200 and 1,700 years BP, which they attribute to short-term pulses of warm Atlantic Water advection. Intermediate periods of lowered IP_{25} and phytoplankton marker contents accordingly point

to a weakened WSC - weakened through a lowered heat and/or volume transport - and probably a broadened EGC that permitted sea ice advances beyond the core site (Fig. 29). Intensified sea ice advection via the Sørkapp Current is possible as well. Such a fluctuating ice margin (due to a variable Atlantic Water inflow) is also described in a recent study by Werner et al. (2011) on base of foraminifer and IRD data obtained from a box core that was recovered at the same core site.

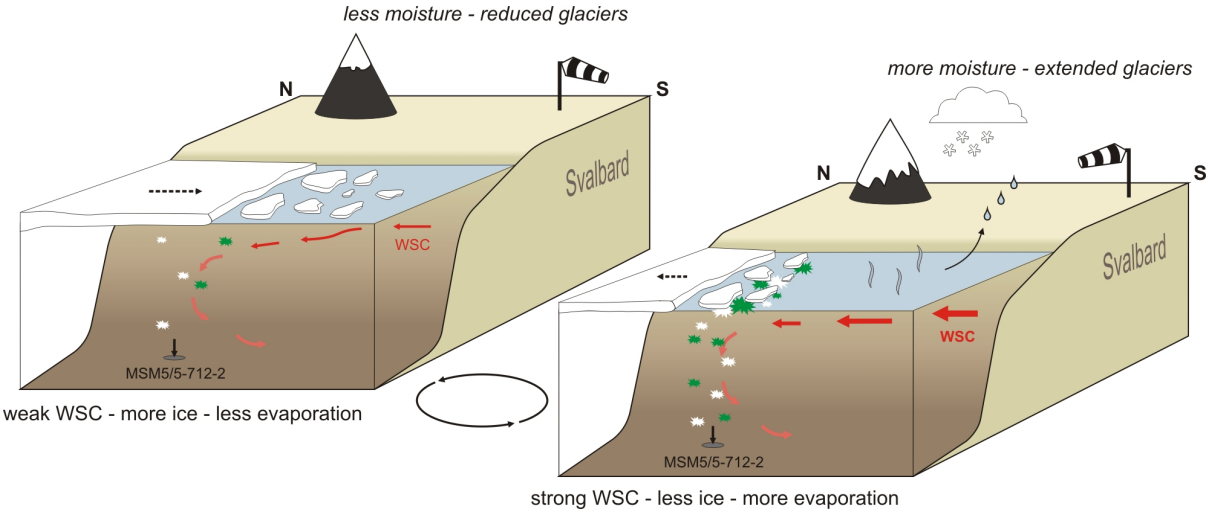

Fig. 29: Scheme illustrating periods of Neoglacial sea ice advance (left) and retreat (right) at the continental margin of West Spitsbergen due to variations in the inflow of warm Atlantic Water via the WSC and/or weakened/strengthened westerlies. Associated fluctuations in the productivity of ice algae (white patches) and phytoplankton (green patches) are indicated. Periods of ice retreat promote glacier growth on Spitsbergen due to an increased moisture supply from the sea.

The notably reduced accumulation of dinosterol and brassicasterol in core MSM5/5-712-2 during the past 1,300 years BP may indicate a deterioration of the sea surface conditions that limited the productivity of phytoplankton at the West Spitsbergen margin. Meanwhile increasing IP_{25} flux rates and highest IRD contents at about 600 years BP suggest an increase in sea ice coverage that also promoted the release of ice-rafted organic material, which could account for maximum TOC values. Maximum IP_{25} concentrations in sediment core MSM5/5-723-2 (Fig. 26) support this Neoglacial sea ice advance.

In contrast to the finding for eastern Fram Strait the Late Holocene increase in IP_{25} flux rates at the East Greenland shelf is accompanied by a continuously rising accumulation of brassicasterol and dinosterol (Fig. 27). Maximum fluxes of IP_{25} and phytoplankton biomarkers in core PS2641-4 point to favourable living conditions for both ice and phytoplankton algae at the East Greenland shelf during the past 1,000 years BP. Further reduced $CaCO_3$ contents in this core hence may be attributed to calcium carbonate

dissolution due to an increased formation of corrosive bottom waters linked to higher sea ice production and/or organic matter (originating from phytoplankton blooms) remineralisation (Steinsund and Hald, 1994). Alternatively, this reduction in $CaCO_3$ may indicate a shift of the provenance of ice rafted (carbonate) material. Highest IP_{25} contents determined for the past 1,000 years BP in all cores are tentatively attributable to the 'Little Ice Age' cooling that is also recorded in further marine (e.g. Andersson et al., 2003; Bendle and Rosell-Melé, 2007; Moros et al., 2006; Spielhagen et al., 2011) and also terrestrial archives from the subpolar North Atlantic (e.g. Nesje et al., 2001; Seppä and Birks, 2002). The occurrence of a broad and severe (i.e. perennial) sea ice cover during this period, however, is contradicted by the elevated phytoplankton marker contents in core PS2641-4. We hence conclude that during the past ca. 1,000 years BP, stable marginal ice zone conditions established at the inner East Greenland shelf, whereas eastern Fram Strait experienced an ice advance that reduced phytoplankton productivity.

With respect to the Late Holocene cooling that is observed at various sites in the subpolar North Atlantic and also in more remote areas, the hypothesis evolved that a continuous transition from a positive towards a negative NAO phase characterised the Holocene climate development (e.g. Andersen et al., 2004). Reduced Siberian river discharge during the past 2,000 years BP and vegetation changes in northeast European Russia, for example, are interpreted to reflect the development of a colder and dryer climate in the Eurasian Arctic and could be related to negative NAO-like conditions (Salonen et al., 2011; Stein et al., 2004). And also Jessen et al. (2011) relate changes in Late Holocene pollen records from southern Greenland and the Labrador Sea to a distinct reduction of south-westerly air masses in favour of colder air originating from the north and thus conclude that the atmospheric circulation pattern in the subpolar North Atlantic likely shifted from a more positive to a more negative NAO. Regarding the comparatively rapid sea ice oscillations at core site MSM5/5-712-2 between 3,000 and 1,200 years BP, we consider that a relationship between sea ice extent and oceanic-atmospheric (i.e. NAO-like) forcing fields, in fact, could explain the observed fluctuations. As no (instrumental) records of the long-term (centennial-to millennial-scale) development of the NAO are available (the first calculation of the NAO index dates back to 1932; Walker and Bliss, 1932), its influence on Late Holocene environmental conditions in the subpolar North Atlantic remains elusive. Shifting NAO conditions, however, could account for respective changes in the strength of westerly storm tracks and Atlantic Water advection to the continental margin of Spitsbergen (Dickson, 2000; Hurrell and Deser, 2009; Kwok and Rothrock, 1999). Previously, the observation of

fluctuating glacier extents in southwest Norway lead Nesje et al. (2001) to establish a relationship between Late Holocene glacier advances and positive NAO phases causing more humid and wet winter conditions over Scandinavia. Similarly, Giraudeau et al. (2010) credit both an increased advection of Atlantic Water into the Norwegian Sea and a coincidently strengthened polar outflow towards the western Nordic Seas to positive NAO intervals during the Late Holocene. Such a seesaw pattern between warm water input through eastern and cold water output via western Fram Strait, however, is not observed in our records. With general regard to the Holocene climatic development, we notice that the sea ice conditions at core site PS2641-4 obviously were less prone to variations in the strength of the oceanic (and atmospheric) circulation system than the sites in eastern Fram Strait. The rapid sea ice fluctuations reflected in the record of core MSM5/5-712-2 during the Neoglacial and the associated changes in the advection of warm (WSC) and polar (EGC) water masses are not fully traceable in the record of core PS2641-4. Due to its location in the vicinity of the Arctic and Atlantic oceanic (and atmospheric) fronts, core MSM5/5-712-2 apparently experienced more significant palaeoceanographic and -environmental changes, while the setting at the inner shelf of East Greenland remained relatively unaffected.

5.6.4 PIP_{25} index and sea ice estimate

We recently demonstrated that the coupling of the environmental (sea surface) information carried by IP_{25} and phytoplankton biomarkers by means of a phytoplankton-IP_{25} index (PIP_{25}) proves a valuable approach to reconstruct (spring) sea ice coverage more comprehensively (Müller et al., 2011). A distinct connection between the sea ice distribution and sedimentary IP_{25} and phytoplankton marker contents is strengthened through correlation analyses of PIP_{25} indices determined on surface sediments from the subpolar North Atlantic with sea ice concentrations derived from satellite and modelling data (Müller et al., 2011). According to the respective phytoplankton biomarker used for the calculation (brassicasterol or dinosterol), this index is specified as P_BIP_{25} or P_DIP_{25}, respectively. Highest PIP_{25} (P_BIP_{25} and P_DIP_{25}) values in the range of 0.75 to 1 seem to reflect extended ice coverage throughout spring and summer, whilst minimum values refer to predominantly ice-free (spring/summer) sea surface conditions. Intermediate values (0.5 - 0.75) characterise sites within the productive marginal ice zone.

Throughout the past 8,000 years BP, P_BIP_{25} and P_DIP_{25} indices calculated for core MSM5/5-712-2 sediments successively rise (Fig. 30) and thus point to a gradual increase in (spring) sea ice coverage at the West Spitsbergen continental margin. Minimum and close to

zero values denote a period of significantly reduced ice cover between 8,200 and 7,800 years BP. With reference to the findings of Müller et al. (2011) these values may refer to a sea ice concentration of less than 20%. Given the infancy of this approach, this interpretation of P_BIP_{25} and P_DIP_{25} values in terms of sea ice concentrations, however, needs to be considered as a very rough estimate. A sustained increase in sea ice occurrences at the core site is reflected by further rising P_BIP_{25} and P_DIP_{25} values, which finally pass the "threshold level" of 0.5 designating marginal ice zone conditions from ca. 4,800 years BP on. Maximum P_BIP_{25} values determined for the past ca. 1,000 years are in the range of 0.75 to 0.80 and thus indicate a shift towards severe ice coverage (presumably > 70% ice concentration).

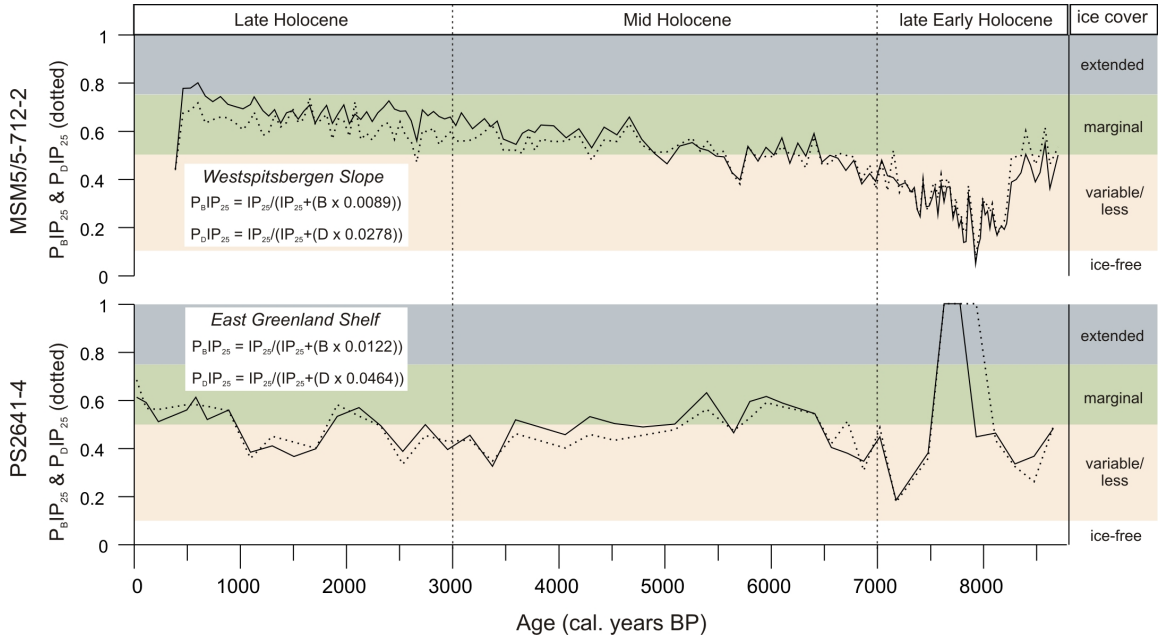

Fig. 30: P_BIP_{25} and P_DIP_{25} indices calculated for sediment cores MSM5/5-712-2 (top) and PS2641-4 (bottom). Indices were calculated using IP_{25}, brassicasterol, and dinosterol accumulation rates and respective balance factors following Müller et al. (2011). Shadings refer to estimates of sea ice conditions (PIP_{25} > 0.1 variable, > 0.5 marginal, > 0.75 extended ice cover) according to Müller et al. (2011).

P_BIP_{25} and P_DIP_{25} indices calculated for core PS2641-4 show minimum values during the late Early Holocene (8,700 - 7,200 years BP; Fig. 30) that point towards a variable or less pronounced sea ice coverage at the inner shelf of East Greenland. Given the lack of brassicasterol and dinosterol between 7,900 and 7,600 years BP, P_BIP_{25} and P_DIP_{25} values are 1 for this interval, which would refer to a significantly extended (spatially and temporally) ice cover. This interpretation, however, omits the possibility of intensively stratified surface waters due to meltwater plumes released through the East Greenland Kejser Franz Joseph fjord system. Throughout the past 7,000 years, P_BIP_{25} and P_DIP_{25} indices of core PS2641-4 fluctuate between values of ca. 0.4 to 0.6 (Fig. 30), which may denote variable to stable

marginal sea ice conditions (20 - 50% ice concentration) in western Fram Strait throughout the Mid and Late Holocene. The observation that P_BIP_{25} and P_DIP_{25} indices obtained from this core are largely in the same range or even lower than those from core MSM5/5-712-2 occurs somewhat surprising as sea ice conditions at the East Greenland shelf are generally considered to be more severe due to the pronounced discharge of sea ice and icebergs via the EGC. In a previous study, the very low contents of IRD in the PS2641-4 sediments have been interpreted to reflect a sedimentation regime that is dominated by meltwater discharge rather than by iceberg rafting (Evans et al., 2002). This prompts the assumption that much of the brassicasterol and dinosterol identified in this core could originate from the adjacent fjord systems and is advected through massive meltwater releases in summer. While calculating the P_BIP_{25} and P_DIP_{25} indices, the amount of "in-situ" phytoplankton accordingly could be overestimated, which would result in (too) low P_BIP_{25} and P_DIP_{25} values.

The short-term variability observed in the biomarker records of core MSM5/5-712-2 during the Late Holocene (Fig. 25), however, is not reproduced by the P_BIP_{25} and P_DIP_{25} indices of this core. The in-phase fluctuations of IP_{25} and phytoplankton marker contents referring to rapid advances and retreats of the sea ice margin seem to be counterbalanced through the index calculation. Coevally high amounts of IP_{25}, brassicasterol, and dinosterol (indicating beneficial ice-edge conditions) as well as coevally low biomarker contents (suggesting an unfavourable/severe ice cover) thus give the same PIP_{25} values - as was already suggested by Müller et al. (2011). We hence conclude that for the proper identification of different sea ice conditions individual biomarker concentrations need to be known and accordingly interpreted.

Nonetheless, we consider these PIP_{25} indices to describe sea ice conditions a promising means, as they may enable a more quantitative assessment of the ice coverage (once the modern analogue calibration data set has been extended) and thus provide valuable information that can be used for e.g. palaeo freshwater budget estimates.

5.7 Conclusions

The Holocene sea ice evolution in eastern and western Fram Strait is reconstructed by means of the sea ice proxy IP_{25}, IRD data and the phytoplankton-derived biomarkers brassicasterol and dinosterol. In line with a lowered Northern Hemisphere insolation and decreasing temperatures, the (spring) sea ice coverage along the western continental margin of Spitsbergen increased continuously throughout the past 8,500 years BP. In contrast, sea ice conditions at the inner shelf of East Greenland probably remained relatively constant

over this period. Estimates of the sea ice conditions based on phytoplankton-IP_{25} indices (P_BIP_{25} and P_DIP_{25}) reveal a Mid Holocene shift from a reduced ice cover to marginal ice zone conditions in eastern Fram Strait, whereas the inner East Greenland shelf experienced a seasonal variable to stable marginal ice cover throughout the past 7,000 years BP. During the Neoglacial, a rapidly advancing and retreating sea ice margin characterised the environmental setting at the West Spitsbergen slope. This points to a highly variable inflow of warm Atlantic Water, which, in turn, could be associated with short-term changes in the oceanic-atmospheric forcing pattern. This variability is not clearly reflected in the core from the East Greenland shelf, where only a delayed Late Holocene ice advance (i.e. a pronounced increase in IP_{25} contents) is observed for the past 1,000 years BP. The use of IP_{25} and phytoplankton markers, however, proves a valuable combinatory approach for the assessment of sea surface conditions. Regarding the P_BIP_{25} and P_DIP_{25} indices we recommend that the reconstruction of sea ice coverage should not be solely based on these ratios but that individual biomarker concentrations need to be considered as well.

Acknowledgements

Robert Spielhagen (IFM-GEOMAR, Kiel, Germany), Christian Hass (AWI-Sylt, Germany) and Jacques Giraudeau (EPOC, Université Bordeaux 1/CNRS, France) are kindly acknowledged for providing AMS ^{14}C datings of the *Maria S. Merian* cores. Financial support was provided by the Deutsche Forschungsgemeinschaft through SPP INTERDYNAMIK (STE 412/24-1).

6. Variability of sea ice conditions in the Fram Strait over the past 30,000 years

Juliane Müller [a], Guillaume Massé [b,c], Rüdiger Stein [a], Simon T. Belt [c]

[a] Alfred Wegener Institute for Polar and Marine Research, 27568 Bremerhaven,Germany
[b] LOCEAN, UMR7159 CNRS/UPMC/IRD/MNHN, 4 Place Jussieu, 75005 Paris, France
[c] SEOES, University of Plymouth, Drake Circus, PL48AA Plymouth, UK

Published in Nature Geoscience (November 2009).

Abstract

Sea ice is a critical component of global climate, contributing to heat reduction (albedo) and deep-water formation which is a driving mechanism of the global thermohaline circulation (Dieckmann and Hellmer, 2003; Rudels, 1996). During the transition from the Last Glacial to the Holocene warm period, fluctuations in this circulation process and variations in sea ice coverage in the northernmost Atlantic are commonly associated with rapid climate shifts (Clark et al., 2002). Here, we use the variable sedimentary abundances of the geochemical biomarkers IP_{25} and brassicasterol, derived from sea ice diatoms and phytoplankton, respectively, to obtain a continuous sea ice record for the past 30,000 years for the northernmost Atlantic (Fram Strait). We identify and characterise different sea ice scenarios ranging from perennial ice cover (Last Glacial Maximum), a stationary sea ice margin (Late Weichselian), seasonal spring sea ice cover (Holocene) and ice-free (Early Bølling) conditions. Our results demonstrate a distinct correlation between sea ice conditions, North Atlantic water advection and known climatic fluctuations in the Nordic Seas during the past 30,000 years, and provide a more detailed sea surface record for future interpretation of other atmospheric and sub-surface oceanographic palaeoclimatic data.

6.1 Introduction

The distribution of sea ice in Fram Strait, the only deep-water connection (~ 2600 m mean water depth) between the Arctic and the Atlantic Ocean, is mainly controlled by the inflow of temperate water from the North Atlantic along the western continental margin of Spitsbergen via the Norwegian Current and Westspitsbergen Current. In contrast, the East Greenland Current carries cold water (and sea ice) southward through this gateway (Rudels, 1996; Fig. 31). The relative contributions of these currents strongly influence the thermohaline circulation, thus contributing to global climate (Rudels, 1996).

Previously, it has been shown that, when detected in marine sediments, a C_{25} isoprenoid lipid (IP_{25}) biosynthesised by Arctic sea ice diatoms acts as a proxy for previous spring sea ice occurrence and subsequent melt (Belt et al., 2007; Massé et al., 2008), while the phytoplankton-derived sterol, brassicasterol (Volkman, 2006), reflects open ocean conditions during summer.

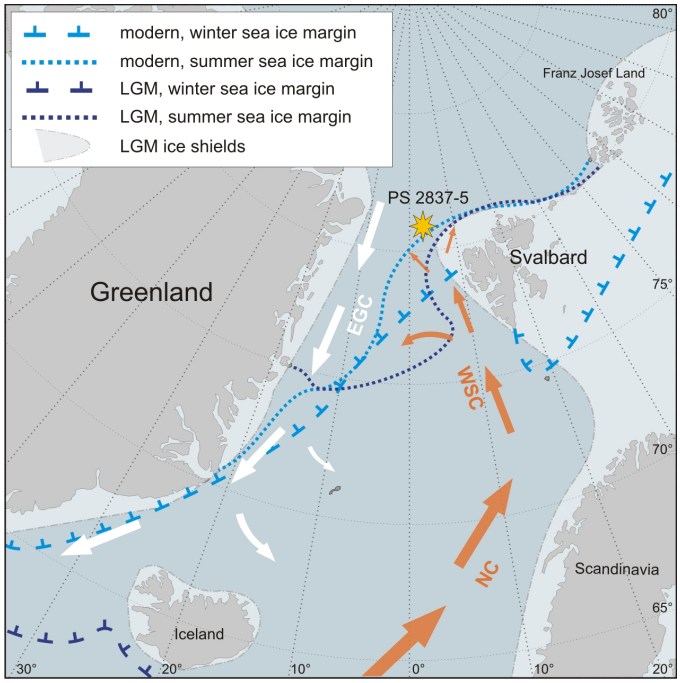

Fig. 31: Map showing the PS2837-5 core site in northern Fram Strait, major ocean currents, and sea ice margins. White-shaded areas indicate the extent of the Greenland, Iceland, and Scandinavian Ice Shields during the Last Glacial Maximum. Orange arrows refer to warm Atlantic water inflow via the Norwegian (NC) and Westspitsbergen Current (WSC); white arrows indicate cold polar water transported by the East Greenland Current (EGC).

In the current study, we present Organic Carbon (OC, global productivity and terrigenous organic carbon input; data from Birgel and Hass, 2004) and fluxes of IP_{25} (sea ice) and brassicasterol (phytoplankton; data from Birgel and Hass, 2004) for a sediment core (PS2837-5) from the western flank of the Yermak Plateau (81°13.99'N, 02°22.85'E, northwest of Spitsbergen, 1042 m water depth; Stein and Fahl, 1997) close to the present day summer sea ice margin in Fram Strait (Fig. 31). We use the previously reported age model of PS2837-5, which is based on 14 AMS ^{14}C ages of tests of the planktic foraminifer *Neogloboquadrina pachyderma* sin. and assumes a marine reservoir correction of 400 years and linear interpolation between ^{14}C-dated horizons (Nørgaard-Pedersen et al., 2003). In the following, ages are given in calibrated calendar years before present.

6.2 Material and methods

The analysis of the IP_{25} biomarker was carried out on freeze-dried sediment material from individual horizons from the PS2837-5 core. Prior to extraction, an internal standard (7-hexylnonadecane) was added to ca. 1.5 g freeze-dried and ground sediment material to permit quantification. Sediments were then extracted using dichloromethane/methanol (3 x

3 ml; 2:1 vol/vol) and ultrasonification (3 x 10 min). The resulting extracts were fractionated to yield hydrocarbon fractions containing IP_{25} using open column chromatography (SiO_2, hexane) and these were analysed using gas chromatography mass spectrometry (GC-MS). GC-MS measurements were carried out on a HP 5890 gas chromatograph (30 m fused silica column; 0.25 mm inner diameter, 0.25 μm film thickness) coupled to a HP 5970 mass selective detector. The GC oven temperature was programmed from 40 to 300 °C at 5 °C/min and held at the final temperature for 10 min. MS operating conditions were 280 °C (ion source) and 70 eV (ionization energy). Deviation for the repeatability of measurements was less than 10%. The identification of the IP_{25} monoene was based on its GC retention time and comparison of its mass spectrum with that of an authentic standard published previously (Belt et al., 2007). Sedimentary IP_{25} concentrations were determined by calculating the relative GC-MS responses of IP_{25} and the internal standard and taking account of the mass of sediment extracted in each case. Temporal fluxes of IP_{25} and brassicasterol were determined by combining sedimentary concentrations with sediment densities and sedimentation rates.

6.3 Results and Discussion

6.3.1 Late Weichselian and Last Glacial Maximum

For much of the interval between 30 and 17 ka BP (Late Weichselian to early deglaciation; Fig. 32), IP_{25}, brassicasterol and OC fluxes are amongst their lowest within the entire record. These near-zero fluxes for all three proxy records, especially during the Last Glacial Maximum (LGM) and the early deglaciation (23.5 - 17 ka BP), are attributable to an almost permanent period of ice cover (Fig. 33.a), possibly resulting from an extension of the Svalbard-Barents-Sea Ice Sheet (SBIS) to the shelf edge during this time (Andersen et al., 1996) and a distinct weakening of warm Atlantic water inflow into northern Fram Strait. Under such conditions, diatom and phytoplankton growth is limited since the presence of a thick ice sheet inhibits light penetration and enhanced stratification reduces nutrient availability. These observations demonstrate that the summer sea ice margin during the LGM must have been located south of ca. 81° N (Fig. 31; Mangerud et al., 1998; Sarnthein et al., 2003a).

Exceptionally, elevated IP_{25} fluxes at about 29.6 ka BP (Fig. 32) probably indicate a short-term thinning of this near-perennial sea ice cover permitting some sea ice algal growth with subsequent release during a brief summer melt period (Fig. 33.a). Between 27 and 24 ka BP (Fig. 32), increased IP_{25} and brassicasterol fluxes indicate favourable conditions for both sea

ice diatom and phytoplankton growth. Enhanced marine OC accumulation has also been observed in other cores from Fram Strait and adjacent areas (Birgel and Stein, 2004; Knies and Stein, 1998) in the vicinity of the SBIS. Since primary production is enhanced at the ice edge (Smith et al., 1987), resulting in higher sedimentary concentrations of marine-derived biomarkers (Birgel et al., 2004), these elevated fluxes of IP_{25} and brassicasterol probably reveal the occurrence of a stationary ice margin (ca. 81° N; 2° E) during this otherwise perennially ice-covered interval (Fig. 33.b).

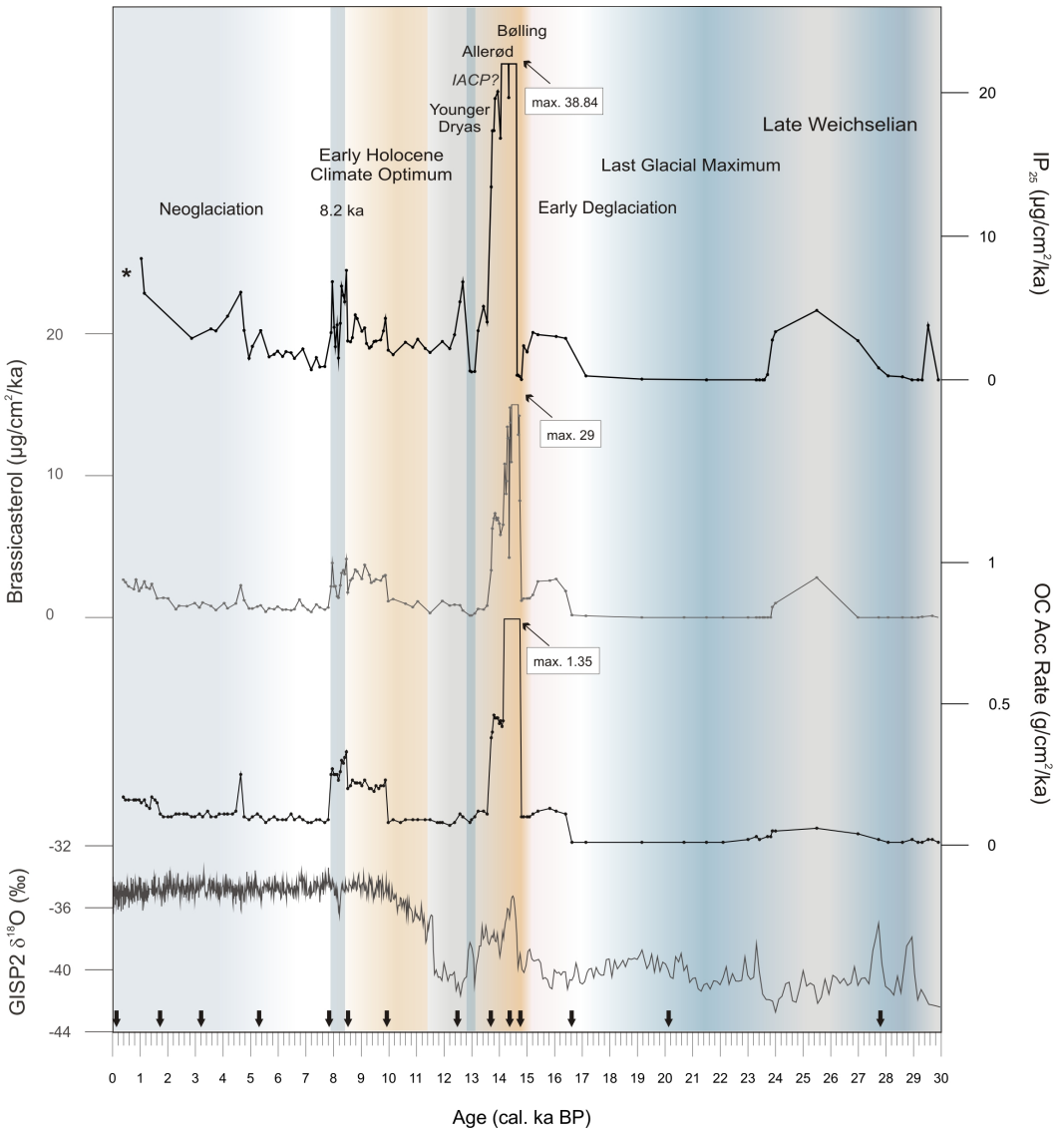

Fig. 32: Temporal evolution of Organic Carbon (OC), brassicasterol, and IP_{25} accumulation rates (fluxes), and $\delta^{18}O$ values from the GISP2 ice core. The named geological epochs (e.g. Late Weichselian) correspond to intervals for which discrete sea ice conditions have been identified. Black arrows refer to ^{14}C AMS datings. * Interval for which IP_{25} was not determined.

A coeval enhancement in ice-rafted debris in PS2837-5 (Nørgaard-Pedersen et al., 2003) provides evidence for the presence of drifting sea ice or icebergs at this time and, in turn,

the occurrence of coastal polynyas. Such polynyas probably resulted from strengthened Atlantic water advection and/or katabatic winds as suggested previously (Knies et al., 1999), with parallel formation of an adjacent stationary ice margin.

6.3.2 Deglaciation to Younger Dryas

Coincident with intensified Atlantic water advection (Stein, 2008a) and the onset of the SBIS disintegration at about 17 ka BP (Andersen et al., 1996; Knies et al., 2001; Knies and Stein, 1998), higher fluxes of IP_{25} occurred, likely as a result of reduced ice thickness and thus better light penetration and nutrient availability suitable for sea ice diatom growth (c.f. 29.6 ka BP event). An increase in brassicasterol and OC fluxes lagged those observed for IP_{25} by ca. 400 yr (Fig. 32), consistent with a progressive retreat of the ice sheet and more frequent summer ice melt and open water conditions. At the onset of the Bølling (ca. 15 ka BP), a notable abrupt warm phase characterised by heavier GISP2 $\delta^{18}O$ values (Grootes et al., 1993), exceptionally high sedimentation rates resulting from huge deglacial meltwater plumes carrying high amounts of terrigenous (Svalbard) material (Birgel and Hass, 2004), led to extremely high OC and brassicasterol fluxes (Fig. 32). Coeval with this rapid warming, a sudden drop in IP_{25} fluxes occurred for ca. 200 yr (14.8 - 14.6 ka BP), reflecting significantly reduced sea ice occurrence (Fig. 33.c). At that time, the Yermak Plateau probably only experienced short-term advances of sea ice, barely sufficient for sea ice diatoms to populate. On the other hand, open water phytoplankton would have benefited dramatically from such essentially ice-free conditions.

The Early Bølling was followed by intervals of variable sea ice cover (ca. 14.6 - 13.2 ka BP), as reflected by the IP_{25} fluxes. Massive sedimentary input continued during this interval, thus promoting an increased burial/preservation of organic matter (the 'ballast effect'; Birgel and Hass, 2004; Knies and Stein, 1998) and peak fluxes of OC, brassicasterol and IP_{25}. A prominent short-term decrease in $\delta^{18}O$ (GISP2), along with reduced IP_{25}, brassicasterol and OC fluxes between 13.2 and 13 ka BP, are consistent with a dramatic temperature decrease over Greenland, and generally unfavourable environmental conditions with extended (perennial) sea ice cover and reduced primary production (Fig. 33.a). These observations, together with an absence of benthic foraminifera in PS2837-5 (Wollenburg et al., 2004), are associated with a deterioration of thermohaline processes and reduced bottom-current activity in Fram Strait (Birgel and Hass, 2004) and demonstrate that this permanent sea ice cover affected both primary production and higher trophic levels, resulting in a widespread ecological decline. In previous studies carried out on PS2837-5, this abrupt cooling event

was tentatively assigned as the Intra-Allerød Cold Period (IACP; Birgel and Hass, 2004; Wollenburg et al., 2004). However, in the North Atlantic, higher ^{14}C reservoir ages have been determined specifically for this interval (500-600 years; Bondevik et al., 2006). Since these were not considered in the original age model for PS2837-5 (Nørgaard-Pedersen et al., 2003), this abrupt cold spell may alternatively be assigned to the Early Younger Dryas (ca. 12.7 ka BP), consistent with the common identification of the Younger Dryas as the major cold period in the Northern Hemisphere following the LGM (Bradley and England, 2008; Slubowska-Woldengen et al., 2008). In further support of this assignment, IP_{25} and brassicasterol fluxes increased during the subsequent Mid-Late Younger Dryas intervals, as sea ice diatom and phytoplankton activity improved due to less severe sea ice conditions (Fig. 32). Such conditions probably resulted from a weak but constant inflow of warm water from the Atlantic via the Westspitsbergen Current, generating climate conditions also suitable for primary productivity, a conclusion consistent with diatom-valve assemblages from the Vøring Plateau in the Norwegian Sea (Koç et al., 1993).

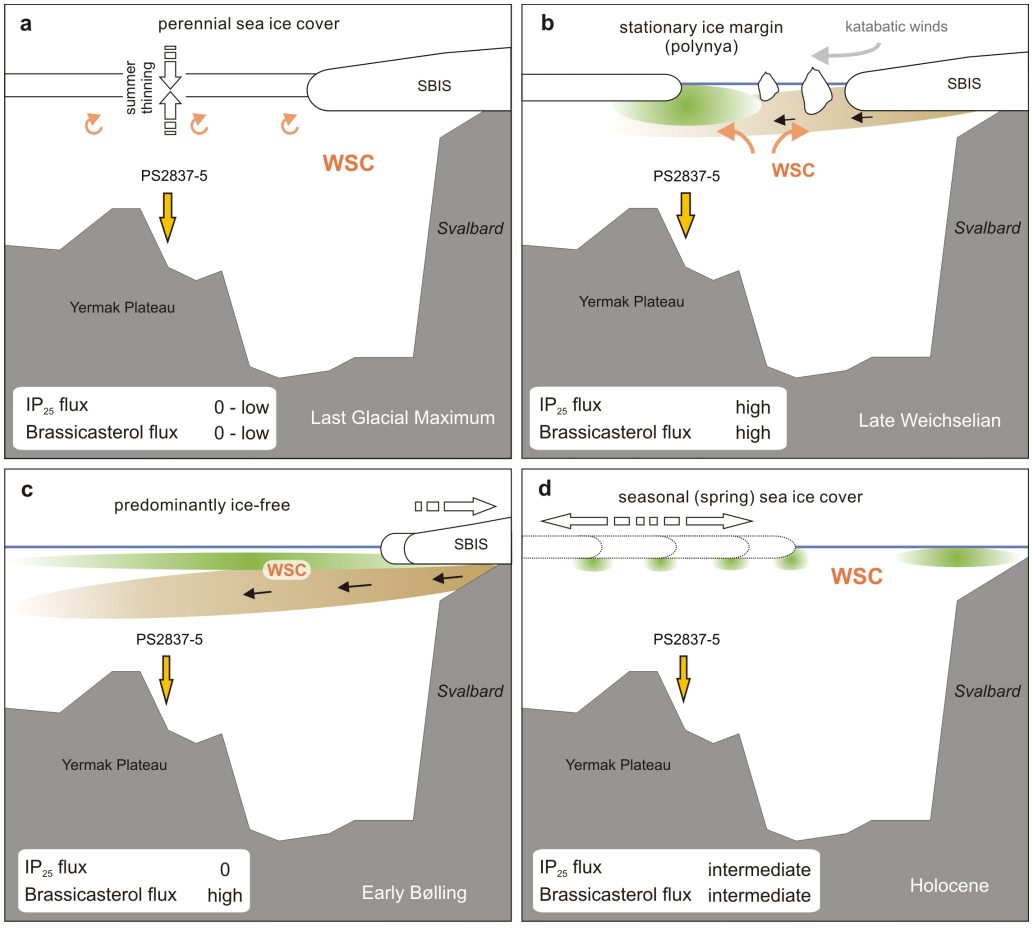

Fig. 33: Schematic illustrations of distinct sea ice conditions at the PS2837-5 core site for selected time intervals (a - d). Green shadings refer to primary productivity while brown shadings indicate input of terrigenous matter. Overview IP_{25} and brassicasterol fluxes are indicated for each interval. WSC = Westspitsbergen Current, SBIS = Svalbard-Barents-Sea Ice Sheet.

6.3.3 The Holocene

An abrupt increase in GISP2 $\delta^{18}O$ values, together with numerous terrestrial and marine records mark the beginning of the Holocene interglacial at around 11.5 ka BP in northern latitudes (Grootes et al., 1993). Enhanced insolation and warm Atlantic water influx to the Nordic seas (Andersen et al., 2004; Koç et al., 1993) resulted in a northward retreat of the Polar Front especially in the Early Holocene as indicated from foraminiferal and diatom distributions (Hald et al., 2007; Koç et al., 1993). This is further evidenced here through the observation of significantly increased brassicasterol and OC fluxes (Fig. 32). However, the co-occurrence of IP_{25} and the absence of IRD (Nørgaard-Pedersen et al., 2003) demonstrate that seasonal sea ice, rather than the presence of polynyas with drifting icebergs and a stationary ice margin, must have prevailed in northern Fram Strait throughout this period, with changes to the IP_{25} fluxes reflecting variability of spring sea ice conditions (Fig. 32, 31.d).

Around 8.4 ka BP, a short-term increase followed by a rapid decrease at 8.2 ka is observed in the brassicasterol and IP_{25} flux records. Subsequently, from ca. 8 - 5 ka BP, IP_{25}, brassicasterol and OC fluxes all remained low, similar to the Early Younger Dryas (or IACP) and the LGM when near-permanent sea ice coverage severely restricted primary production. The '8.2 ka event', a significant cold spell probably caused by the outburst of a giant glacial meltwater lake in North America (Kleiven et al., 2008), likely triggered an abrupt increase in sea ice coverage at the western Yermak Plateau at the end of the Early Holocene Climate Optimum. Although the GISP2 $\delta^{18}O$ decline at 8.2 ka BP describes a relatively short-term atmospheric cooling event in Greenland, the longer-term minimum fluxes of IP_{25} and brassicasterol in northern Fram Strait suggest a more prolonged deterioration in the marine conditions, with near-perennial sea ice cover. This is reversed in the Late Holocene (since ca. 5 ka BP) with slightly increasing OC and brassicasterol fluxes indicative of an amelioration of the environmental conditions at the Yermak Plateau. Concurrent higher fluxes of IP_{25} point to the re-establishment of seasonal sea ice conditions in Northern Fram Strait. These observations are consistent with the widespread evidence for a neoglacial period in the northern North Atlantic during the Holocene (Hald et al., 2007; Stein, 2008a).

6.4 Summary and Conclusions

This is the first application of the novel sea ice biomarker IP_{25} in determining Arctic sea ice records prior to the Holocene. We also show how the variable occurrence of IP_{25}, when

considered alongside other geochemical proxies such as brassicasterol from phytoplankton, can reveal more specific palaeo sea ice scenarios. The co-occurrence of both biomarkers refers to either seasonal sea ice cover (Early and Late Holocene) or a stationary ice margin (Late Weichselian) enabling spring sea ice diatom and summer phytoplankton growth, with the latter scenario evidenced further by the additional enhancement of sedimentary IRD (Nørgaard-Pedersen et al., 2003). In contrast, near-zero occurrences of both biomarkers (LGM and Early Younger Dryas/IACP), result from unfavourable environmental conditions for both organism classes during extreme cold periods with near-perennial sea ice cover. In addition, the predominant occurrence of IP_{25} (early deglaciation) or brassicasterol (Early Bølling) indicates the progressive thinning of the sea ice cover, or sea ice-free conditions, respectively. As such, the relationship between IP_{25} and brassicasterol fluxes is strongly dependent on the specific sea ice conditions, shown further by the variable correlation between these two biomarkers at different intervals across the record (Fig. 32).

As shown, our biomarker-based observations and interpretations align strongly with previous palaeoclimate records for northern Fram Strait (Andersen et al., 1996; Birgel and Hass, 2004; Knies et al., 1999; Wollenburg et al., 2004), but they also provide more specific palaeoceanographic information. Firstly, during intervals of the Late Weichselian, our biomarker record indicates extended periods of near-perennial sea ice cover (29 - 27.5 ka BP and 23.5 - 17 ka BP; Fig. 32), yet high fluxes of planktic and benthic foraminifera have been identified previously in PS2837-5, and these were attributed to a stronger though, significantly, subsurface input of warm Atlantic water (Nørgaard-Pedersen et al., 2003; Wollenburg et al., 2004) during so-called high-productive events (Hebbeln et al., 1994). We suggest that a temperate subsurface layer, causing thinning and short-term opening of the ice sheet during summer months (Fig. 33.a), was sufficient for short-term blooms of phytoplankton-grazing foraminifera without significant deposition of marine surface-water or sea ice-derived biomarkers (23.5 - 17 ka BP). Secondly, significantly higher biomarker fluxes are observed during an interval (27 - 24 ka BP) barren of planktic foraminifers (Nørgaard-Pedersen et al., 2003) which may be ascribed to enhanced sedimentary carbonate dissolution (Knies et al., 1999; Nørgaard-Pedersen et al., 2003; Steinsund and Hald, 1994; Wollenburg et al., 2004) as a consequence of elevated sea surface primary productivity at the ice edge during polynya conditions. These observations further reinforce the importance of evaluating the significance of individual proxies when carrying out integrated palaeoclimate reconstructions.

Biomarker data are available at doi:10.1594/PANGAEA.728973.

Acknowledgements

We thank Steven J. Rowland and Daniel Birgel for discussions on the use of selected biomarkers and for provision of some geochemical data from PS2837-5. Financial support was provided by the Deutsche Forschungsgemeinschaft (DFG), STE 412/24-1, the European Research Council (ERC StG project 203441) and the UK Natural Environmental Research Council (NE/D013216/1).

7. Conclusions and Outlook

7.1 Conclusions

Within the framework of this thesis both the applicability of the novel sea ice proxy IP_{25} and its significance for palaeoceanographic and -climatic reconstructions were evaluated.

The reliability of IP_{25} to satisfactorily reflect a previous ice cover has been demonstrated by means of the surface sediment study outlined in chapter 4. Major outcome of this study is that the coupling of IP_{25} with phytoplankton-derived biomarkers (referring to mainly ice-free conditions) considerably improves the reconstruction of sea surface conditions. This combination importantly prevents the misleading interpretation of ambiguous low or zero IP_{25} contents and even enables discrimination between ice-free, seasonal, stable ice-edge, and permanent ice cover conditions. Thus a phytoplankton-IP_{25} (PIP_{25}) index was established to combine the different biomarker information. In co-operation with colleagues from the numerical modelling department this study was complemented with satellite and model data, which finally permitted qualitative and quantitative comparison between biomarker results and observed sea ice conditions. Correlation analyses of the PIP_{25} index of surface sediments with numerically modelled and satellite-derived sea ice data yielded good results and thus provided a first step towards quantitative sea ice reconstructions.

The reconstruction of Holocene sea ice conditions in Fram Strait and the use of the PIP_{25} index are described in chapter 5. The combinatory biomarker approach significantly improved the assessment of sea surface conditions and enabled the identification of rapid sea ice fluctuations during the Neoglacial, which were brought into context with changes of the oceanic (and atmospheric) circulation patterns. By means of PIP_{25} indices, a Middle Holocene shift from less sea ice cover to marginal ice zone conditions was reconstructed. The distinct Neoglacial short-term variations, however, are not reflected by the PIP_{25} indices, which strengthens that in-phase fluctuations of the respective biomarkers are unfortunately balanced out through the PIP_{25} calculation. This needs to be considered for the use of these indices.

The first identification of IP_{25} in pre-Holocene sediments as shown in chapter 6 importantly extended the temporal application of the novel ice proxy. Previous estimates of the Last Glacial Maximum sea ice conditions in Fram Strait thus could be proven (or discarded, where required). Abrupt climatic perturbations during the last glacial-interglacial transition were associated with highly variable oceanic circulation patterns and extreme sea ice fluctuations, which were successively reconstructed by means of the IP_{25} and

phytoplankton biomarker records. These findings highlight the susceptibility of Arctic sea ice to climate change and thus motivate the further use of IP_{25} to elucidate palaeo sea ice conditions.

7.2 Outlook

The data presented within this work contribute to the knowledge about the use of the novel sea ice proxy IP_{25} for palaeoceanographic sea ice reconstructions and the evolution of the sea ice cover in Fram Strait during the past 30,000 years. Suggestions were made how the information carried by IP_{25} could be interpreted to ensure a comprehensive assessment of sea surface conditions. Given the juvenescence of IP_{25} there are still many open questions and uncertainties that require consideration and illumination during future IP_{25} studies.

With regard to the herein documented approach to establish a "modern-analogue" type of calibration between IP_{25} (or rather PIP_{25}) data and satellite- or model-based sea ice maps to quantitatively reconstruct sea ice coverage, much more biomarker information is needed to validate this attempt. IP_{25} studies on surface sediments from (ideally) the whole Arctic Ocean would provide the required amount and density of data to verify the quantitative PIP_{25} sea ice estimate. Those studies would also gather environmental information about the spatial distribution of IP_{25} producing sea ice diatoms and reveal possible ecological restrictions. In this regard, the identification of the IP_{25} source diatom species (either through analyses of sedimentary or, more reliably, in-ice diatom assemblages) would fill a distinct gap of knowledge. Sediment trap studies (as they are already performed at the AWI) would additionally elucidate the actual export rates of IP_{25} and possible alteration mechanisms that affect IP_{25} on its way from the sea surface through the water column towards the sea floor.

Further IP_{25} studies performed on a multitude of sediment cores from the high northern latitudes would extend not only the spatial but also the temporal range of this proxy. Comparisons of IP_{25} based sea ice estimates between different core sites thus could even provide basis for an "atlas" of palaeo (time-slice) sea ice coverage. In particular the localisation of palaeo sea ice margins would be of high interest as they denote areas of contrasting sea surface conditions that control atmospheric and oceanic interactions. The importance and use of such work for palaeoceanographic and climate studies would be indisputable.

With respect to the herein conducted IP_{25} analyses of sediment cores from the inner East Greenland shelf and the West Spitsbergen continental margin, it became evident that

especially the latter constitutes a promising study area to record climatically induced changes in the oceanographic setting of the Fram Strait. It may be expected that sediment cores from the more distal East Greenland shelf or continental slope also serve as valuable archives to track the discharge history of the EGC. Sea ice reconstruction studies from both sides of the Fram Strait would surely support the investigation of a potential seesawing in the strength of Atlantic water in- and Arctic water (ice) outflow during ancient climates (e.g. during Pleistocene glacials and interglacials). This, in turn, would help to estimate which impact palaeo sea ice oscillations had on the North Atlantic thermohaline circulation and hence on global climate. The opportunity to recover respectively old sediment material by means of common shipboard facilities or new invented coring devices such as the MeBo sea floor drill rig (MARUM, Bremen) that can be deployed and operated from standard research vessels thus should be used to retrieve such core material for IP_{25} analyses.

Apart from Fram Strait, further target areas as, for example, the Bering Strait - representing the minor Arctic gateway counterpart - occur rather interesting for studying IP_{25} to amend the reconstruction of climate relevant ocean-ice-atmosphere interactions. The ascertainment of teleconnections between short- and long-term variations in the glacial-marine setting (not only of the Arctic gateways) would certainly contribute to the understanding of the role that the high latitudes play in driving and amplifying global climate variability.

8 References

Aagaard, K., 1981. On the deep circulation in the Arctic Ocean. Deep Sea Research Part A. Oceanographic Research Papers, 28(3): 251-268.

Aagaard, K., 1982. Inflow from the Atlantic Ocean to the Polar Basin. In: L. Rey (Editor), The Arctic Ocean. Comité Arctique International, Monaco, pp. 69-82.

Aagaard, K. and Carmack, E.C., 1989. The Role of Sea Ice and Other Fresh Water in the Arctic Circulation. J. Geophys. Res., 94.

Aagaard, K. and Carmack, E.C., 1994. The Arctic Ocean and Climate: A Perspective. In: O.M. Johannessen, R.D. Muench and J.E. Overland (Editors), The Polar Oceans and Their Role in Shaping the Global Environment. Geophysical Monograph Series. American Geophysical Union, Washington DC, pp. 5-20.

Aagaard, K. and Coachman, L.K., 1968. The East Greenland Current north of Denmark Strait. Arctic, 21(3): 181-200.

Aagaard, K., Foldvik, A. and Hillman, S.R., 1987. The West Spitsbergen Current: Disposition and Water Mass Transformation. Journal of Geophysical Research, 92(4): 3778-3784.

Abelmann, A., 1992. Diatom assemblages in Arctic sea ice--indicator for ice drift pathways. Deep Sea Research Part A. Oceanographic Research Papers, 39(2, Part 1): S525-S538.

Alley, R.B., Mayewski, P.A., Sowers, T., Stuiver, M., Taylor, K.C. and Clark, P.U., 1997. Holocene climatic instability: A prominent, widespread event 8200 yr ago. Geology, 25(6): 483-486.

Andersen, C., Koç, N., Jennings, A. and Andrews, J.T., 2004. Nonuniform response of the major surface currents in the Nordic Seas to insolation forcing: Implications for the Holocene climate variability. Paleoceanography, 19: PA 2003.

Andersen, E.S., Dokken, T.M., Elverhøi, A., Solheim, A. and Fossen, I., 1996. Late quaternary sedimentation and glacial history of the western Svalbard continental margin. Marine Geology, 133(3-4): 123-156.

Andersson, C., Risebrobakken, B., Jansen, E. and Dahl, S.O., 2003. Late Holocene surface ocean conditions of the Norwegian Sea (Vøring Plateau). Paleoceanography, 18(2): 1044.

Andrews, J.T., Belt, S.T., Olafsdottir, S., Massé, G., Vare, L., 2009. Sea ice and marine climate variability for NW Iceland/Denmark Strait over the last 2000 cal. yr BP. The Holocene, 19: 775-784.

Andrews, J.T., Helgadottir, G., Geirsdottir, A. and Jennings, A.E., 2001. Multicentury-Scale Records of Carbonate (Hydrographic?) Variability on the Northern Iceland Margin over the Last 5000 Years. Quaternary Research, 56(2): 199-206.

Andrews, J.T., Jennings, A.E., Coleman, G.C. and Eberl, D.D., 2010. Holocene variations in mineral and grain-size composition along the East Greenland glaciated margin (ca 67°-70°N): Local versus long-distance sediment transport. Quaternary Science Reviews, 29(19-20): 2619-2632.

Bauch, D., Carstens, J. and Wefer, G., 1997. Oxygen isotope composition of living Neogloboquadrina pachyderma (sin.) in the Arctic Ocean. Earth and Planetary Science Letters, 146(1-2): 47-58.

Bauch, H.A., Erlenkeuser, H., Spielhagen, R.F., Struck, U., Matthiessen, J., Thiede, J. and Heinemeier, J., 2001. A multiproxy reconstruction of the evolution of deep and surface waters in the subarctic Nordic seas over the last 30,000†yr. Quaternary Science Reviews, 20(4): 659-678.

Bauch, H.A. and Kandiano, E.S., 2007. Evidence for early warming and cooling in North Atlantic surface waters during the last interglacial. Paleoceanography, 22(1): PA1201.

Bauerfeind, E., Leipe, T. and Ramseier, R.O., 2005. Sedimentation at the permanently ice-covered Greenland continental shelf (74°57.7'N/12°58.7'W): significance of biogenic and lithogenic particles in particulate matter flux. Journal of Marine Systems, 56(1-2): 151-166.

Baumannn, K.-H., Meggers, H. and Henrich, R., 1986. Variations in surface water mass conditions in the Norwegian-Greenland Sea: Evidence from Pliocene/Pleistocene calcareous plankton records (Sites 644, 909, 909). In: J. Thiede, A.M. Myhre, J.V. Firth, G.L. Johnson and W.F. Ruddiman (Editors), Proceedings of the Ocean Drilling Program, Scientific Results. College Station, Texas, pp. 493-514.

Belkin, I.M., Levitus, S., Antonov, J. and Malmberg, S.-A., 1998. "Great Salinity Anomalies" in the North Atlantic. Progress In Oceanography, 41(1): 1-68.

Belt, S.T., Allard, W.G., Masse, G., Robert, J.-M. and Rowland, S.J., 2000a. Highly branched isoprenoids (HBIs): identification of the most common and abundant sedimentary isomers. Geochimica et Cosmochimica Acta, 64(22): 3839-3851.

Belt, S.T., Allard, W.G., Rintatalo, J., Johns, L.A., van Duin, A.C.T. and Rowland, S.J., 2000b. Clay and acid catalysed isomerisation and cyclisation reactions of highly branched isoprenoid (HBI) alkenes: implications for sedimentary reactions and distributions. Geochimica et Cosmochimica Acta, 64(19): 3337-3345.

Belt, S.T., Massé, G., Rowland, S.J., Poulin, M., Michel, C. and LeBlanc, B., 2007. A novel chemical fossil of palaeo sea ice: IP_{25}. Organic Geochemistry, 38(1): 16-27.

Belt, S.T., Massé, G., Vare, L.L., Rowland, S.J., Poulin, M., Sicre, M.-A., Sampei, M. and Fortier, L., 2008. Distinctive ^{13}C isotopic signature distinguishes a novel sea ice biomarker in Arctic sediments and sediment traps. Marine Chemistry, 112(3-4): 158-167.

Belt, S.T., Vare, L.L., Massé, G., Manners, H.R., Price, J.C., MacLachlan, S.E., Andrews, J.T. and Schmidt, S., 2010. Striking similarities in temporal changes to spring sea ice occurrence across the central Canadian Arctic Archipelago over the last 7000 years. Quaternary Science Reviews, 29(25-26): 3489-3504.

Bendle, J.A.P. and Rosell-Melé, A., 2007. High-resolution alkenone sea surface temperature variability on the North Icelandic Shelf: implications for Nordic Seas palaeoclimatic development during the Holocene. The Holocene, 17(1): 9-24.

Berger, A., 1978. Long-term variations of caloric insolation resulting from the earth's orbital elements. Quaternary Research, 9(2): 139-167.

Birgel, D. and Hass, H.C., 2004. Oceanic and atmospheric variations during the last deglaciation in the Fram Strait (Arctic Ocean): a coupled high-resolution organic-geochemical and sedimentological study. Quaternary Science Reviews, 23(1-2): 29-47.

Birgel, D. and Stein, R., 2004. Northern Fram Strait and Yermak Plateau: distribution, variability and burial of organic carbon and paleoenvironmental implications. In: R. Stein and G.M. MacDonald (Editors), The Organic Carbon Cycle in the Arctic Ocean. Springer Verlag, New York.

Birgel, D., Stein, R. and Hefter, J., 2004. Aliphatic lipids in recent sediments of the Fram Strait/Yermak Plateau (Arctic Ocean): composition, sources and transport processes. Marine Chemistry, 88(3-4): 127-160.

Birks, H.H., 1991. Holocene vegetational history and climatic change in west Spitsbergen - plant macrofossils from Skardtjørna, an Arctic lake. The Holocene, 1(3): 209-218.

Blumer, M., Guillard, R.R.L. and Chase, T., 1971. Hydrocarbons of marine phytoplankton. Marine Biology, 8(3): 183-189.

Bohrmann, G., Henrich, R. and Thiede, J., 1990. Miocene to Quaternary Paleoceanography in the Northen North Atlantic: Variability in carbonate and biogenic opal accumulation. In: U. Bleil and J. Thiede (Editors), Geological History of the Polar Oceans: Arctic Versus Antarctic. Kluwer Academic Publishers, Dordrecht Boston London, pp. 647-675.

Bondevik, S., Mangerud, J., Birks, H.H., Gulliksen, S. and Reimer, P., 2006. Changes in North Atlantic Radiocarbon Reservoir Ages During the Allerød and Younger Dryas. Science, 312: 1514-1517.

Bonnet, S., de Vernal, A., Hillaire-Marcel, C., Radi, T. and Husum, K., 2010. Variability of sea-surface temperature and sea-ice cover in the Fram Strait over the last two millennia. Marine Micropaleontology, 74(3-4): 59-74.

Boon, J.J., Rijpstra, W.I.C., Lange, F.d., de Leeuw, J.W., Yoshioka, M. and Shimizu, Y., 1979. Black Sea sterol—a molecular fossil for dinoflagellate blooms Nature, 277: 125-127.

Bordovskiy, O.K., 1965. Sources of organic matter in marine basins. Marine Geology, 3(1-2): 5-31.

Bourke, R., Weigel, A. and Paquette, R., 1988. The Westward Turning Branch of the West Spitsbergen Current. Journal of Geophysical Research, 93(C11): 14065-14077.

Boyd, T.J. and D'Asaro, E.A., 1994. Cooling of the West Spitsbergen Current: Wintertime Observations West of Svalbard. J. Geophys. Res., 99(C11): 22597-22618.

Bradley, R.S. and England, J.H., 2008. The Younger Dryas and the Sea of Ancient Ice. Quaternary Research, 70(1): 1-10.

Broecker, W., S., 1992. The strength of the Nordic Heat Pump. In: E. Bard, Broecker, W. S. (Editor), The Last Deglaciation:Absolute and Radiocarbon Chronologies. NATO Scientific Affairs Division. Springer-Verlag, Berlin Heidelberg.

Broecker, W.S., 1991. The great ocean conveyer. Oceanography, 4: 79-89.

Broecker, W.S., Peteet, D.M. and Rind, D., 1985. Does the ocean-atmosphere system have more than one stable mode of operation? Nature, 315(6014): 21-26.

Brown, T., Belt, S., Philippe, B., Mundy, C., Massé, G., Poulin, M. and Gosselin, M., in press. Temporal and vertical variations of lipid biomarkers during a bottom ice diatom bloom in the Canadian Beaufort Sea: further evidence for the use of the IP25 biomarker as a proxy for spring Arctic sea ice. Polar Biology.

Brown, T.A., 2011. Production and preservation of the Arctic sea ice diatom biomarker IP25, University of Plymouth, 291 pp.

Budéus, G., 2007. Short Cruise Report RV Maria S. Merian Cruise MSM05/5, University of Hamburg, Institute of Oceanography; http://www.ifm.zmaw.de/leitstelle-meteormerian/reisen-des-fs-maria-s-merian/.

Calvo, E., Grimalt, J. and Jansen, E., 2002. High resolution U37K sea surface temperature reconstruction in the Norwegian Sea during the Holocene. Quaternary Science Reviews, 21(12-13): 1385-1394.

Carstens, J.r. and Wefer, G., 1992. Recent distribution of planktonic foraminifera in the Nansen Basin, Arctic Ocean. Deep Sea Research Part A. Oceanographic Research Papers, 39(2, Part 1): S507-S524.

Chapman, M.R., Shackleton, N.J. and Duplessy, J.-C., 2000. Sea surface temperature variability during the last glacial-interglacial cycle: assessing the magnitude and pattern of climate change in the North Atlantic. Palaeogeography, Palaeoclimatology, Palaeoecology, 157(1-2): 1-25.

Clark, D.L., 1982. Origin, nature and world climate effect of Arctic Ocean ice-cover. Nature, 300(5890): 321-325.

Clark, P.U., Pisias, N.G., Stocker, T.F. and Weaver, A.J., 2002. The role of the thermohaline circulation in abrupt climate change. Nature, 415(6874): 863-869.

Clarke, G.K.C., Leverington, D.W., Teller, J.T. and Dyke, A.S., 2004. Paleohydraulics of the last outburst flood from glacial Lake Agassiz and the 8200 BP cold event. Quaternary Science Reviews, 23(3-4): 389-407.

CLIMAP-Project-Members, 1981. Seasonal reconstruction of the earths surface at the last glacial maximum. Geological Society of America, Map and Chart Series, 36: 18.

Comiso, J., 1999 (updated 2008). Bootstrap Sea Ice Concentrations from NIMBUS-7 SMMR and DMSP SSM/I, 1979-2003, Digital Media. National Snow and Ice Data Center, Boulder, Colorado USA.

Comiso, J.C., Wadhams, P., Pedersen, L.T. and Gersten, R.A., 2001. Seasonal and interannual variability of the Odden ice tongue and a study of environmental effects. J. Geophys. Res., 106: 9093-9116.

Cornford, C., Gardner, P. and Burgess, C., 1998. Geochemical truths in large data sets. I: Geochemical screening data. Organic Geochemistry, 29(1-3): 519-530.

Cronin, T.M., Gemery, L., Briggs Jr, W.M., Jakobsson, M., Polyak, L. and Brouwers, E.M., 2010. Quaternary Sea-ice history in the Arctic Ocean based on a new Ostracode sea-ice proxy. Quaternary Science Reviews, 29(25-26): 3415-3429.

Darby, D.A., 2008. Arctic perennial ice cover over the last 14 million years. Paleoceanography, 23(1): PA1S07.

Darby, D.A. and Bischof, J.F., 2004. A Holocene record of changing Arctic Ocean ice drift analogous to the effects of the Arctic Oscillation. Paleoceanography, 19(1): PA1027.

Darby, D.A., Ortiz, J., Polyak, L., Lund, S., Jakobsson, M. and Woodgate, R.A., 2009. The role of currents and sea ice in both slowly deposited central Arctic and rapidly deposited Chukchi-Alaskan margin sediments. Global and Planetary Change, 68(1-2): 58-72.

de Vernal, A., Eynaud, F., Henry, M., Hillaire-Marcel, C., Londeix, L., Mangin, S., Matthiessen, J., Marret, F., Radi, T., Rochon, A., Solignac, S. and Turon, J.L., 2005. Reconstruction of sea-surface conditions at middle to high latitudes of the Northern Hemisphere during the Last

Glacial Maximum (LGM) based on dinoflagellate cyst assemblages. Quaternary Science Reviews, 24(7-9): 897-924.

de Vernal, A., Henry, M., Matthiessen, J., Mudie, P.J., Rochon, A., Boessenkool, K.P., Eynaud, F., Grøsfjeld, K., Guiot, J., Hamel, D., Harland, R., Head, M.J., Kunz-Pirrung, M., Levac, E., Loucheur, V., Peyron, O., Pospelova, V., Radi, T., Turon, J.-L. and Voronina, E., 2001. Dinoflagellate cyst assemblages as tracers of sea-surface conditions in the northern North Atlantic, Arctic and sub-Arctic seas: the new 'n = 677' data base and its application for quantitative palaeoceanographic reconstruction. Journal of Quaternary Science, 16(7): 681-698.

Delworth, T., Manabe, S. and Stouffer, R.J., 1993. Interdecadal Variations of the Thermohaline Circulation in a Coupled Ocean-Atmosphere Model. Journal of Climate, 6(11): 1993-2011.

Dembicki Jr, H., 1992. The effects of the mineral matrix on the determination of kinetic parameters using modified Rock Eval pyrolysis. Organic Geochemistry, 18(4): 531-539.

Dickson, R.R., Meincke, J., Malmberg, S.-A. and Lee, A.J., 1988. The "great salinity anomaly" in the Northern North Atlantic 1968-1982. Progress In Oceanography, 20(2): 103-151.

Dickson, R.R., Osborn, T. J., Hurrell, J. W., Meincke, J., Blindheim, J., Adlandsvik, B., Vinje, T., Alekseev, G. and Maslowski, W., 2000. The Arctic Ocean Response to the North Atlantic Oscillation. Journal of Climate, 13: 2671–2696.

Dieckmann, G.S. and Hellmer, H.H., 2003. The Importance of Sea Ice: An Overview. In: D.N. Thomas and G.S. Dieckmann (Editors), Sea Ice. Blackwell Publishing, Oxford, pp. 1-21.

Dima, M. and Lohmann, G., 2007. A hemispheric mechanism for the Atlantic Multidecadal Oscillation. J. Climate, 20(11): 2706-2719.

Dowdeswell, J.A. and Cofaigh, C.Ó., 2002. Glacier-Influenced Sedimentation on High-Latitude Continental Margins. Special Publications. Geological Society, London, 203 pp.

Eglinton, G., 1966. Recent advances in organic geochemistry. Geologische Rundschau, 55(3): 551-567.

Eglinton, G. and Hamilton, R.J., 1967. Leaf Epicuticular Waxes. Science, 156(3780): 1322-1335.

Eglinton, T.I. and Eglinton, G., 2008. Molecular proxies for paleoclimatology. Earth and Planetary Science Letters, 275(1-2): 1-16.

Eicken, H., 2003. From the microscopic, to the macroscopic, to the regional scale: Growth, microstructure and properties of sea ice. In: G.S.D. David N. Thomas (Editor), Sea Ice: An introduction to its Physics, Chemistry, Biology and Geology. Blackwell, Oxford, pp. 22-81.

Eicken, H., Gradinger, R., Salganek, M., Shirasawa, K., Perovich, D. and Leppäranta, M., 2009. Field Techniques for Sea Ice Research. University of Alaska Press, Fairbanks, 566 pp.

Eicken, H., Reimnitz, E., Alexandrov, V., Martin, T., Kassens, H. and Viehoff, T., 1997. Sea-ice processes in the Laptev Sea and their importance for sediment export. Continental Shelf Research, 17(2): 205-233.

Elverhøi, A., Andersen, E.S., Dokken, T., Hebbeln, D., Spielhagen, R., Svendsen, J.I., Sørflaten, M., Rørnes, A., Hald, M. and Forsberg, C.F., 1995. The Growth and Decay of the Late Weichselian Ice Sheet in Western Svalbard and Adjacent Areas Based on Provenance Studies of Marine Sediments. Quaternary Research, 44(3): 303-316.

Engen, Ø., Faleide, J.I. and Dyreng, T.K., 2008. Opening of the Fram Strait gateway: A review of plate tectonic constraints. Tectonophysics, 450(1-4): 51-69.

Espitalié, J., Laporte, J.L., Madec, M., Marquis, F., Leplat, P., Paulet, J. and Boutefeu, A., 1977. Methode rapide de characterisation des roches-mere de leur potential petrolier et de leur degre d'évolution. Revue de l'Institute Francçais du Pétrole, 32: 23-42.

Evans, J., 2000. Late Weichselian and Holocene sedimentation in Kejser Franz Josephs Fjord and on the adjacent continental margin, East Greenland. PhD thesis, University of Cambridge, 150 pp.

Evans, J., Dowdeswell, J.A., Grobe, H., Niessen, F., Stein, R., Hubberten, H.-W. and Whittington, R.J., 2002. Late Quaternary sedimentation in Kejser Franz Jospeh Fjord and the continental margin of East Greenland. In: J.A. Dowdeswell and C.Ó. Cofaigh (Editors), Glacier-Influenced Sedimentation on High-Latidtude Continental Margins. Geological Society, London, pp. 149-179.

Ewing, M. and Donn, W.L., 1956. A Theory of Ice Ages. Science, 123(3207): 1061-1066.

Fahl, K. and Nöthig, E.-M., 2007. Lithogenic and biogenic particle fluxes on the Lomonosov Ridge (central Arctic Ocean) and their relevance for sediment accumulation: Vertical vs. lateral transport. Deep Sea Research Part I: Oceanographic Research Papers, 54(8): 1256-1272.

Fahl, K. and Stein, R., 1997. Modern organic carbon deposition in the Laptev Sea and the adjacent continental slope: surface water productivity vs. terrigenous input. Organic Geochemistry, 26(5-6): 379-390.

Forwick, M. and Vorren, T.O., 2009. Late Weichselian and Holocene sedimentary environments and ice rafting in Isfjorden, Spitsbergen. Palaeogeography, Palaeoclimatology, Palaeoecology, 280(1-2): 258-274.

Frolov, I.E., Gudkovich, Z.M., Radionov, V.F., Shirochkov, A.V. and Timokhov, L.A., 2005. A brief history of Arctic exploration, in: The Arctic Basin - Results from the Russian drifting Stations. Springer, Berlin Heidelberg New York, pp. 1-29.

Fronval, T. and Jansen, E., 1996. Late Neogene Paleoclimates and Paleoceanography in the Iceland-Norwegian Sea: Evidence from the Iceland and Voring Plateau. In: J. Thiede, A.M. Myhre, J.V. Firth, G.L. Johnson and W.F. Ruddiman (Editors), Proceedings of the Ocean Drilling Program, Scientific Results. College Station, Texax, pp. 455-468.

Gaines, S.M., Eglinton, G. and Rullkötter, J., 2009. Echoes of Life: What fossil molecules reveal about earth history. Oxford University Press, New York.

Gelpi, E., Schneider, H., Mann, J. and Oró, J., 1970. Hydrocarbons of geochemical significance in microscopic algae. Phytochemistry, 9(3): 603-612.

Gerdes, R.d., Karcher, M.J., Kauker, F. and Schauer, U., 2003. Causes and development of repeated Arctic Ocean warming events. Geophys. Res. Lett., 30(19): 1980.

Giraudeau, J., Grelaud, M., Solignac, S., Andrews, J.T., Moros, M. and Jansen, E., 2010. Millennial-scale variability in Atlantic water advection to the Nordic Seas derived from Holocene coccolith concentration records. Quaternary Science Reviews, 29(9-10): 1276-1287.

Gloersen, P., Campbell, W.J., Cavalieri, D.J., Comiso, J.C., Parkinson, C.L. and Zwally, H.J., 1992. Arctic and Antarctic Sea Ice, 1978-1987: Satellite Passive-Microwave Observations and Analysis. NASA SP, 511, Washington, D.C.

Goad, L. and Withers, N., 1982. Identification of 27-nor-(24R)-24-methylcholesta-5,22-dien-3β-ol and brassicasterol as the major sterols of the marine dinoflagellateGymnodinium simplex. Lipids, 17(12): 853-858.

Gosselin, M., Levasseur, M., Wheeler, P.A., Horner, R.A. and Booth, B.C., 1997. New measurements of phytoplankton and ice algal production in the Arctic Ocean. Deep Sea Research Part II: Topical Studies in Oceanography, 44(8): 1623-1644.

Gradinger, R., 2009. Sea-ice algae: Major contributors to primary production and algal biomass in the Chukchi and Beaufort Seas during May/June 2002. Deep Sea Research Part II: Topical Studies in Oceanography, 56(17): 1201-1212.

Gradinger, R., Friedrich, C. and Spindler, M., 1999. Abundance, biomass and composition of the sea ice biota of the Greenland Sea pack ice. Deep Sea Research Part II: Topical Studies in Oceanography, 46(6-7): 1457-1472.

Gradinger, R. and Ikävalko, J., 1998. Organism incorporation into newly forming Arctic sea ice in the Greenland Sea. Journal of Plankton Research, 20(5): 871-886.

Green, C.L., Green, J.A.M. and Bigg, G.R., 2011. Simulating the impact of freshwater inputs and deep-draft icebergs formed during a MIS 6 Barents Ice Sheet collapse. Paleoceanography, 26(2): PA2211.

Gregory, J.M., Dixon, K.W., Stouffer, R.J., Weaver, A.J., Driesschaert, E., Eby, M., Fichefet, T., Hasumi, H., Hu, A., Jungclaus, J.H., Kamenkovich, I.V., Levermann, A., Montoya, M., Murakami, S., Nawrath, S., Oka, A., Sokolov, A.P. and Thorpe, R.B., 2005. A model intercomparison of changes in the Atlantic thermohaline circulation in response to increasing atmospheric CO2 concentration. Geophys. Res. Lett., 32(12): L12703.

Gregory, T.R., Smart, C.W., Hart, M.B., Massé, G., Vare, L.L. and Belt, S.T., 2010. Holocene palaeoceanographic changes in Barrow Strait, Canadian Arctic: foraminiferal evidence. Journal of Quaternary Science, 25(6): 903-910.

Grootes, P.M. and Stuiver, M., 1997. Oxygen 18/16 variability in Greenland snow and ice with 10-3 to 10-5-year time resolution. J. Geophys. Res., 102(C12): 26455-26470.

Grootes, P.M., Stuiver, M., White, J.W.C., Johnsen, S. and Jouzel, J., 1993. Comparison of oxygen isotope records from the GISP2 and GRIP Greenland ice cores. Nature, 366(6455): 552-554.

Grossi, V., Beker, B., Geenevasen, J.A.J., Schouten, S., Raphel, D., Fontaine, M.-F. and Sinninghe Damste, J.S., 2004. C25 highly branched isoprenoid alkenes from the marine benthic diatom Pleurosigma strigosum. Phytochemistry, 65(22): 3049-3055.

Haas, C. and Druckenmiller, M., 2009. Ice Thickness and Roughness Measurements. In: H. Eicken et al. (Editors), Field Techniques for Sea Ice Research. University of Alaska Press, Fairbanks, pp. 49-116.

Haas, C., Hendricks, S. and Doble, M., 2006. Comparison of the sea-ice thickness distribution in the Lincoln Sea and adjacent Arctic Ocean in 2004 and 2005. Annals of Glaciology, 44: 247-252.

Hald, M., Andersson, C., Ebbesen, H., Jansen, E., Klitgaard-Kristensen, D., Risebrobakken, B.r., Salomonsen, G.R., Sarnthein, M., Sejrup, H.P. and Telford, R.J., 2007. Variations in temperature and extent of Atlantic Water in the northern North Atlantic during the Holocene. Quaternary Science Reviews, 26(25-28): 3423-3440.

Hald, M., Dokken, T. and Mikalsen, G., 2001. Abrupt climatic change during the last interglacial-glacial cycle in the polar North Atlantic. Marine Geology, 176(1-4): 121-137.

Haugan, P.M., 1999. Structure and heat content of the West Spitsbergen Current. Polar Research, 18(2): 183-188.

Hays, J.D., Imbrie, J. and Shackleton, N.J., 1976. Variations in the Earth's Orbit: Pacemaker of the Ice Ages. Science, 194(4270): 1121-1132.

Hebbeln, D., 1992. Weichselian glacial history of the Svalbard area: correlating the marine and terrestrial records. Boreas, 21(3): 295-302.

Hebbeln, D., 2000. Flux of ice-rafted detritus from sea ice in the Fram Strait. Deep Sea Research Part II: Topical Studies in Oceanography, 47(9-11): 1773-1790.

Hebbeln, D. and Berner, H., 1993. Surface sediment distribution in the Fram Strait. Deep Sea Research Part I: Oceanographic Research Papers, 40(9): 1731-1745.

Hebbeln, D., Dokken, T., Andersen, E.S., Hald, M. and Elverhøi, A., 1994. Moisture supply for northern ice-sheet growth during the Last Glacial Maximum. Nature, 370: 357-360.

Hebbeln, D. and Wefer, G., 1997. Late Quaternary Paleoceanography in the Fram Strait. Paleoceanography, 12.

Hedges, J.I., Clark, W.A., Quay, P.D., Richey, J.E., Devol, A.H. and Santos, U.d.M., 1986. Compositions and fluxes of particulate organic material in the Amazon River. Limnology and Oceanography, 31(4): 717-738.

Henrich, R.d., 1998. Dynamics of Atlantic water advection to the Norwegian-Greenland Sea -- a time-slice record of carbonate distribution in the last 300 ky. Marine Geology, 145(1-2): 95-131.

Henrich, R.d., Baumann, K.-H., Huber, R. and Meggers, H., 2002. Carbonate preservation records of the past 3 Myr in the Norwegian-Greenland Sea and the northern North Atlantic: implications for the history of NADW production. Marine Geology, 184(1-2): 17-39.

Hillaire-Marcel, C. and de Vernal, A., 2008. Stable isotope clue to episodic sea ice formation in the glacial North Atlantic. Earth and Planetary Science Letters, 268(1-2): 143-150.

Hilmer, M. and Jung, T., 2000. Evidence for a recent change in the link between the North Atlantic Oscillation and Arctic Sea ice export. Geophys. Res. Lett., 27(7): 989-992.

Hjort, C., 1973. A sea correction for East Greenland. Geologiska Forenungen i Stockholm Forhandlungar, 95: 132-134.

Horner, R., 1985a. Ecology of sea ice microalgae. In: R. Horner (Editor), Sea Ice Biota. CRC Press, Florida, pp. 83-103.

Horner, R., 1985b. Sea Ice Biota. CRC Press, Florida, 224 pp.

Horner, R. and Alexander, V., 1972. Algal populations in arctic sea ice: An investigation of heterotrophy. Limnology and Oceanography, 17(3): 454-458.

Huang, W.-Y. and Meinschein, W.G., 1979. Sterols as ecological indicators. Geochimica et Cosmochimica Acta, 43(5): 739-745.

Hubberten, H.-W., 1995. Die Expedition ARKTIS-X/2 mit FS Polarstern 1994 (The Expedition ARKTIS-X/2 of RV Polarstern in 1994), Alfred Wegener Institute for Polar and Marine Research, Bremerhaven.

Huber, R., Meggers, H., Baumann, K.H. and Henrich, R., 2000. Recent and Pleistocene carbonate dissolution in sediments of the Norwegian-Greenland Sea. Marine Geology, 165(1-4): 123-136.

Hughen, K.A., Baillie, M.G.L., Bard, E., Beck, J.W., Bertrand, C.J.H., Blackwell, P.G., Buck, C.E., Burr, G.S., Cutler, K.B., Damon, P.E., Edwards, R.L., Fairbanks, R.G., Friedrich, M., Guilderson, T.P., Kromer, B., McCormac, G., Manning, S., Ramsey, C.B., Reimer, P.J., Reimer, R.W., Remmele, S., Southon, J.R., Stuiver, M., Talamo, S., Taylor, F.W., van der Plicht, J. and Weyhenmeyer, C.E., 2004. Marine04 marine radiocarbon age calibration, 0-26 cal kyr BP. Radiocarbon, 46(3): 1059-1086.

Hughes, N.E., Wilkinson, J.P. and Wadhams, P., 2011. Multi-satellite sensor analysis of fast-ice development in the Norske Øer Ice Barrier, northeast Greenland. Annals of Glaciology, 52(57): 151-168.

Humlum, O., Elberlin, B., Hormes, A., Fjordheim, K., Hansen, O.H., Heinemeier, J., 2005. Late-Holocene glacier growth in Svalbard, documented by subglacial relict vegetation and living soil microbes. The Holocene, 15: 396-407.

Hurrell, J.W. and Deser, C., 2009. North Atlantic climate variability: The role of the North Atlantic Oscillation. Journal of Marine Systems, 78(1): 28-41.

Hurrell, J.W. and Deser, C., 2010. North Atlantic climate variability: The role of the North Atlantic Oscillation. Journal of Marine Systems, 79(3-4): 231-244.

Imbrie, J., Boyle, E.A., Clemens, S.C., Duffy, A., Howard, W.R., Kukla, G., Kutzbach, J., Martinson, D.G., McIntyre, A., Mix, A.C., Molfino, B., Morley, J.J., Peterson, L.C., Pisias, N.G., Prell, W.L., Raymo, M.E., Shackleton, N.J. and Toggweiler, J.R., 1992. On the Structure and Origin of Major Glaciation Cycles 1. Linear Responses to Milankovitch Forcing. Paleoceanography, 7(6): 701-738.

Jakobsson, M., Backman, J., Rudels, B., Nycander, J., Frank, M., Mayer, L., Jokat, W., Sangiorgi, F., O/'Regan, M., Brinkhuis, H., King, J. and Moran, K., 2007. The early Miocene onset of a ventilated circulation regime in the Arctic Ocean. Nature, 447(7147): 986-990.

Jansen, E., Fronval, T., Rack, F. and Channell, J.E.T., 2000. Pliocene-Pleistocene Ice Rafting History and Cyclicity in the Nordic Seas During the Last 3.5 Myr. Paleoceanography, 15(6): 709-721.

Jennings, A., Andrews, J. and Wilson, L., 2011. Holocene environmental evolution of the SE Greenland Shelf North and South of the Denmark Strait: Irminger and East Greenland current interactions. Quaternary Science Reviews, 30(7-8): 980-998.

Jennings, A.E., Knudsen, K.L., Hald, M., Hansen, C.V. and Andrews, J.T., 2002. A mid-Holocene shift in Arctic sea-ice variability on the East Greenland Shelf. The Holocene, 12(1): 49-58.

Jessen, S.P., Rasmussen, T.L., Nielsen, T. and Solheim, A., 2010. A new Late Weichselian and Holocene marine chronology for the western Svalbard slope 30,000-0 cal years BP. Quaternary Science Reviews, 29(9-10): 1301-1312.

Johns, L., Wraige, E.J., Belt, S.T., Lewis, C.A., Masse, G., Robert, J.M. and Rowland, S.J., 1999. Identification of a C-25 highly branched isoprenoid (HBI) diene in Antarctic sediments, Antarctic sea-ice diatoms and cultured diatoms. Organic Geochemistry, 30(11): 1471-1475.

Jokat, W., 2004. The Expedition ARKTIS XIX/4 of the Research Vessel Polarstern in 2003 Reports of Legs 4a and 4b, Alfred Wegener Institute for Polar and Marine Research, Bremerhaven.

Jones, G.A. and Keigwin, L.D., 1988. Evidence from Fram Strait (78° N) for early deglaciation. Nature, 336: 56-59.

Justwan, A. and Koç, N., 2008. A diatom based transfer function for reconstructing sea ice concentrations in the North Atlantic. Marine Micropaleontology, 66(3-4): 264-278.

Kanazawa, A., Yoshioka, M. and Teshima, S.-I., 1971. The occurrence of brassicasterol in the diatoms, *Cyclotella nana* and *Nitzschia closterium*. Bulletin of the Japanese Society of Scientific Fisheries, 37: 889-903.

Karcher, M.J., Gerdes, R.d., Kauker, F. and Kˆberle, C., 2003. Arctic warming: Evolution and spreading of the 1990s warm event in the Nordic seas and the Arctic Ocean. J. Geophys. Res., 108(C2): 3034.

Kaufman, D.S., Schneider, D.P., McKay, N.P., Ammann, C.M., Bradley, R.S., Briffa, K.R., Miller, G.H., Otto-Bliesner, B.L., Overpeck, J.T., Vinther, B.M. and Arctic Lakes 2k Project, M., 2009. Recent Warming Reverses Long-Term Arctic Cooling. Science, 325(5945): 1236-1239.

Kauker, F., Gerdes, R., Karcher, M., Koeberle, C. and Lieser, J.L., 2003. Variability of Arctic and North Atlantic sea ice: A combined analysis of model results and observations from 1978 to 2001. J. Geophys. Res., 108(C6): 3182.

Kerr, R.A., 1992. Unmasking a Shifty Climate System. Science, 255(5051): 1508-1510.

Kierdorf, C., 2006. Variability of organic carbon along the ice-covered polar continental margin of East Greenland, University of Bremen, Bremerhaven, 241 pp.

Killops, S. and Killops, V., 2005. Introduction to Organic Geochemistry, 2nd edition. Blackwell Publishing, Malden, Oxford, Carlton.

Kleiven, H.F., Kissel, C., Laj, C., Ninnemann, U.S., Richter, T.O. and Cortijo, E., 2008. Reduced North Atlantic Deep Water Coeval with the Glacial Lake Agassiz Freshwater Outburst. Science, 319: 60-64.

Knies, J., 2005. Climate-induced changes in sedimentary regimes for organic matter supply on the continental shelf off northern Norway. Geochimica et Cosmochimica Acta, 69(19): 4631-4647.

Knies, J. and Gaina, C., 2008. Middle Miocene ice sheet expansion in the Arctic: Views from the Barents Sea. Geochem. Geophys. Geosyst., 9(2): Q02015.

Knies, J., Kleiber, H.-P., Matthiessen, J., M¸ller, C. and Nowaczyk, N., 2001. Marine ice-rafted debris records constrain maximum extent of Saalian and Weichselian ice-sheets along the northern Eurasian margin. Global and Planetary Change, 31(1-4): 45-64.

Knies, J., Matthiessen, J., Mackensen, A., Stein, R., Vogt, C., Frederichs, T. and Nam, S.-I., 2007. Effects of Arctic freshwater forcing on thermohaline circulation during the Pleistocene. Geology, 35: 1075-1078.

Knies, J., Matthiessen, J., Vogt, C. and Stein, R., 2002. Evidence of 'Mid-Pliocene (˜3 Ma) global warmth' in the eastern Arctic Ocean and implications for the Svalbard/Barents Sea ice sheet during the late Pliocene and early Pleistocene (˜3 – 1.7 Ma). Boreas, 31(1): 82-93.

Knies, J. and Stein, R., 1998. New aspects of organic carbon deposition and its paleoceanographic implications along the northern Barents Sea margin during the last 30,000 years. Paleoceanography, 13(4): 384-394.

Knies, J., Vogt, C. and Stein, R., 1999. Late Quaternary growth and decay of the Svalbard/Barents Sea ice sheet and paleoceanographic evolution in the adjacent Arctic Ocean. Geo-Marine Letters, 18(3): 195-202.

Koç Karpuz, N. and Schrader, H., 1990. Surface Sediment Diatom Distribution and Holocene Paleotemperature Variations in the Greenland, Iceland and Norwegian Sea. Paleoceanography, 5: 557-580.

Koç, N., Jansen, E. and Haflidason, H., 1993. Paleoceanographic reconstructions of surface ocean conditions in the Greenland, Iceland and Norwegian seas through the last 14 ka based on diatoms. Quaternary Science Reviews, 12(2): 115-140.

Kohly, A., 1998. Diatom flux and species composition in the Greenland and Norwegian Sea in 1991-1992. Marine Geology, 145: 293-312.

Krause, G. and Schauer, U., 2001. The Expeditions ARKTIS XVI/1 and ARKTIS XVI/2 of the Research Vessel Polarstern in 2000., Alfred Wegener Institute for Polar and Marine Research, Bremerhaven.

Krylov, A.A., Andreeva, I.A., Vogt, C., Backman, J., Krupskaya, V.V., Grikurov, G.E., Moran, K. and Shoji, H., 2008. A shift in heavy and clay mineral provenance indicates a middle Miocene onset of a perennial sea ice cover in the Arctic Ocean. Paleoceanography, 23(1): PA1S06.

Kwok, R., 2000. Recent Changes in Arctic Ocean Sea Ice Motion Associated with the North Atlantic Oscillation. GEOPHYSICAL RESEARCH LETTERS, 27(6): 775-778.

Kwok, R., Cunningham, G.F. and Pang, S.S., 2004. Fram Strait sea ice outflow. J. Geophys. Res., 109(C1): C01009.

Kwok, R. and Rothrock, D.A., 1999. Variability of Fram Strait ice flux and North Atlantic Oscillation. J. Geophys. Res., 104(C3): 5177-5189.

Langford, F.F. and Blanc-Valleron, M.M., 1990. Interpreting Rock-Eval pyrolysis data using graphs of pyrolyzable hydrocarbons vs. total organic carbon. American Association of Petroleum Geologists Bulletin, 74: 799-804.

Laskar, J., Robutel, P., Joutel, F., Gastineau, M., Correia, A.C.M. and Levrard, B., 2004. A long-term numerical solution for the insolation quantities of the Earth. Astronomy and Astrophysics, 428(1): 261-285.

Lemke, P., 2003. The Expedition ARKTIS XVIII/1a, b of the research vessel Polarstern in 2002, Alfred Wegener Institute for Polar and Marine Research, Bremerhaven.

Lemke, P., J. Ren, R.B. Alley, I. Allison, J. Carrasco, G. Flato, Y. Fujii, G. Kaser, P. Mote, R.H. Thomas and T. Zhang, 2007. Observations: Changes in Snow, Ice and Frozen Ground. In: S. Solomon, D. Qin, M. Manning, Z. Chen, M. Marquis, K.B. Averyt, M. Tignor and H.L. Miller (eds.) (Editor), Climate Change 2007: The Physical Science Basis. Contribution of Working Group I to the Fourth Assessment Report of the Intergovernmental Panel on Climate Change. Cambridge University Press, Cambridge and New York.

Light, B., Eicken, H., Maykut, G.A. and Grenfell, T.C., 1998. The effect of included participates on the spectral albedo of sea ice. J. Geophys. Res., 103(C12): 27739-27752.

Lisiecki, L.E. and Raymo, M.E., 2005. A Pliocene-Pleistocene stack of 57 globally distributed benthic δ18O records. Paleoceanography, 20(1): PA1003.

Lisitzin, A.P., 2002. Sea-Ice and Iceberg Sedimentation in the Ocean: Recent and Past. Springer, Berlin Heidelberg New York.

Lorenz, S.J. and Lohmann, G., 2004. Acceleration technique for Milankovitch type forcing in a coupled atmosphere-ocean circulation model: method and application for the Holocene. Climate Dynamics, 23(7): 727-743.

Macdonald, R.W., Sakshaug, E. and Stein, R., 2004. The Arctic Ocean: Modern Status and Recent Climate Change. In: R. Stein and R.W. Macdonald (Editors), The Organic Carbon Cycle In The Arctic Ocean. Springer, Berlin Heidelberg New York, pp. 6-20.

Madureira, L.A.S., van Kreveld, S.A., Eglinton, G., Conte, M.H., Ganssen, G., van Hinte, J.E. and Ottens, J.J., 1997. Late Quaternary High-Resolution Biomarker and Other Sedimentary Climate Proxies in a Northeast Atlantic Core. Paleoceanography, 12(2): 255-269.

Mangerud, J., Dokken, T., Hebbeln, D., Heggen, B., Ingolfsson, O., Landvik, J.Y., Mejdahl, V., Svendsen, J.I. and Vorren, T.O., 1998. Fluctuations of the Svalbard-Barents sea ice sheet during the last 150 000 years. Quaternary Science Reviews, 17(1-3): 11-42.

Mangerud, J. and Svendsen, J.I., 1992. The last interglacial-glacial period on Spitsbergen, Svalbard. Quaternary Science Reviews, 11(6): 633-664.

Martin, T. and Wadhams, P., 1999. Sea-ice flux in the East Greenland Current. Deep Sea Research Part II: Topical Studies in Oceanography, 46(6-7): 1063-1082.

Massé, G., Rowland, S.J., Sicre, M.-A., Jacob, J., Jansen, E. and Belt, S.T., 2008. Abrupt climate changes for Iceland during the last millennium: Evidence from high resolution sea ice reconstructions. Earth and Planetary Science Letters, 269: 565-569.

Matthiessen, J., Baumann, K.-H., Schröder-Ritzrau, A., Hass, C., Andruleit, H., Baumann, A., Jensen, S., Kohly, A., Pflaumann, U., Samtleben, C., Schäfer, P. and Thiede, J., 2001. Distribution of calcareous, siliceous and organic-walled planktic mircofossils in surface sediments of the Nordic Seas and their relation to surface-water mass. In: P. Schäfer, Ritzrau, W., Schlüter, M., Thiede, J. (Editor), The Northern North Atlantic: A changing environment. Springer, Berlin Heidelberg New York, pp. 105-127.

Matthiessen, J. and Brenner, W., 1996. Dinoflagellate Cyst Ecostratigraphy of Pliocene-Pleistocene Sediments from the Yermak Plateau (Arctic Ocean, Hole 911A). In: J. Thiede, A.M. Myhre, J.V. Firth, G.L. Johnson and W.F. Ruddiman (Editors), Proceedings of the Ocean Drilling Program, Scientific Results. College Station, Texas, pp. 243-253.

Matthiessen, J. and Knies, J., 2001. Dinoflagellate cyst evidence for warm interglacial conditions at the northern Barents Sea margin during marine oxygen isotope stage 5. Journal of Quaternary Science, 16(7): 727-737.

Matthiessen, J., Knies, J., Vogt, C. and Stein, R., 2009. Pliocene palaeoceanography of the Arctic Ocean and subarctic seas. Philosophical Transactions of the Royal Society A: Mathematical, Physical and Engineering Sciences, 367(1886): 21-48.

McManus, J.F., Oppo, D.W., Keigwin, L.D., Cullen, J.L. and Bond, G.C., 2002. Thermohaline Circulation and Prolonged Interglacial Warmth in the North Atlantic. Quaternary Research, 58(1): 17-21.

Meyers, P.A., 1994. Preservation of elemental and isotopic source identification of sedimentary organic matter. Chemical Geology, 114(3-4): 289-302.

Meyers, P.A., 1997. Organic geochemical proxies of paleoceanographic, paleolimnologic, and paleoclimatic processes. Organic Geochemistry, 27(5-6): 213-250.

Miller, G.H., Alley, R.B., Brigham-Grette, J., Fitzpatrick, J.J., Polyak, L., Serreze, M.C. and White, J.W.C., 2010a. Arctic amplification: can the past constrain the future? Quaternary Science Reviews, 29(15-16): 1779-1790.

Miller, G.H., Brigham-Grette, J., Alley, R.B., Anderson, L., Bauch, H.A., Douglas, M.S.V., Edwards, M.E., Elias, S.A., Finney, B.P., Fitzpatrick, J.J., Funder, S.V., Herbert, T.D., Hinzman, L.D., Kaufman, D.S., MacDonald, G.M., Polyak, L., Robock, A., Serreze, M.C., Smol, J.P., Spielhagen, R., White, J.W.C., Wolfe, A.P. and Wolff, E.W., 2010b. Temperature and precipitation history of the Arctic. Quaternary Science Reviews, 29(15-16): 1679-1715.

Moros, M., Andrews, J.T., Eberl, D.D. and Jansen, E., 2006. Holocene history of drift ice in the northern North Atlantic: Evidence for different spatial and temporal modes. Paleoceanography, 21(2): PA2017.

Müller, J., Massé, G., Stein, R. and Belt, S.T., 2009. Variability of sea-ice conditions in the Fram Strait over the past 30,000 years. Nature Geoscience, 2(11): 772-776. doi:10.1038/ngeo665.

Müller, J., Wagner, A., Fahl, K., Stein, R., Prange, M. and Lohmann, G., 2011. Towards quantitative sea ice reconstructions in the northern North Atlantic: A combined biomarker and numerical modelling approach. Earth and Planetary Science Letters, 306 (3-4): 137-148. doi:10.1016/j.epsl.2011.04.011.

Müller, P.J., 1977. C/N ratios in Pacific deep-sea sediments: Effect of inorganic ammonium and organic nitrogen compounds sorbed by clays. Geochimica et Cosmochimica Acta, 41(6): 765-776.

Müller, P.J., Kirst, G., Ruhland, G., von Storch, I. and Rosell-Melé, A., 1998. Calibration of the alkenone paleotemperature index U37K' based on core-tops from the eastern South Atlantic and the global ocean (60°N-60°S). Geochimica et Cosmochimica Acta, 62(10): 1757-1772.

Nam, S.-I., Stein, R., Grobe, H. and Hubberten, H., 1995. Late Quaternary glacial-interglacial changes in sediment composition at the East Greenland continental margin and their paleoceanographic implications. Marine Geology, 122(3): 243-262.

Nansen, F., 1930. In Nacht und Eis, 1. Brockhaus, Leipzig, 527 pp.

Nesje, A., Matthews, J.A., Dahl, S.O., Berrisford, M.S. and Andersson, C., 2001. Holocene glacier fluctuations of Flatebreen and winter-precipitation changes in the Jostedalsbreen region, western Norvay, based on glaciolacustrine sediment records The Holocene, 11(3): 267-280.

NGRIP-Members, 2004. High-resolution record of Northern Hemisphere climate extending into the last interglacial period. Nature, 431(7005): 147-151.

Nørgaard-Pedersen, N., Mikkelsen, N., Lassen, S.J., Kristoffersen, Y. and Sheldon, E., 2007. Reduced sea ice concentrations in the Arctic Ocean during the last interglacial period revealed by sediment cores off northern Greenland. Paleoceanography, 22(1): PA1218.

Nørgaard-Pedersen, N., Spielhagen, R.F., Erlenkeuser, H., Grootes, P.M., Heinemeier, J. and Knies, J., 2003. Arctic Ocean during the Last Glacial Maximum: Atlantic and polar domains of surface water mass distribution and ice cover. Paleoceanography, 18(3): 1063-1082.

NSIDC, Boulder, USA. http://nsidc.org/data/seaice_index/archives/, accessed August 2010.

NSIDC, http://nsidc.org/; accessed April 2011. National Snow and Ice Data Center, University of Colorado at Boulder, USA.

Nürnberg, D., Wollenburg, I., Dethleff, D., Eicken, H., Kassens, H., Letzig, T., Reimnitz, E. and Thiede, J., 1994. Sediments in Arctic sea ice: Implications for entrainment, transport and release. Marine Geology, 119(3-4): 185-214.

Otto-Bliesner, B.L., Marshall, S.J., Overpeck, J.T., Miller, G.H., Hu, A. and CAPE-Last-Interglacial-Project-members, 2006. Simulating Arctic Climate Warmth and Icefield Retreat in the Last Interglaciation. Science, 311(5768): 1751-1753.

Peinert, R., Antia, A., Bauerfeind, E., von Bodungen, B., Haupt, O., Krumbholz, M., Peeken, I., Ramseier, R.O., Voss, M. and Zeitzschel, B., 2001. Particle Flux Variability in the Polar and Atlantic Biogeochemical Provinces of the Nordic Seas. In: P. Schäfer, Ritzrau, W., Schlüter, M., Thiede, J. (Editor), The Northern North Atlantic: A Changing Environment. Springer, Berlin, pp. 53-68.

Perovich, D.K., Grenfell, T.C., Light, B., Elder, B.C., Harbeck, J., Polashenski, C., Tucker, W.B., III and Stelmach, C., 2009. Transpolar observations of the morphological properties of Arctic sea ice. J. Geophys. Res., 114.

Peters, K.E., Walters, C.C. and Moldowan, J.M., 2005. The Biomarker Guide, 1+2. Cambridge University Press, Cambridge, 1131 pp.

Pflaumann, U., Duprat, J., Pujol, C. and Labeyrie, L.D., 1996. SIMMAX: A Modern Analog Technique to Deduce Atlantic Sea Surface Temperatures from Planktonic Foraminifera in Deep-Sea Sediments. Paleoceanography, 11(1): 15-35.

Pflaumann, U., Sarnthein, M., Chapman, M., d'Abreu, L., Funnell, B., Huels, M., Kiefer, T., Maslin, M., Schulz, H., Swallow, J., van Kreveld, S., Vautravers, M., Vogelsang, E. and Weinelt, M., 2003. Glacial North Atlantic: Sea-surface conditions reconstructed by GLAMAP 2000. Paleoceanography, 18: 1065.

Polyak, L., Alley, R.B., Andrews, J.T., Brigham-Grette, J., Cronin, T.M., Darby, D.A., Dyke, A.S., Fitzpatrick, J.J., Funder, S., Holland, M., Jennings, A.E., Miller, G.H., O'Regan, M., Savelle, J., Serreze, M., St. John, K., White, J.W.C. and Wolff, E., 2010. History of sea ice in the Arctic. Quaternary Science Reviews, 29(15-16): 1757-1778.

Pryce, R.J., 1971. The occurrence of bound, water-soluble squalene, 4,4-dimethyl sterols, 4[alpha]-methyl sterols and sterols in leaves of Kalanchoe blossfeldiana. Phytochemistry, 10(6): 1303-1307.

Ramseier, R.O., Garrity, C., Bauerfeind, E. and Peinert, R., 1999. Sea-ice impact on long-term particle flux in the Greenland Sea's Is Odden-Nordbukta region, 1985-1996. J. Geophys. Res., 104(C3): 5329-5343.

Ramseier, R.O., Garrity, C., Martin, T., 2001. An Overview of Sea-Ice Conditions in the Greenland Sea and the Relationship of Oceanic Sedimentation to the Ice Regime. In: P. Schäfer, Ritzrau, W., Schlüter, M., Thiede, J. (Editor), The Northern North Atlantic: A Changing Environment. Springer, Berlin, pp. 19-38.

Rasmussen, T.L., Thomsen, E., Slubowska, M.A., Jessen, S., Solheim, A. and Koç, N., 2007. Paleoceanographic evolution of the SW Svalbard margin (76°N) since 20,000 14C yr BP. Quaternary Research, 67(1): 100-114.

Raymo, M.E., Hodell, D. and Jansen, E., 1992. Response of Deep Ocean Circulation to Initiation of Northern Hemisphere Glaciation (3-2 MA). Paleoceanography, 7(5): 645-672.

Rey, F., Noji, T.T. and Miller, L.A., 2000. Seasonal phytoplankton development and new production in the central Greenland Sea. Sarsia, 85(4): 329-344.

Richardson, K., Markager, S., Buch, E., Lassen, M.F. and Kristensen, A.S., 2005. Seasonal distribution of primary production, phytoplankton biomass and size distribution in the Greenland Sea. Deep Sea Research Part I: Oceanographic Research Papers, 52(6): 979-999.

Risebrobakken, B.r., Moros, M., Ivanova, E.V., Chistyakova, N. and Rosenberg, R., 2010. Climate and oceanographic variability in the SW Barents Sea during the Holocene. The Holocene.

Robson, J.N. and Rowland, S.J., 1988. Biodegradation of highly branched isoprenoid hydrocarbons: A possible explanation of sedimentary abundance. Organic Geochemistry, 13(4-6): 691-695.

Roeckner, E., Brokopf, R., Esch, M., Giorgetta, M., Hagemann, S., Kornblueh, L., Manzini, E., Schlese, U. and Schulzweida, U., 2006. Sensitivity of Simulated Climate to Horizontal and Vertical Resolution in the ECHAM5 Atmosphere Model. Journal of Climate, 19(16): 3771-3791.

Romankevich, E.A., 1984. Geochemistry of Organic Matter in the Ocean. Springer, Berlin Heidelberg New York Tokyo, 335 pp.

Rontani, J.-F., Belt, S.T., Vaultier, F. and Brown, T.A., in press. Visible light induced photo-oxidation of highly branched isoprenoid (HBI) alkenes: significant dependence on number and nature of double bonds. Organic Geochemistry.

Rowland, S.J., Belt, S.T., Wraige, E.J., Masse, G., Roussakis, C. and Robert, J.M., 2001. Effects of temperature on polyunsaturation in cytostatic lipids of Haslea ostrearia. Phytochemistry, 56(6): 597-602.

Rowland, S.J. and Robson, J.N., 1990. The widespread occurrence of highly branched acyclic C20, C25 and C30 hydrocarbons in recent sediments and biota--A review. Marine Environmental Research, 30(3): 191-216.

Rudels, B., 1996. The thermohaline circulation of the Arctic Ocean and the Greenland Sea. In: P. Wadhams, J.A. Dowdeswell and A.N. Schofield (Editors), The Arctic And Environmental Change. Gordon and Breach, Amsterdam, pp. 87-99.

Rudels, B., Bjork, G., Nilsson, J., Winsor, P., Lake, I. and Nohr, C., 2005. The interaction between waters from the Arctic Ocean and the Nordic Seas north of Fram Strait and along the East Greenland Current: results from the Arctic Ocean-02 Oden expedition. Journal of Marine Systems, 55(1-2): 1-30.

Rudels, B., Fahrbach, E., Meincke, J., Budeus, G. and Eriksson, P., 2002. The East Greenland Current and its contribution to the Denmark Strait overflow. ICES J. Mar. Sci., 59(6): 1133-1154.

Rudels, B., J. Friedrich, H. and Quadfasel, D., 1999. The Arctic Circumpolar Boundary Current. Deep Sea Research Part II: Topical Studies in Oceanography, 46(6-7): 1023-1062.

Rudels, B. and Quadfasel, D., 1991. Convection and deep water formation in the Arctic Ocean-Greenland Sea System. Journal of Marine Systems, 2(3-4): 435-450.

Saenko, O.A., Eby, M. and Weaver, A.J., 2004. The effect of sea-ice extent in the North Atlantic on the stability of the thermohaline circulation in global warming experiments. Climate Dynamics, 22(6): 689-699.

Sakshaug, E., 2004. Primary and secondary production in the Arctic Seas. In: R. Stein and R.W. Macdonald (Editors), The organic carbon cycle in the Arctic Ocean. Springer-Verlag, Heidelberg, pp. 57-82.

Salonen, J.S., Seppö, H., Väliranta, M., Jones, V.J., Self, A., Heikkilä, M., Kultti, S. and Yang, H., 2011. The Holocene thermal maximum and late-Holocene cooling in the tundra of NE European Russia. Quaternary Research, 75(3): 501-511.

Salvigsen, O., Forman, S.L. and Miller, G.H., 1992. Thermophilous molluscs on Svalbard during the Holocene and their paleoclimatic implications. Polar Research, 11(1): 1-10.

Sarnthein, M., Pflaumann, U. and Weinelt, M., 2003a. Past extent of sea ice in the northern North Atlantic inferred from foraminiferal paleotemperature estimates. Paleoceanography, 18(2): 1047-1058.

Sarnthein, M., Van Kreveld, S., Erlenkeuser, H., Grootes, P.M., Kucera, M., Pflaumann, U. and Schulz, M., 2003b. Centennial-to-millennial-scale periodicities of Holocene climate and sediment injections off the western Barents shelf, 75°N. Boreas, 32(3): 447-461.

Schauer, U., Rudels, B., Jones, E.P., Anderson, L.G., Muench, R.D., Björk, G., Swift, J.H., Ivanov, V. and Larsson, A.-M., 2002. Confluence and redistribution of Atlantic water in the Nansen, Amundsen and Makarov basins. Annals Geophysicae, 20: 257-273.

Schlitzer, R., 2009. Ocean Data View, http://odv.awi.de.

Schlüter, M. and Sauter, E., 2000. Biogenic silica cycle in surface sediments of the Greenland Sea. Journal of Marine Systems, 23(4): 333-342.

Schubert, C.J. and Stein, R., 1996. Deposition of organic carbon in Arctic Ocean sediments: terrigenous supply vs marine productivity. Organic Geochemistry, 24(4): 421-436.

Seppä, H. and Birks, H.J.B., 2002. Holocene Climate Reconstructions from the Fennoscandian Tree-Line Area Based on Pollen Data from Toskaljavri. Quaternary Research, 57(2): 191-199.

Serreze, M.C., Holland, M.M. and Stroeve, J., 2007. Perspectives on the Arctic's Shrinking Sea-Ice Cover. Science, 315(5818): 1533-1536.

Slubowska-Woldengen, M., Koç, N., Rasmussen, T.L., Klitgaard-Kristensen, D., Hald, M. and Jennings, A.E., 2008. Time-slice reconstructions of ocean circulation changes on the continental shelf in the Nordic and Barents Seas during the last 16,000 cal yr B.P. Quaternary Science Reviews, 27(15-16): 1476-1492.

Slubowska-Woldengen, M., Rasmussen, T.L., Koc, N., Klitgaard-Kristensen, D., Nilsen, F. and Solheim, A., 2007. Advection of Atlantic Water to the western and northern Svalbard shelf since 17,500 cal yr BP. Quaternary Science Reviews, 26(3-4): 463-478.

Smith, S.L., Smith, W.O., Codispoti, L.A. and Wilson, D.L., 1985. Biological observations in the marginal ice zone of the East Greenland Sea. Journal of Marine Research, 43: 693-717.

Smith, W.O., Jr., Baumann, M.E.M., Wilson, D.L. and Aletsee, L., 1987. Phytoplankton Biomass and Productivity in the Marginal Ice Zone of the Fram Strait During Summer 1984. J. Geophys. Res., 92: 6777-6786.

Solomon, S., Qin, D., Manning, M., Chen, Z., Marquis, M., Averyt, K.B., Tignor, M., Miller, H.L. and (eds.), 2007. Contribution of Working Group I to the Fourth Assessment Report of the Intergovernmental Panel on Climate Change, 2007, Cambridge and New York.

Spielhagen, R.F., Baumann, K.-H., Erlenkeuser, H., Nowaczyk, N.R., Nørgaard-Pedersen, N., Vogt, C. and Weiel, D., 2004. Arctic Ocean deep-sea record of northern Eurasian ice sheet history. Quaternary Science Reviews, 23(11-13): 1455-1483.

Spielhagen, R.F., Kirstin Werner, Steffen Aagaard Sørensen, Katarzyna Zamelczyk, Evguenia Kandiano, Gereon Budeus, Katrine Husum, Thomas M. Marchitto and Hald, a.M., 2011. Enhanced Modern Heat Transfer to the Arctic by Warm Atlantic Water. Science, 331: 450-453.

Spreen, G., Kaleschke, L. and Heygster, G., 2008. Sea ice remote sensing using AMSR-E 89-Ghz channels. Journal of Geophysical Research, 113(C02S03).

Spreen, G., Kern, S., Stammer, D., Forsberg, R., Haarpaintner, J. and rg, 2006. Satellite-based estimates of sea-ice volume flux through Fram Strait. Annals of Glaciology, 44: 321-328.

St. John, K., 2008. Cenozoic ice-rafting history of the central Arctic Ocean: Terrigenous sands on the Lomonosov Ridge. Paleoceanography, 23(1): PA1S05.

Steele, M. and Boyd, T., 1998. Retreat of the cold halocline layer in the Arctic Ocean. J. Geophys. Res., 103(C5): 10419-10435.

Steele, M., Morley, R. and Ermold, W., 2001. PHC: A Global Ocean Hydrography with a High-Quality Arctic Ocean. Journal of Climate, 14(9): 2079-2087.

Stein, R., 1990. Organic carbon content/sedimentation rate relationship and its paleoenvironmental significance for marine sediments. Geo-Marine Letters, 10(1): 37-44.

Stein, R., 2008a. Arctic Ocean Sediments: Processes, Proxies, And Paleoenvironment. Developments in Marine Geology, 2. Elsevier, Amsterdam, 592 pp.

Stein, R., 2008b. Glacio-marine sedimentary processes. In: R. Stein (Editor), Arctic Ocean Sediments: Processes, Proxies, and Paleoenvironment. Elsevier, Amsterdam Boston Heidelberg London New York Oxford Paris, pp. 87-126.

Stein, R., Boucsein, B. and Meyer, H., 2006. Anoxia and high primary production in the Paleogene central Arctic Ocean: First detailed records from Lomonosov Ridge. Geophys. Res. Lett., 33(18): L18606.

Stein, R., Dittmers, K., Fahl, K., Kraus, M., Matthiessen, J., Niessen, F., Pirrung, M., Polyakova, Y., Schoster, F., Steinke, T. and Futterer, D.K., 2004. Arctic (palaeo) river discharge and environmental change: evidence from the Holocene Kara Sea sedimentary record. Quaternary Science Reviews, 23(11-13): 1485-1511.

Stein, R. and Fahl, K., 1997. Scientific Cruise Report of the Arctic Expedition ARK-XIII/2 of RV Polarstern in 1997 Alfred Wegener Institute for Polar and Marine Research, Bremerhaven.

Stein, R. and Macdonald, R.W., 2004a. Geochemical Proxies used for Organic Carbon Source Identification in Arctic Ocean Sediments. In: R. Stein and R.W. Macdonald (Editors), The Organic Carbon Cycle In The Arctic Ocean. Springer, Berlin, pp. 24-32.

Stein, R. and Macdonald, R.W., 2004b. The organic carbon cycle in the Arctic Ocean. Springer, Berlin, 363 pp.

Stein, R., Nam, S.-I., Grobe, H. and Hubberten, H.-W., 1996. Late Quaternary glacial history and short-term ice-rafted debris fluctuations along the East Greenland continental margin. In: J.T. Andrews, W.E.N. Austin, H. Bergsten and A.E. Jennings (Editors), Late Quaternary Palaeoceanography of the North Atlantic Margins. Geological Society, London, pp. 135-151.

Stein, R. and Stax, R., 1991. Late quaternary organic carbon cycles and paleoproductivity in the Labrador Sea. Geo-Marine Letters, 11(2): 90 - 95.

Steinsund, P.I. and Hald, M., 1994. Recent calcium carbonate dissolution in the Barents Sea: Paleoceanographic applications. Marine Geology, 117(1-4): 303-316.

Stevenson, F.J. and Cheng, C.N., 1972. Organic geochemistry of the Argentine Basin sediments: Carbon-nitrogen relationships and Quaternary correlations. Geochimica et Cosmochimica Acta, 36(6): 653-671.

Stickley, C. E., St John, K., Koç, N., Jordan, R. W., Passchier, S., Pearce, R.B., Kearns, L.E., 2009. Evidence for middle Eocene Arctic sea ice from diatoms and ice-rafted debris. Nature 460(7253): 376-379.

Stuiver, M. and Grootes, P.M., 2000. GISP2 Oxygen Isotope Ratios. Quaternary Research, 53(3): 277-284.

Stuiver, M. and Reimer, P.J., 1993. Extended (super 14) C data base and revised CALIB 3.0 (super 14) C age calibration program. Radiocarbon, 35(1): 215-230.

Stuiver, M., Reimer, P.J., Bard, E., Beck, J.W., Burr, G.S., Hughen, K.A., Kromer, B., McCormac, G., van der Plicht Johannes and Spurk, M., 1998. INTCAL98 radiocarbon age calibration, 24,000-0 cal BP. Radiocarbon, 40(3): 1041-1083.

Stuiver, M., Reimer, P.J. and Reimer, R.W., 2005. CALIB 5.0 (program and documentation), http://calib.qub.ac.uk/calib/.

Svendsen, J.I., Alexanderson, H., Astakhov, V.I., Demidov, I., Dowdeswell, J.A., Funder, S., Gataullin, V., Henriksen, M., Hjort, C., Houmark-Nielsen, M., Hubberten, H.W., Ingolfsson, O., Jakobsson, M., Kjär, K.H., Larsen, E., Lokrantz, H., Lunkka, J.P., Lysa, A., Mangerud, J., Matiouchkov, A., Murray, A., Mˆller, P., Niessen, F., Nikolskaya, O., Polyak, L., Saarnisto, M., Siegert, C., Siegert, M.J., Spielhagen, R.F. and Stein, R., 2004. Late Quaternary ice sheet history of northern Eurasia. Quaternary Science Reviews, 23(11-13): 1229-1271.

Svendsen, J.I. and Mangerud, J., 1997. Holocene glacial and climatic variations on Spitsbergen, Svalbard. The Holocene, 7: 45-57.

Swerpel, S., 1985. The Hornsund Fiord: Water Masses. Polish Polar Research, 6: 475-496.

Teller, J.T., Leverington, D.W. and Mann, J.D., 2002. Freshwater outbursts to the oceans from glacial Lake Agassiz and their role in climate change during the last deglaciation. Quaternary Science Reviews, 21(8-9): 879-887.

Thiede, J., Winkler, A., Wolf-Welling, T., Eldholm, O., Myhre, A.M., Baumann, K.-H., Henrich, R. and Stein, R., 1998. Late Cenozoic history of the polar North Atlantic: Results from Ocean Drilling. Quaternary Science Reviews, 17(1-3): 185-208.

Thornalley, D.J.R., McCave, I.N. and Elderfield, H., 2010. Freshwater input and abrupt deglacial climate change in the North Atlantic. Paleoceanography, 25: PA1201.

Tissot, B.P. and Welte, D.H., 1984. Petroleum Formation and Occurrence. Springer, Berlin Heidelberg New York Tokyo, 699 pp.

Untersteiner, N., 1982. The Sea-Air Interface. In: L. Rey (Editor), The Arctic Ocean. Macmillan Press, London, pp. 113-130.

Van Nieuwenhove, N., Bauch, H.A., Eynaud, F., Kandiano, E., Cortijo, E. and Turon, J.-L., 2011. Evidence for delayed poleward expansion of North Atlantic surface waters during the last interglacial (MIS 5e). Quaternary Science Reviews, 30(7-8): 934-946.

Vare, L.L., Massé, G. and Belt, S.T., 2010. A biomarker-based reconstruction of sea ice conditions for the Barents Sea in recent centuries. The Holocene: DOI: 10.1177/0959683609355179.

Vare, L.L., Massé, G., Gregory, T.R., Smart, C.W. and Belt, S.T., 2009. Sea ice variations in the central Canadian Arctic Archipelago during the Holocene. Quaternary Science Reviews, 28(13-14): 1354-1366.

Vellinga, M. and Wood, R., 2008. Impacts of thermohaline circulation shutdown in the twenty-first century. Climatic Change, 91(1): 43-63.

Vinje, T., 1977. Sea ice conditions in the European sector of the marginal seas of the Arctic, 1966-1975. Norsk Polarinstitutt Årbok 1975: 163-174.

Vinje, T., 2001a. Anomalies and Trends of Sea-Ice Extent and Atmospheric Circulation in the Nordic Seas during the Period 1864–1998. Journal of Climate, 14(3): 255-267.

Vinje, T., 2001b. Fram Strait Ice Fluxes and Atmospheric Circulation: 1950–2000. Journal of Climate 14(16): 3508-3517.

Vinje, T., Nordlund, N. and Kvambekk, Å., 1998. Monitoring ice thickness in Fram Strait. J. Geophys. Res., 103(C5): 10437-10449.

Vinje, T.E., 1982. The Drift Pattern of Sea Ice in the Arctic with particular Reference to the Atlantic Approach. In: L. Rey (Editor), The Arctic Ocean. Macmillan Press, London, pp. 43-68.

Vogt, C., Knies, J., Spielhagen, R.F. and Stein, R., 2001. Detailed mineralogical evidence for two nearly identical glacial/deglacial cycles and Atlantic water advection to the Arctic Ocean during the last 90,000 years. Global and Planetary Change, 31(1-4): 23-44.

Vogt, P.R., 1986. Geophysical and geochemical signatures and plate tectonics. In: B.G. Hurdle (Editor), The Nordic Seas. Springer, New York Berlin Heidelberg Tokyo, pp. 413-662.

Volkman, J.K., 1986. A review of sterol markers for marine and terrigenous organic matter. Organic Geochemistry, 9(2): 83-99.

Volkman, J.K., 2006. Lipid markers for marine organic matter. In: J.K. Volkman (Editor), Handbook of Environmental Chemistry. Springer-Verlag, Berlin, Heidelberg, pp. 27-70.

Volkman, J.K., Barrett, S.M., Blackburn, S.I., Mansour, M.P., Sikes, E.L. and Gelin, F., 1998. Microalgal biomarkers: A review of recent research developments. Organic Geochemistry, 29(5-7): 1163-1179.

Volkman, J.K., Barrett, S.M. and Dunstan, G.A., 1994. C25 and C30 highly branched isoprenoid alkenes in laboratory cultures of two marine diatoms. Organic Geochemistry, 21(3-4): 407-414.

Volkman, J.K., Barrett, S.M., Dunstan, G.A. and Jeffrey, S.W., 1993. Geochemical significance of the occurrence of dinosterol and other 4-methyl sterols in a marine diatom. Organic Geochemistry, 20(1): 7-15.

Wadhams, P., 1990. Evidence for thinning of the Arctic ice cover north of Greenland. Nature, 345(6278): 795-797.

Wadhams, P., 1992. Sea Ice Thickness Distribution in the Greenland Sea and Eurasian Basin, May 1987. J. Geophys. Res., 97(C4): 5331-5348.

Wadhams, P., 1997. Ice thickness in the Arctic Ocean: The statistical reliability of experimental data. J. Geophys. Res., 102(C13): 27951-27959.

Wadhams, P., 2000. Ice in the Ocean. Gordon and Breach, Amsterdam.

Wadhams, P., Comiso, J.C., Prussen, E., Wells, S., Brandon, M., Aldworth, E., Viehoff, T., Allegrino, R. and Crane, D.R., 1996. The development of the Odden ice tongue in the Greenland Sea during winter 1993 from remote sensing and field observations. J. Geophys. Res., 101: 213-235.

Wakeham, S.G. and Canuel, E.A., 2006. Degradation and preservation of organic matter in marine sediments. In: O. Hutzinger and J.K. Volkman (Editors), The Handbook of Environmental Chemistry. Springer Verlag, Berlin Heidelberg New York, pp. 295-321.

Walker, G.T. and Bliss, E.W., 1932. World Weather V. Mem. Roy. Meteor. Soc., 4: 53-84.

Wassmann, P., Bauerfeind, E., Fortier, M., Fukuchi, M., Hargrave, B., Moran, B., Noji, T., Nöthig, E.-M., Olli, K., Peinert, R., Sasaki, H. and Shevchenko, V., 2004. Particulate Organic Carbon Flux to the Arctic Ocean Sea Floor. In: R. Stein and R.W. Macdonald (Editors), The Organic Carbon Cycle in the Arctic Ocean. Springer, Berlin Heidelberg, pp. 101-138.

Watson, A.J., Messias, M.J., Fogelqvist, E., Van Scoy, K.A., Johannessen, T., Oliver, K.I.C., Stevens, D.P., Rey, F., Tanhua, T., Olsson, K.A., Carse, F., Simonsen, K., Ledwell, J.R., Jansen, E., Cooper, D.J., Kruepke, J.A. and Guilyardi, E., 1999. Mixing and convection in the Greenland Sea from a tracer-release experiment. Nature, 401(6756): 902-904.

Werner, K., Spielhagen, R.F., Bauch, D., Hass, H.C., Kandiano, E., Zamelczyk, K., 2011. Atlantic Water advection to the eastern Fram Strait - Multiproxy evidence for late Holocene variability. Palaeogeography, Palaeoclimatology, Palaeoecology, 308, (3-4): 264-276.

Wiktor, J., 1999. Early spring microplankton development under fast ice covered fjords of Svalbard, Arctic Oceanologia, 41(1): 51-72.

Wolf, T.C.W. and Thiede, J., 1991. History of terrigenous sedimentation during the past 10 m.y. in the North Atlantic (ODP Legs 104 and 105 and DSDP Leg 81). Marine Geology, 101(1-4): 83-102.

Wolf-Welling, T., Cremer, M., O'Connell, S., Winkler, A. and Thiede, J., 1996. Cenozoic Arctic Gateway Paleoclimate Variability: Indications from Changes in Coarse-Fraction Composition. In: J. Thiede, A.M. Myhre, J.V. Firth, G.L. Johnson and W.F. Ruddiman (Editors), Proceedings of the Ocean Drilling Program, Scientific Results. College Station, Texas, pp. 515-567.

Wollenburg, J.E., Knies, J. and Mackensen, A., 2004. High-resolution paleoproductivity fluctuations during the past 24 kyr as indicated by benthic foraminifera in the marginal Arctic Ocean. Palaeogeography, Palaeoclimatology, Palaeoecology, 204(3-4): 209-238.

Wyrtki, K., 1961. The thermohaline circulation in relation to the general circulation in the oceans. Deep Sea Research (1953), 8(1): 39-64.

Xu, Y., Jaffe, R., Wachnicka, A. and Gaiser, E.E., 2006. Occurrence of C25 highly branched isoprenoids (HBIs) in Florida Bay: Paleoenvironmental indicators of diatom-derived organic matter inputs. Organic Geochemistry, 37(7): 847-859.

Youngblood, W.W. and Blumer, M., 1973. Alkanes and alkenes in marine benthic algae. Marine Biology, 21(3): 163-172.

Yunker, M.B., Belicka, L.L., Harvey, H.R. and Macdonald, R.W., 2005. Tracing the inputs and fate of marine and terrigenous organic matter in Arctic Ocean sediments: A multivariate analysis of lipid biomarkers. Deep Sea Research Part II: Topical Studies in Oceanography, 52(24-26): 3478-3508.

Zhang, J., Rothrock, D.A. and Steele, M., 1998. Warming of the Arctic Ocean by a strengthened Atlantic Inflow: Model results. Geophys. Res. Lett., 25(10): 1745-1748.

Zonneveld, K.A.F., Versteegh, G.J.M., Kasten, S., Eglinton, T.I., Emeis, K.-C., Huguet, C., Koch, B.P., de Lange, G.J., de Leeuw, J.W., Middelburg, J.J., Mollenhauer, G., Prahl, F.G., Rethemeyer, J. and Wakeham, S.G., 2010. Selective preservation of organic matter in marine environments; processes and impact on the sedimentary record. Biogeosciences, 7(2): 483-511.

9. Appendix

The appendices A - C provide data that are presented and discussed in this thesis. Further data that were collected within the framework of this thesis will be archived within PANGAEA and made available whilst these results are published.

Appendix A includes data presented in chapter 4.

Appendix A1: Biomarker concentrations of surface sediments.

Appendix A2: P_BIP_{25}, P_DIP_{25} and $P_{Alk}IP_{25}$ indices of surface sediments.

Appendix A3: Satellite and NAOSIM sea ice data.

Appendix B includes data presented in chapter 5.

Appendix B1: Biomarker data, P_BIP_{25} and P_DIP_{25} indices of sediment core MSM5/5-712-2.

Appendix B2: Bulk and biomarker data, P_BIP_{25}, P_DIP_{25} indices of sediment core PS2641-4.

Appendix B3: IP_{25} data of sediment core MSM5/5-723-2.

Appendix B4: TOC and $CaCO_3$ contents of sediment cores MSM5/5-712-2 and MSM5/5-723-2.

Appendix C includes data presented in chapter 6.

Appendix C: IP_{25} data of sediment core PS2837-5.

Appendix A1: Biomarker data of surface sediments from the West Spitsbergen and East Greenland margin (chapter 4)

Station	Latitude	Longitude	Water depth (m)	IP25 (µg/g sed)	IP25 (µg/g TOC)	Brassicasterol (µg/g sed)	Brassicasterol (µg/g TOC)	Dinosterol (µg/g sed)	Dinosterol (µg/g TOC)
PS57/127-1	79.0333	10.51	-307	0.01	0.76	4.38	234.22	0.88	47.15
PS57/130-1	77.7833	9.68	-388	0.01	0.85	0.93	108.52	0.22	25.57
PS57/131-2	77.1683	11.1	-320	0.00	0.59	1.07	129.33	0.22	26.25
PS57/136-2	77.81	15.8817	-589	0.00	0.28	1.57	93.35	0.14	8.09
PS57/137-2	77.77	15.065	-1442	0.01	0.41	2.12	100.42	0.30	14.15
PS57/138-1	76.6817	12.995	-1013	0.00	0.54	0.55	63.38	0.15	17.18
PS57/145-1	76.335	13.9283	-1502	0.00	0.17	1.02	85.54	0.20	16.93
PS57/166-2	79.13	4.893	-527	0.01	0.67	1.30	100.45	0.27	21.16
PS62/002-3	61.7947	-39.3738	-1928	0.00	0.00	0.40	201.45	0.06	30.77
PS62/003-3	61.701	-39.0676	-2192	0.00	0.00	1.58	686.33	0.17	73.10
PS62/004-2	61.5258	-38.1232	-2564	0.00	0.00	0.50	134.12	0.11	28.83
PS62/012-2	64.6243	-31.6933	-2431	0.00	0.00	0.26	111.09	0.04	19.14
PS62/015-4	67.9307	-25.4291	-1013	0.02	3.88	0.80	135.21	0.23	39.64
PS62/017-1	67.8508	-24.582	-1502	0.03	4.11	1.45	234.00	0.27	43.71
PS62/020-1	70.9989	-18.9151	-1374	0.02	2.59	0.75	116.60	0.14	22.06
PS62/022-3	72.4906	-12.6063	-527	0.01	1.65	1.08	152.59	0.20	27.60
PS62/026-3	74.332	-8.213	-3341	0.01	0.83	0.85	97.79	0.16	17.93
PS62/027-1	74.824	-7.008	-3510	0.01	0.82	0.72	93.70	0.13	16.91
PS62/028-1	74.849	-6.915	-3477	0.00	0.70	0.66	95.18	0.12	16.86
PS62/029-2	74.799	-7.084	-3471	0.00	0.00	0.45	70.93	0.10	15.86
PS62/038-1	74.767	-5.026	-3603	0.00	0.00	0.24	85.30	0.04	15.03
PS62/041-1	74.684	-5.012	-3602	0.00	0.00	0.68	101.85	0.12	17.70
PS62/044-1	74.7901	-5.6937	-3558	0.00	0.61	0.66	84.02	0.14	17.83
PS62/046-3	74.808	-8.152	-3395	0.01	0.87	0.76	101.84	0.18	23.49
PS62/048-1	74.841	-8.142	-3458	0.01	0.93	0.89	119.30	0.14	19.26
PS62/050-1	74.867	-8.154	-3383	0.01	0.97	0.67	95.52	0.15	21.12
PS64/487-1	76.149	-17.283	-234	0.03	6.40	0.39	72.86	0.13	24.86
PS64/488-1	76.1828	-15.181	-320	0.02	2.43	0.31	35.44	0.11	12.10
PS64/489-1	76.2356	-11.0017	-315	0.01	2.77	0.34	77.81	0.07	16.23
PS64/490-1	76.397	-9.9913	-264	0.01	3.47	0.23	86.95	0.08	28.52
PS64/504-1	75.7209	-8.0882	-2324	0.00	1.23	0.25	63.49	0.07	18.41
PS64/508-1	75.9817	-9.1974	-1087	0.01	1.48	0.12	30.33	0.04	10.20
PS64/511-1	76.1658	-10.0127	-288	0.01	1.96	0.30	67.15	0.08	17.37
PS64/516-1	76.4749	-11.4143	-314	0.01	1.38	0.34	54.61	0.09	14.27
PS64/528-1	75.5895	-7.5765	-3187	0.00	0.66	0.20	33.73	0.05	9.10
PS64/531-1	75.7817	-8.3472	-2023	0.01	1.29	0.30	55.93	0.10	18.96
PS64/573-1	74.765	-16.7318	-388	0.03	2.72	0.61	59.81	0.20	19.88
PS64/582-1	74.4423	-14.1948	-589	0.01	2.28	0.29	65.28	0.09	19.93
PS64/583-1	74.3977	-13.8936	-1442	0.01	1.47	0.25	48.59	0.07	13.65
PS2630-7	73.16	-18.0683	-287	0.02	4.89	0.41	127.24	0.10	32.81
PS2642-2	72.79	-25.8217	-759	0.01	8.47	0.22	217.63	0.05	51.80
PS2648-3	70.525	-22.51	-109	0.03	3.77	1.40	202.29	0.22	31.80
PS2651-3	71.15	-25.5417	-773	0.00	2.60	0.35	251.33	0.09	63.88
PS2654-6	70.9217	-26.5833	-942	0.00	3.51	0.31	234.65	0.09	66.11

Appendix A1: Biomarker data of surface sediments from the West Spitsbergen and East Greenland margin (chapter 4)

Station	Latitude	Longitude	Water depth (m)	n-C15 alkane (µg/g sed)	n-C15 alkane (µg/g TOC)	n-C17 alkane (µg/g sed)	n-C17 alkane (µg/g TOC)	n-C19 alkane (µg/g sed)	n-C19 alkane (µg/g TOC)
PS57/127-1	79.0333	10.51	-307	0.24	12.91	0.42	22.49	0.37	20.01
PS57/130-1	77.7833	9.68	-388	0.44	51.61	0.44	51.57	0.43	50.49
PS57/131-2	77.1683	11.1	-320	0.47	57.12	0.46	55.09	0.46	55.10
PS57/136-2	77.81	15.8817	-589	0.93	55.18	1.02	60.84	1.77	105.17
PS57/137-2	77.77	15.065	-1442	0.84	39.70	0.87	41.15	0.99	46.71
PS57/138-1	76.6817	12.995	-1013	0.61	70.28	0.54	62.32	0.65	74.60
PS57/145-1	76.335	13.9283	-1502	0.46	38.54	0.48	40.64	0.44	36.60
PS57/166-2	79.13	4.893	-527	0.05	4.26	0.21	16.46	0.22	16.97
PS62/002-3	61.7947	-39.3738	-1928	0.00	1.72	0.01	6.20	0.01	5.66
PS62/003-3	61.701	-39.0676	-2192	0.01	3.13	0.01	6.44	0.02	7.53
PS62/004-2	61.5258	-38.1232	-2564	0.01	3.69	0.02	4.59	0.02	4.17
PS62/012-2	64.6243	-31.6933	-2431	0.01	5.58	0.02	7.10	0.01	5.36
PS62/015-4	67.9307	-25.4291	-1013	0.04	7.58	0.05	8.98	0.04	7.13
PS62/017-1	67.8508	-24.582	-1502	0.07	10.57	0.07	11.19	0.06	9.34
PS62/020-1	70.9989	-18.9151	-1374	0.08	13.26	0.09	14.84	0.08	12.53
PS62/022-3	72.4906	-12.6063	-527	0.11	15.71	0.11	15.65	0.09	12.87
PS62/026-3	74.332	-8.213	-3341	0.08	9.76	0.14	16.60	0.14	16.19
PS62/027-1	74.824	-7.008	-3510	0.07	8.84	0.09	11.48	0.09	11.07
PS62/028-1	74.849	-6.915	-3477	0.05	7.91	0.09	12.91	0.08	12.22
PS62/029-2	74.799	-7.084	-3471	0.01	1.74	0.06	9.68	0.08	12.66
PS62/038-1	74.767	-5.026	-3603	0.01	2.37	0.02	8.40	0.03	11.68
PS62/041-1	74.684	-5.012	-3602	0.03	5.00	0.07	11.13	0.09	12.92
PS62/044-1	74.7901	-5.6937	-3558	0.03	4.19	0.09	11.73	0.09	11.78
PS62/046-3	74.808	-8.152	-3395	0.13	16.85	0.11	14.14	0.10	12.74
PS62/048-1	74.841	-8.142	-3458	0.06	8.50	0.09	12.03	0.09	11.83
PS62/050-1	74.867	-8.154	-3383	0.04	5.98	0.08	10.94	0.08	11.95
PS64/487-1	76.149	-17.283	-234	0.01	0.95	0.02	4.62	0.02	4.21
PS64/488-1	76.1828	-15.181	-320	0.03	3.37	0.07	7.73	0.05	5.65
PS64/489-1	76.2356	-11.0017	-315	0.01	2.41	0.03	7.56	0.03	6.96
PS64/490-1	76.397	-9.9913	-264	0.01	4.96	0.03	12.59	0.03	10.49
PS64/504-1	75.7209	-8.0882	-2324	0.01	3.11	0.06	14.20	0.06	15.31
PS64/508-1	75.9817	-9.1974	-1087	0.01	2.34	0.05	11.35	0.05	13.27
PS64/511-1	76.1658	-10.0127	-288	0.01	1.67	0.03	5.79	0.03	6.05
PS64/516-1	76.4749	-11.4143	-314	0.00	0.28	0.02	3.32	0.03	4.77
PS64/528-1	75.5895	-7.5765	-3187	0.01	1.64	0.04	6.81	0.05	8.69
PS64/531-1	75.7817	-8.3472	-2023	0.04	7.48	0.10	18.45	0.09	15.98
PS64/573-1	74.765	-16.7318	-388	0.05	5.05	0.10	9.32	0.07	7.07
PS64/582-1	74.4423	-14.1948	-589	0.03	6.11	0.05	10.83	0.04	9.07
PS64/583-1	74.3977	-13.8936	-1442	0.06	12.63	0.08	16.09	0.07	13.31
PS2630-7	73.16	-18.0683	-287	0.02	4.92	0.04	12.06	0.03	9.90
PS2642-2	72.79	-25.8217	-759	0.00	0.67	0.01	6.36	0.01	9.46
PS2648-3	70.525	-22.51	-109	0.15	21.98	0.24	35.49	0.18	26.19
PS2651-3	71.15	-25.5417	-773	0.00	1.97	0.01	8.00	0.01	8.76
PS2654-6	70.9217	-26.5833	-942	0.00	1.43	0.01	7.16	0.01	5.62

Appendix A2: PIP25 indices of surface sediments from the West Spitsbergen and East Greenland margin (chapter 4)

Station	Latitude	Longitude	PBIP25 index	PDIP25 index	PAIkIP25 index
PS57/127-1	79.0333	10.51	0.19	0.19	0.27
PS57/130-1	77.7833	9.68	0.36	0.33	0.13
PS57/131-2	77.1683	11.1	0.25	0.25	0.09
PS57/136-2	77.81	15.8817	0.18	0.34	0.03
PS57/137-2	77.77	15.065	0.23	0.30	0.08
PS57/138-1	76.6817	12.995	0.38	0.32	0.07
PS57/145-1	76.335	13.9283	0.13	0.13	0.04
PS57/166-2	79.13	4.893	0.33	0.32	0.33
PS62/002-3	61.7947	-39.3738	0.00	0.00	0.00
PS62/003-3	61.701	-39.0676	0.00	0.00	0.00
PS62/004-2	61.5258	-38.1232	0.00	0.00	0.00
PS62/012-2	64.6243	-31.6933	0.00	0.00	0.00
PS62/015-4	67.9307	-25.4291	0.68	0.59	0.82
PS62/017-1	67.8508	-24.582	0.56	0.58	0.78
PS62/020-1	70.9989	-18.9151	0.62	0.63	0.64
PS62/022-3	72.4906	-12.6063	0.44	0.47	0.51
PS62/026-3	74.332	-8.213	0.38	0.41	0.35
PS62/027-1	74.824	-7.008	0.39	0.42	0.42
PS62/028-1	74.849	-6.915	0.35	0.38	0.37
PS62/029-2	74.799	-7.084	0.00	0.00	0.00
PS62/038-1	74.767	-5.026	0.00	0.00	0.00
PS62/041-1	74.684	-5.012	0.00	0.00	0.00
PS62/044-1	74.7901	-5.6937	0.35	0.34	0.38
PS62/046-3	74.808	-8.152	0.38	0.35	0.35
PS62/048-1	74.841	-8.142	0.36	0.42	0.44
PS62/050-1	74.867	-8.154	0.42	0.41	0.48
PS64/487-1	76.149	-17.283	0.86	0.79	0.95
PS64/488-1	76.1828	-15.181	0.83	0.75	0.80
PS64/489-1	76.2356	-11.0017	0.72	0.72	0.82
PS64/490-1	76.397	-9.9913	0.74	0.64	0.77
PS64/504-1	75.7209	-8.0882	0.58	0.50	0.51
PS64/508-1	75.9817	-9.1974	0.78	0.68	0.60
PS64/511-1	76.1658	-10.0127	0.68	0.63	0.80
PS64/516-1	76.4749	-11.4143	0.65	0.59	0.82
PS64/528-1	75.5895	-7.5765	0.59	0.52	0.52
PS64/531-1	75.7817	-8.3472	0.63	0.50	0.46
PS64/573-1	74.765	-16.7318	0.77	0.67	0.78
PS64/582-1	74.4423	-14.1948	0.72	0.63	0.71
PS64/583-1	74.3977	-13.8936	0.69	0.61	0.49
PS2630-7	73.16	-18.0683	0.74	0.69	0.83
PS2642-2	72.79	-25.8217	0.74	0.71	0.93
PS2648-3	70.525	-22.51	0.57	0.64	0.55
PS2651-3	71.15	-25.5417	0.43	0.38	0.79
PS2654-6	70.9217	-26.5833	0.52	0.44	0.87

Appendix A3: Satellite and NAOSIM sea ice data from the West Spitsbergen and East Greenland margin (chapter 4)

Station	Latitude	Longitude	Satellite sea ice concentration (%)	NAOSIM sea ice concentration (%)	NAOSIM sea ice thickness (m)
PS57/127-1	79.0333	10.51	15	25	0.5
PS57/130-1	77.7833	9.68	5	25	0.5
PS57/131-2	77.1683	11.1	5	25	0.5
PS57/136-2	77.81	15.8817	n.d.	n.d.	n.d.
PS57/137-2	77.77	15.065	n.d.	n.d.	n.d.
PS57/138-1	76.6817	12.995	15	35	0.5
PS57/145-1	76.335	13.9283	15	45	0.5
PS57/166-2	79.13	4.893	15	35	0.5
PS62/002-3	61.7947	-39.3738	5	5	0
PS62/003-3	61.701	-39.0676	5	5	0
PS62/004-2	61.5258	-38.1232	5	5	0
PS62/012-2	64.6243	-31.6933	5	5	0
PS62/015-4	67.9307	-25.4291	65	75	1.5
PS62/017-1	67.8508	-24.582	45	65	0.5
PS62/020-1	70.9989	-18.9151	65	95	2.5
PS62/022-3	72.4906	-12.6063	25	35	0.5
PS62/026-3	74.332	-8.213	15	35	0.5
PS62/027-1	74.824	-7.008	15	25	0
PS62/028-1	74.849	-6.915	15	25	0
PS62/029-2	74.799	-7.084	15	25	0
PS62/038-1	74.767	-5.026	5	35	0.5
PS62/041-1	74.684	-5.012	5	35	0.5
PS62/044-1	74.7901	-5.6937	5	35	0.5
PS62/046-3	74.808	-8.152	15	25	0
PS62/048-1	74.841	-8.142	15	25	0
PS62/050-1	74.867	-8.154	15	25	0
PS64/487-1	76.149	-17.283	95	95	3.5
PS64/488-1	76.1828	-15.181	95	95	2.5
PS64/489-1	76.2356	-11.0017	85	85	1.5
PS64/490-1	76.397	-9.9913	75	75	1.5
PS64/504-1	75.7209	-8.0882	25	35	0.5
PS64/508-1	75.9817	-9.1974	55	45	0.5
PS64/511-1	76.1658	-10.0127	65	75	1.5
PS64/516-1	76.4749	-11.4143	85	85	1.5
PS64/528-1	75.5895	-7.5765	25	25	0.5
PS64/531-1	75.7817	-8.3472	35	45	0.5
PS64/573-1	74.765	-16.7318	85	95	2.5
PS64/582-1	74.4423	-14.1948	65	75	1.5
PS64/583-2	74.3977	-13.8936	65	75	1.5
PS2630-7	73.16	-18.0683	85	95	2.5
PS2642-2	72.79	-25.8217	n.d.	n.d.	n.d.
PS2648-3	70.525	-22.51	n.d.	75	5.5
PS2651-3	71.15	-25.5417	n.d.	n.d.	n.d.
PS2654-6	70.9217	-26.5833	n.d.	n.d.	n.d.

mean spring (March-April-May) sea ice concentrations (thicknesses) ± 5% (± 0.5 m) averaged over the period 1979-2003

n.d.: not determined

Appendix B1: Biomarker data and PIP25 indices of sediment core MSM5/5-712-2

Depth (m)	IP25 (ng/g sed)	IP25 (µg/g TOC)	Brassicasterol (µg/g sed)	Brassicasterol (µg/g TOC)	Dinosterol (µg/g sed)	Dinosterol (µg/g TOC)	PBIP25 index	PDIP25 index
0.10	2.86	0.23	0.41	33.47	0.13	10.57	0.40	0.41
0.11	8.65	0.69	0.28	22.15	0.15	12.00	0.75	0.65
0.12	9.69	0.76	0.31	24.19	0.16	12.48	0.75	0.66
0.13	11.16	0.87	0.31	24.29	0.16	12.35	0.77	0.69
0.14	8.67	0.68	0.33	25.99	0.18	14.17	0.71	0.61
0.15	7.92	0.63	0.34	27.08	0.15	12.35	0.69	0.62
0.16	8.16	0.66	0.31	25.27	0.15	12.17	0.71	0.63
0.17	7.25	0.61	0.33	27.47	0.14	11.40	0.68	0.63
0.18	6.95	0.60	0.33	28.40	0.14	12.38	0.66	0.61
0.19	5.67	0.50	0.28	24.80	0.13	11.65	0.66	0.58
0.20	6.55	0.57	0.30	26.27	0.13	11.36	0.67	0.62
0.21	6.78	0.63	0.26	24.66	0.12	10.78	0.71	0.65
0.22	4.60	0.46	0.24	23.74	0.12	11.84	0.65	0.55
0.23	4.52	0.44	0.26	25.12	0.11	10.75	0.62	0.57
0.24	4.44	0.44	0.22	22.19	0.08	7.91	0.65	0.64
0.25	4.31	0.42	0.28	27.40	0.10	9.39	0.59	0.59
0.26	6.44	0.62	0.34	33.36	0.13	12.87	0.64	0.61
0.27	6.67	0.62	0.34	32.02	0.10	9.69	0.65	0.67
0.28	7.46	0.68	0.45	41.08	0.15	13.95	0.61	0.61
0.29	8.80	0.80	0.46	41.81	0.17	15.53	0.64	0.62
0.30	9.25	0.82	0.43	37.93	0.12	10.47	0.67	0.72
0.31	7.07	0.63	0.46	40.47	0.15	13.11	0.59	0.60
0.32	6.99	0.64	0.37	34.50	0.14	12.60	0.64	0.62
0.33	6.74	0.64	0.31	29.64	0.12	11.34	0.67	0.64
0.34	4.87	0.49	0.32	32.07	0.13	13.45	0.59	0.54
0.35	5.35	0.54	0.29	29.42	0.10	10.33	0.63	0.63
0.36	5.34	0.53	0.24	24.51	0.11	10.66	0.67	0.62
0.37	4.72	0.46	0.31	30.39	0.12	12.17	0.59	0.55
0.38	5.80	0.56	0.32	31.04	0.08	7.80	0.63	0.70
0.39	5.75	0.53	0.35	32.48	0.16	14.76	0.61	0.54
0.40	5.77	0.55	0.30	28.88	0.14	13.64	0.64	0.56
0.41	5.06	0.48	0.32	30.14	0.14	13.32	0.60	0.53
0.42	5.78	0.54	0.31	28.89	0.14	12.91	0.64	0.57
0.43	6.05	0.58	0.29	28.02	0.13	12.13	0.66	0.60
0.44	5.96	0.59	0.25	24.91	0.12	12.22	0.69	0.61
0.45	4.52	0.45	0.23	22.30	0.12	12.26	0.65	0.54
0.46	4.18	0.43	0.22	22.44	0.08	8.76	0.64	0.61
0.47	4.51	0.47	0.23	24.15	0.12	12.11	0.65	0.55
0.48	4.80	0.46	0.30	28.80	0.14	13.25	0.60	0.53
0.49	3.66	0.36	0.32	31.43	0.15	14.31	0.52	0.44
0.50	5.11	0.52	0.26	26.33	0.12	12.27	0.65	0.58
0.51	5.72	0.55	0.32	31.25	0.14	13.34	0.62	0.57
0.52	6.12	0.59	0.32	30.89	0.14	13.30	0.64	0.59
0.53	4.69	0.46	0.27	26.66	0.14	13.92	0.62	0.52
0.54	4.69	0.48	0.28	28.83	0.12	12.78	0.61	0.55
0.55	5.55	0.53	0.32	30.86	0.13	12.92	0.62	0.57
0.56	3.46	0.34	0.23	22.89	0.10	9.59	0.58	0.53
0.57	3.31	0.35	0.18	18.72	0.09	9.90	0.64	0.53
0.59	4.32	0.43	0.31	31.01	0.12	12.02	0.57	0.54
0.60	3.66	0.33						
0.61	4.10	0.41	0.24	24.69	0.10	10.07	0.61	0.57
0.62	4.42	0.44	0.30	30.31	0.09	9.24	0.58	0.60
0.63	4.34	0.43	0.27	26.92	0.11	10.62	0.60	0.57
0.64	3.69	0.35	0.32	29.82	0.12	11.44	0.52	0.49
0.65	4.09	0.38						
0.66	3.84	0.37	0.36	34.25	0.13	12.11	0.50	0.49
0.67	3.75	0.35	0.29	27.18	0.13	12.23	0.55	0.48
0.68	4.92	0.45	0.36	32.68	0.12	11.40	0.56	0.56
0.69	4.30	0.40	0.33	30.59	0.14	13.28	0.55	0.49
0.70	4.37	0.41	0.29	27.45	0.12	11.22	0.58	0.54
0.72	4.42	0.41	0.30	28.03	0.13	11.84	0.58	0.53

Appendix B1: Biomarker data and PIP25 indices of sediment core MSM5/5-712-2

Depth [cm]	IP25 (ng/g sed)	IP25 (µg/g TOC)	Brassicasterol (µg/g sed)	Brassicasterol (µg/g TOC)	Dinosterol (µg/g sed)	Dinosterol (µg/g TOC)	PBIP25 index	PDIP25 index
0.74	4.62	0.45	0.39	37.68	0.13	12.76	0.53	0.53
0.76	5.34	0.50	0.38	35.41	0.14	12.67	0.57	0.56
0.78	3.52	0.35	0.35	34.49	0.14	13.52	0.49	0.45
0.80	4.33	0.44	0.30	30.66	0.12	12.27	0.58	0.54
0.82	4.19	0.43	0.33	33.90	0.12	12.14	0.54	0.53
0.84	5.49	0.57	0.32	32.87	0.11	11.88	0.62	0.60
0.86	3.19	0.34	0.27	29.45	0.10	10.38	0.52	0.51
0.88	3.00	0.31	0.33	34.17	0.10	10.77	0.46	0.48
0.90	2.78	0.30	0.36	38.38	0.09	10.05	0.42	0.49
0.92	3.26	0.35	0.31	33.50	0.10	10.41	0.50	0.52
0.94	4.19	0.43	0.38	38.89	0.11	11.52	0.51	0.54
0.96	2.84	0.31	0.28	31.32	0.10	10.49	0.49	0.49
0.98	2.89	0.33	0.30	34.08	0.08	9.25	0.48	0.53
1.00	2.62	0.29	0.30	32.57	0.09	10.16	0.45	0.47
1.01			0.29	29.59	0.08	8.41		
1.02	2.65	0.27	0.30	31.08	0.09	9.04	0.45	0.49
1.04	1.70	0.17	0.25	26.18	0.08	8.42	0.39	0.40
1.06	1.74	0.19	0.30	32.32	0.10	11.13	0.36	0.35
1.08	3.06	0.32	0.30	30.46	0.10	9.83	0.49	0.51
1.10	2.49	0.26	0.31	31.65	0.09	9.74	0.43	0.46
1.12	2.74	0.27	0.27	26.37	0.10	9.79	0.49	0.47
1.14	2.77	0.28	0.31	31.10	0.10	10.24	0.46	0.47
1.16	3.09	0.31	0.26	26.07	0.10	9.60	0.53	0.51
1.18	2.75	0.27	0.35	34.49	0.10	9.50	0.42	0.48
1.20	2.88	0.28	0.26	25.58	0.10	9.73	0.51	0.48
1.22	2.59	0.26	0.30	29.33	0.12	11.46	0.45	0.42
1.24	3.71	0.35	0.29	27.06	0.10	9.14	0.55	0.55
1.26	2.72	0.27	0.34	34.53	0.11	11.37	0.43	0.44
1.28	2.69	0.28	0.30	30.96	0.11	11.41	0.46	0.44
1.30	2.64	0.25	0.31	29.28	0.09	8.59	0.44	0.48
1.32	2.35	0.25	0.34	35.55	0.08	8.83	0.39	0.47
1.34	2.66	0.28	0.32	33.72	0.10	10.20	0.44	0.46
1.36	1.93	0.17	0.35	31.77	0.10	9.38	0.34	0.37
1.38	2.42	0.25	0.37	38.39	0.10	10.59	0.38	0.43
1.40	1.61	0.18	0.28	31.26	0.10	11.34	0.35	0.34
1.42	2.31	0.27	0.28	32.63	0.09	10.91	0.44	0.44
1.44	1.47	0.14	0.23	21.84	0.10	9.15	0.37	0.33
1.46	1.34	0.15	0.22	24.31	0.04	4.95	0.37	0.49
1.48	1.50	0.16	0.28	29.50	0.10	10.70	0.34	0.32
1.50	1.84	0.20	0.33	35.08	0.10	10.75	0.35	0.37
1.52	1.52	0.17	0.32	35.92	0.11	11.93	0.31	0.31
1.53	1.67	0.18	0.32	35.90	0.11	11.66	0.33	0.34
1.54	1.03	0.11	0.31	33.29	0.10	10.52	0.24	0.26
1.55	1.03	0.12	0.36	39.70	0.10	11.66	0.21	0.24
1.56	1.64	0.19	0.29	32.48	0.09	10.07	0.35	0.37
1.57	1.06	0.12	0.30	32.11	0.10	10.73	0.25	0.26
1.58	1.13	0.13	0.31	34.74	0.10	11.57	0.26	0.26
1.59	1.24	0.14	0.29	33.25	0.08	8.64	0.28	0.34
1.60	1.41	0.16	0.27	31.19	0.08	9.10	0.33	0.36
1.61	1.08	0.12	0.36	39.92	0.08	9.08	0.22	0.30
1.62	1.42	0.16	0.26	28.45	0.07	7.82	0.34	0.39
1.63	1.20	0.13	0.31	33.39	0.08	8.95	0.27	0.32
1.64	1.63	0.18	0.31	34.88	0.09	9.59	0.33	0.38
1.65	1.50	0.17	0.29	32.33	0.09	10.00	0.33	0.35
1.66	0.70	0.08	0.25	29.38	0.08	8.85	0.21	0.23
1.67	1.00	0.12	0.28	32.88	0.08	8.84	0.25	0.30
1.68	0.69	0.08	0.30	35.13	0.08	8.84	0.18	0.22
1.69	0.75	0.09	0.28	31.98	0.08	9.52	0.21	0.23
1.70	0.43	0.05	0.30	32.65	0.07	7.45	0.12	0.17
1.71	0.56	0.06	0.38	39.57	0.09	9.38	0.12	0.17
1.72	1.50	0.17	0.33	37.02	0.09	10.02	0.30	0.35

Appendix B1: Biomarker data and PIP25 indices of sediment core MSM5/5-712-2

Depth [cm]	IP25 (ng/g sed)	IP25 (µg/g TOC)	Brassicasterol (µg/g sed)	Brassicasterol (µg/g TOC)	Dinosterol (µg/g sed)	Dinosterol (µg/g TOC)	PBIP25 index	PDIP25 index
1.73	1.02	0.11	0.33	36.50	0.09	9.57	0.23	0.28
1.74	0.51	0.06	0.29	33.17	0.08	8.75	0.14	0.18
1.75	0.17	0.02	0.36	40.55	0.08	9.34	0.04	0.06
1.76	0.36	0.04	0.30	34.78	0.08	8.75	0.10	0.13
1.77	0.59	0.07	0.36	41.29	0.08	9.44	0.13	0.19
1.78	1.21	0.14	0.30	34.27	0.09	10.25	0.27	0.30
1.79	0.94	0.11	0.31	35.76	0.08	9.48	0.22	0.27
1.80	1.00	0.12	0.31	35.86	0.08	9.74	0.24	0.28
1.81	0.80	0.09	0.37	40.52	0.08	8.81	0.17	0.24
1.82	1.07	0.12	0.33	37.68	0.09	10.19	0.23	0.28
1.83	0.78	0.09	0.34	38.01	0.09	10.14	0.18	0.22
1.84	0.53	0.06	0.30	34.25	0.10	11.03	0.15	0.15
1.85	0.62	0.08	0.29	35.52	0.10	11.82	0.17	0.17
1.86	0.66	0.08	0.29	34.92	0.09	10.70	0.18	0.19
1.87	0.74	0.09	0.35	41.84	0.09	10.85	0.17	0.21
1.88	0.74	0.09	0.30	35.50	0.07	7.99	0.19	0.26
1.90	1.53	0.17	0.27	30.47	0.06	6.43	0.35	0.46
1.92	1.66	0.19	0.28	31.87	0.06	6.95	0.36	0.47
1.94	1.89	0.20	0.28	30.28	0.07	7.42	0.39	0.47
1.96	2.89	0.28	0.32	31.02	0.07	6.75	0.46	0.57
1.98	2.25	0.23	0.30	30.72	0.07	7.52	0.42	0.50
2.00	1.88	0.19	0.33	33.01	0.08	7.86	0.35	0.43
2.02	2.09	0.21	0.31	31.12	0.07	7.25	0.39	0.48
2.04	1.67	0.16	0.15	14.61	0.04	3.57	0.51	0.59
2.06	1.74	0.17	0.34	32.67	0.07	6.90	0.32	0.43
2.09	2.39	0.23	0.27	26.09	0.07	7.31	0.46	0.51

Appendix B2: Bulk and biomarker data and PIP25 indices of sediment core PS2641-4 (chapter 5)

Depth (m)	TOC (wt.%)	CaCO3 (wt.%)	IP25 (ng/g sed)	IP25 (µg/g TOC)	Brassicasterol (µg/g sed)	Brassicasterol (µg/g TOC)	Dinosterol (µg/g sed)	Dinosterol (µg/g TOC)	PBIP25 index	PDIP25 index
0.01	1.17	0.41	5.07	0.43	0.26	22.46	0.05	4.31	0.63	0.71
0.05	1.23	0.03	4.36	0.35	0.25	20.19	0.07	5.86	0.61	0.59
0.10	1.10	0.78	3.70	0.34	0.29	26.45	0.06	5.67	0.53	0.59
0.15	1.10	0.52	3.52	0.32						
0.25	1.12	0.32	3.70	0.33	0.24	21.40	0.06	5.13	0.58	0.61
0.35	1.05	0.78	4.60	0.44	0.24	22.78	0.07	6.80	0.63	0.61
0.45	0.92	0.70	2.79	0.30	0.21	22.97	0.04	4.85	0.54	0.60
0.55	0.99	0.84	2.66	0.27	0.17	17.33	0.05	4.64	0.58	0.58
0.65	1.02	1.05	1.47	0.14	0.19	19.07	0.06	5.59	0.41	0.38
0.75	1.03	0.52	1.79	0.17	0.21	20.41	0.05	4.58	0.43	0.48
0.85	1.04	0.41	1.37	0.13	0.19	18.72	0.04	3.83	0.39	0.45
0.95	0.96	0.62	1.22	0.13	0.15	15.81	0.04	4.12	0.42	0.43
1.05	0.92	0.68	1.92	0.21	0.14	15.01	0.03	3.25	0.56	0.61
1.15	0.88	0.76	2.35	0.27	0.15	16.57	0.04	5.02	0.59	0.56
1.25	0.88	0.98	1.49	0.17	0.12	14.17	0.03	3.74	0.52	0.52
1.35	0.90	0.69	0.88	0.10	0.11	12.72	0.04	4.19	0.41	0.36
1.45	0.88	0.67	1.23	0.14	0.10	11.55	0.03	3.63	0.52	0.48
1.55	0.86	0.81	1.34	0.16	0.17	19.52	0.04	4.45	0.42	0.46
1.65	0.87	0.82	1.20	0.14	0.12	13.61	0.03	3.87	0.48	0.46
1.75	0.82	0.89	0.73	0.09	0.12	15.08	0.03	3.60	0.35	0.37
1.85	0.82	0.13	1.40	0.17	0.11	12.98	0.04	4.29	0.54	0.49
1.95	0.81	0.89	1.68	0.21						
2.05	0.81	0.89	1.24	0.15	0.12	14.99	0.04	4.93	0.48	0.43
2.15	0.83	0.95	1.54	0.18	0.11	13.35	0.04	4.72	0.56	0.48
2.25	0.83	0.67	1.16	0.14	0.09	11.34	0.03	3.95	0.53	0.46
2.35	0.78	1.08	1.69	0.22	0.14	18.56	0.04	5.61	0.51	0.48
2.45	0.77	0.91	1.04	0.14	0.09	11.09	0.02	3.19	0.52	0.50
2.55	0.81	0.92	1.82	0.22	0.09	10.81	0.03	3.76	0.65	0.59
2.65	0.83	1.07	1.05	0.13	0.10	12.00	0.03	3.05	0.49	0.50
2.75	0.79	0.88	1.49	0.19	0.08	10.58	0.03	3.66	0.62	0.55
2.85	0.80	0.97	2.04	0.25	0.10	13.05	0.03	3.82	0.64	0.62
2.95	0.80	1.03	2.21	0.28	0.13	15.92	0.04	4.45	0.61	0.60
3.05	0.85	0.95	2.04	0.24						
3.15	0.87	0.86	1.90	0.22	0.13	15.03	0.03	3.95	0.57	0.57
3.25	0.84	1.36	1.63	0.19	0.20	23.56	0.05	5.80	0.43	0.45
3.35	0.88	1.16	1.23	0.14	0.16	18.74	0.03	2.86	0.40	0.54
3.45	0.88	1.22	0.91	0.10	0.14	15.89	0.04	4.99	0.37	0.33
3.55	0.84	1.58	1.40	0.17	0.14	16.82	0.03	3.77	0.47	0.51
3.65	0.85	1.39	0.40	0.05	0.15	17.16	0.04	4.77	0.20	0.19
3.75	0.86	1.35	1.17	0.14						
3.85	0.90	0.96	1.50	0.17	0.20	22.17	0.06	6.45	0.40	0.38
3.95	0.78	1.04	0.87	0.11	0.00	0.00	0.00	0.00	1.00	1.00
4.05	0.80	1.11	1.49	0.19	0.00	0.00	0.00	0.00	1.00	1.00
4.15	0.79	1.35	1.34	0.17	0.14	17.15	0.00	0.00	0.47	1.00
4.25	0.86	1.13	1.47	0.17	0.14	16.26	0.04	4.81	0.49	0.46
4.35	0.85	1.46	1.09	0.13	0.18	20.81	0.05	5.77	0.36	0.35
4.45	0.77	1.60	1.11	0.14	0.16	20.38	0.07	8.84	0.39	0.28
4.55	0.82	1.62	1.72	0.21	0.15	18.37	0.04	4.66	0.51	0.52
4.65	0.79	1.66			0.19	23.94	0.06	7.12		
4.75	0.80	1.56	1.35	0.17	0.18	21.95	0.04	5.08	0.41	0.44
4.95	0.86	2.09	0.00	0.00	0.22	25.50	0.06	6.46	0.00	0.00
5.05	0.82	1.56			0.16	19.19	0.04	5.03		
5.15	0.81	2.00	0.24	0.03	0.19	23.92	0.07	8.15	0.10	0.08
5.25	0.79	2.32	0.80	0.10	0.18	22.18	0.05	6.59	0.29	0.27

Appendix B3: IP25 data of sediment core MSM5/5-723-2 (chapter 5)

Depth (m)	IP25 (ng/g sed)	IP25 (µg/g OC)
0.08	6.21	0.46
0.10	6.25	0.46
0.12	6.28	0.47
0.14	6.65	0.49
0.17	5.10	0.38
0.20	5.29	0.39
0.22	5.04	0.38
0.24	4.88	0.38
0.26	4.61	0.35
0.28	4.25	0.33
0.30	4.15	0.32
0.32	3.64	0.28
0.34	4.38	0.35
0.36	3.69	0.27
0.38	3.48	0.27
0.40	3.27	0.26
0.42	3.89	0.30
0.44	4.44	0.33
0.46	3.97	0.30
0.48	3.98	0.30
0.50	3.37	0.26
0.52	2.93	0.22
0.54	3.28	0.27
0.56	2.74	0.21
0.58	3.32	0.25
0.60	2.94	0.23
0.62	2.80	0.22
0.64	2.99	0.23
0.66	3.28	0.26
0.68	3.17	0.25
0.70	2.54	0.20
0.72	2.84	0.23
0.74	2.64	0.23
0.76	2.70	0.24
0.78	2.58	0.22
0.80	2.81	0.24
0.82	2.76	0.24
0.84	2.46	0.22
0.86	2.42	0.21
0.88	2.36	0.21
0.90	2.34	0.21
0.92	2.55	0.21
0.94	2.22	0.19
0.96	2.27	0.19
0.98	2.81	0.23
1.00	2.46	0.21
1.04	2.47	0.20
1.06	2.54	0.21
1.08	1.99	0.17
1.10	2.11	0.18
1.12	2.06	0.17
1.16	2.25	0.20
1.18	2.02	0.17
1.20	1.87	0.17
1.22	2.25	0.20
1.24	1.59	0.15
1.26	1.65	0.15
1.28	1.86	0.17
1.30	1.74	0.15
1.32	1.76	0.16

Appendix B3: IP25 data of sediment core MSM5/5-723-2 (chapter 5)

Depth (m)	IP25 (ng/g sed)	IP25 (µg/g OC)
1.34	1.90	0.17
1.36	1.66	0.15
1.38	1.58	0.15
1.40	1.58	0.15
1.42	1.75	0.16
1.44	1.63	0.16
1.46	1.33	0.13
1.48	1.48	0.13
1.50	1.41	0.13
1.52	1.25	0.12
1.54	1.11	0.10
1.56	1.66	0.14
1.58	1.26	0.11
1.60	0.82	0.07
1.62	1.51	0.13
1.66	1.21	0.11
1.68	1.50	0.13
1.70	1.74	0.15
1.72	1.31	0.11
1.74	1.62	0.14
1.78	1.42	0.14
1.80	0.99	0.09
1.82	1.35	0.13
1.84	0.99	0.09
1.86	1.21	0.12
1.88	1.06	0.10
1.90	0.92	0.08
1.92	1.30	0.12
1.94	1.34	0.13
1.96	1.13	0.11
1.98	1.11	0.11
2.00	0.92	0.09

Appendix B4: TOC and CaCO3 contents of *Maria S. Merian* sediment cores (chapter 5)

MSM5/5-712-2 Depth (m)	TOC (wt.%)	CaCO3 (wt.%)
0.10	1.23	14.78
0.11	1.25	13.83
0.12	1.27	13.78
0.13	1.28	14.05
0.14	1.27	14.29
0.15	1.25	14.21
0.16	1.25	14.35
0.17	1.20	15.31
0.18	1.17	15.36
0.19	1.14	15.46
0.20	1.14	15.58
0.21	1.07	16.08
0.22	1.00	15.59
0.23	1.02	14.94
0.24	1.01	14.06
0.25	1.02	14.07
0.26	1.03	14.46
0.27	1.07	14.60
0.28	1.09	14.89
0.29	1.10	14.63
0.30	1.12	14.69
0.31	1.13	14.79
0.32	1.09	15.12
0.33	1.05	15.21
0.34	0.99	15.45
0.35	1.00	15.56
0.36	1.00	15.68
0.37	1.02	16.03
0.38	1.03	15.57
0.39	1.08	14.85
0.40	1.05	14.17
0.41	1.06	13.88
0.42	1.07	13.59
0.43	1.05	12.68
0.44	1.01	12.36
0.45	1.02	12.19
0.46	0.97	12.14
0.47	0.97	12.38
0.48	1.04	12.90
0.49	1.03	12.18
0.50	0.98	11.67
0.51	1.04	11.42
0.52	1.04	11.27
0.53	1.01	11.21
0.54	0.98	16.17
0.55	1.04	10.41
0.56	1.02	10.72
0.57	0.95	9.06
0.58	1.00	11.12
0.59	1.00	11.49
0.60	1.10	7.34
0.61	0.99	10.21
0.62	1.01	10.55
0.63	1.01	10.29
0.64	1.06	9.83
0.65	1.09	9.67
0.66	1.05	8.95
0.67	1.07	9.31
0.68	1.10	9.62
0.69	1.08	9.15
0.70	1.07	9.53
0.71	1.04	9.94
0.72	1.07	9.87
0.73	1.04	10.63
0.74	1.02	10.47

MSM5/5-723-2 Depth (m)	TOC (wt.%)	CaCO3 (%)
0.08	1.35	16.38
0.11	1.36	16.36
0.13	1.33	16.08
0.14	1.35	15.97
0.16	1.33	15.74
0.18	1.32	13.81
0.19	1.32	14.79
0.20	1.34	14.29
0.21	1.32	12.95
0.22	1.32	15.59
0.23	1.30	13.31
0.24	1.27	14.21
0.25	1.30	14.52
0.26	1.32	16.39
0.27	1.28	13.30
0.28	1.27	18.48
0.29	1.29	23.01
0.30	1.29	14.60
0.31	1.27	14.63
0.32	1.29	24.13
0.33	1.25	18.52
0.34	1.25	10.89
0.35	1.25	15.75
0.36	1.35	19.29
0.37	1.27	16.83
0.38	1.29	13.87
0.39	1.27	12.24
0.40	1.24	14.68
0.41	1.28	11.92
0.42	1.31	13.99
0.43	1.35	13.92
0.44	1.35	12.84
0.45	1.32	10.98
0.46	1.31	17.64
0.47	1.34	13.08
0.48	1.31	19.37
0.49	1.33	11.98
0.50	1.32	15.97
0.51	1.36	12.49
0.52	1.32	16.00
0.53	1.28	12.96
0.54	1.22	18.67
0.55	1.25	10.07
0.56	1.28	8.14
0.57	1.30	19.74
0.58	1.33	20.47
0.59	1.28	19.90
0.60	1.26	12.92
0.61	1.27	10.40
0.62	1.27	15.35
0.63	1.27	16.99
0.64	1.28	10.51
0.65	1.26	12.18
0.66	1.27	15.49
0.67	1.27	23.71
0.68	1.27	9.65
0.69	1.26	12.73
0.70	1.28	12.12
0.71	1.23	12.27
0.72	1.26	12.34
0.73	1.19	12.89
0.74	1.16	13.42
0.75	1.22	12.19
0.76	1.14	13.87
0.77	1.15	12.79

Appendix B4: TOC and CaCO3 contents of *Maria S. Merian* sediment cores (chapter 5)

MSM5/5-712-2 Depth (m)	TOC (wt.%)	CaCO3 (wt.%)
0.75	1.06	10.28
0.76	1.08	10.07
0.77	1.04	9.19
0.78	1.01	9.09
0.79	0.98	9.30
0.80	0.98	8.91
0.81	0.97	8.10
0.82	0.98	8.89
0.83	0.99	9.10
0.84	0.97	8.82
0.85	0.98	8.58
0.86	0.93	8.04
0.87	0.93	8.92
0.88	0.95	9.50
0.89	0.94	9.11
0.90	0.94	9.52
0.91	0.96	10.03
0.92	0.93	9.23
0.93	0.96	8.62
0.94	0.98	9.29
0.95	0.94	8.76
0.96	0.91	8.39
0.97	0.89	8.66
0.98	0.88	9.86
0.99	0.87	9.76
1.00	0.92	10.65
1.01	0.98	10.43
1.02	0.98	9.81
1.03	0.98	9.96
1.04	0.97	10.36
1.05	0.96	9.74
1.06	0.92	10.25
1.07	0.96	10.45
1.08	0.97	10.04
1.09	0.97	9.30
1.10	0.97	10.02
1.11	0.98	9.52
1.12	1.02	9.63
1.13	1.04	10.89
1.14	0.99	10.28
1.15	0.97	9.50
1.16	0.99	11.09
1.17	1.03	10.65
1.18	1.02	10.38
1.19	1.02	10.40
1.20	1.03	10.42
1.21	1.04	10.67
1.22	1.01	9.95
1.23	1.05	10.02
1.24	1.07	10.11
1.25	1.00	10.08
1.26	0.99	10.25
1.27	0.98	10.36
1.28	0.98	9.87
1.29	0.99	10.59
1.30	1.06	9.54
1.31	0.96	10.11
1.32	0.96	10.55
1.33	0.97	11.24
1.34	0.96	10.79
1.35	0.98	10.41
1.36	1.11	10.46
1.37	0.92	12.57
1.38	0.96	11.90
1.39	1.04	11.69

MSM5/5-723-2 Depth (m)	TOC (wt.%)	CaCO3 (%)
0.78	1.17	11.82
0.79	1.19	11.86
0.80	1.19	12.28
0.81	1.15	11.88
0.82	1.15	12.04
0.83	1.17	14.11
0.84	1.13	12.24
0.85	1.18	13.41
0.86	1.16	13.79
0.87	1.14	11.92
0.88	1.11	11.81
0.89	1.07	11.38
0.90	1.10	12.13
0.91	1.14	12.32
0.92	1.22	11.79
0.93	1.15	12.41
0.94	1.17	11.73
0.95	1.15	11.89
0.96	1.18	11.32
0.97	1.20	10.38
0.98	1.20	9.69
0.99	1.20	10.97
1.00	1.18	9.48
1.01	1.20	9.11
1.02	1.18	8.70
1.03	1.21	8.68
1.04	1.23	8.92
1.05	1.22	9.85
1.06	1.20	9.81
1.07	1.24	9.95
1.08	1.15	10.51
1.09	1.21	10.41
1.10	1.17	9.79
1.11	1.18	9.78
1.12	1.18	9.07
1.13	1.19	9.23
1.14	1.16	8.57
1.15	1.14	8.76
1.16	1.15	8.83
1.17	1.17	8.21
1.18	1.17	8.05
1.19	1.11	9.10
1.20	1.13	8.02
1.21	1.11	7.26
1.22	1.12	8.83
1.23	1.10	9.19
1.24	1.06	8.09
1.25	1.09	8.95
1.26	1.12	9.42
1.27	1.13	9.56
1.28	1.12	9.38
1.29	1.14	9.26
1.30	1.15	8.78
1.31	1.08	10.54
1.32	1.09	10.71
1.33	1.10	13.24
1.34	1.09	5.49
1.35	1.07	10.60
1.36	1.09	10.29
1.37	1.10	9.64
1.38	1.06	7.50
1.39	1.04	11.20
1.40	1.03	9.74
1.41	1.03	12.71
1.42	1.06	11.72

Appendix B4: TOC and CaCO3 contents of *Maria S. Merian* sediment cores (chapter 5)

MSM5/5-712-2 Depth (m)	TOC (wt.%)	CaCO3 (wt.%)
1.40	0.89	12.64
1.41	1.05	11.74
1.42	0.86	13.91
1.43	0.90	13.61
1.44	1.06	11.49
1.45	0.99	12.46
1.46	0.90	11.91
1.47	0.92	12.17
1.48	0.95	13.13
1.49	0.94	14.45
1.50	0.93	14.51
1.51	0.91	13.80
1.52	0.89	15.18
1.53	0.90	16.16
1.54	0.92	15.67
1.55	0.90	15.26
1.56	0.89	14.49
1.57	0.92	15.54
1.58	0.89	16.21
1.59	0.88	14.92
1.60	0.88	13.83
1.61	0.89	13.59
1.62	0.90	11.69
1.63	0.92	12.01
1.64	0.90	12.30
1.65	0.88	12.50
1.66	0.86	12.26
1.67	0.85	11.65
1.68	0.87	12.21
1.69	0.86	11.83
1.70	0.91	11.99
1.71	0.97	12.60
1.72	0.90	12.99
1.73	0.89	12.18
1.74	0.88	12.07
1.75	0.89	11.96
1.76	0.87	11.80
1.77	0.87	12.12
1.78	0.88	10.90
1.79	0.87	11.24
1.80	0.86	11.65
1.81	0.90	11.14
1.82	0.89	11.54
1.83	0.89	11.07
1.84	0.87	11.24
1.85	0.81	10.20
1.86	0.83	10.06
1.87	0.84	10.54
1.88	0.85	11.58
1.89	0.88	12.26
1.90	0.88	12.83
1.91	0.88	12.47
1.92	0.88	13.14
1.93	0.92	12.69
1.94	0.94	11.96
1.95	0.98	12.27
1.96	1.03	12.37
1.97	0.99	12.49
1.98	0.97	11.78
1.99	0.99	11.67
2.00	1.00	11.53
2.01	1.00	10.25
2.02	1.01	10.31
2.03	1.02	9.69
2.04	1.05	9.68

MSM5/5-723-2 Depth (m)	TOC (wt.%)	CaCO3 (%)
1.43	1.05	12.46
1.44	1.04	12.65
1.45	1.09	10.02
1.46	1.06	11.89
1.47	1.07	10.95
1.48	1.09	11.21
1.49	1.10	10.99
1.50	1.06	11.19
1.51	1.07	10.84
1.52	1.05	11.32
1.53	1.08	11.14
1.54	1.14	10.39
1.55	1.17	12.58
1.56	1.17	11.37
1.57	1.18	11.69
1.58	1.15	12.18
1.59	1.12	12.58
1.60	1.14	10.64
1.61	1.14	11.06
1.62	1.15	10.68
1.63	1.21	10.49
1.64	1.13	10.25
1.65	1.11	9.28
1.66	1.11	8.41
1.67	1.17	8.74
1.68	1.18	9.15
1.69	1.18	9.48
1.70	1.19	9.98
1.71	1.18	11.34
1.72	1.17	10.16
1.73	1.10	8.82
1.74	1.15	8.74
1.75	1.16	8.70
1.78	1.11	9.21
1.79	1.05	8.61
1.80	1.06	9.25
1.81	1.07	10.18
1.82	1.05	9.88
1.83	1.07	9.33
1.84	1.07	9.45
1.85	1.06	9.97
1.86	1.05	9.27
1.87	1.05	10.61
1.88	1.03	9.95
1.89	1.08	9.40
1.90	1.11	9.91
1.91	1.12	9.55
1.92	1.14	10.55
1.93	1.14	9.38
1.94	1.18	9.31
1.95	1.10	10.65
1.96	1.08	11.62
1.97	1.07	11.75
1.98	1.04	11.70
1.99	1.04	12.02
2.00	1.02	11.90
2.05	1.05	9.89
2.07	1.01	10.66
2.09	1.02	10.40

Appendix C: IP25 data of sediment core PS2837-5 (chapter 6)

depth (m)	IP25 (µg/g sed)	IP25 (µg/g TOC)
0.32	0.65	55.17
0.35	0.45	37.58
0.70	0.33	28.62
0.82	0.39	34.03
0.85	0.39	33.96
0.92	0.49	40.67
1.00	0.27	24.48
1.02	0.40	35.07
1.05	0.17	16.19
1.07	0.26	24.07
1.12	0.40	35.81
1.17	0.18	17.31
1.20	0.19	18.21
1.22	0.21	21.89
1.25	0.18	18.96
1.27	0.21	21.93
1.30	0.19	17.96
1.32	0.16	16.53
1.37	0.23	24.03
1.42	0.08	8.59
1.45	0.15	16.62
1.47	0.09	10.11
1.50	0.10	11.21
1.55	0.12	13.07
1.57	0.25	24.91
1.60	0.13	14.94
1.62	0.08	9.16
1.65	0.13	15.28
1.67	0.05	6.54
1.70	0.14	14.94
1.72	0.21	21.75
1.75	0.19	20.42
1.77	0.18	17.77
1.80	0.24	23.10
1.82	0.14	13.83
1.85	0.13	12.88
1.87	0.14	13.00
1.90	0.23	20.79
1.92	0.21	19.19
1.97	0.18	15.79
2.00	0.18	15.54
2.02	0.13	11.62
2.05	0.13	11.10
2.07	0.12	11.44
2.10	0.16	14.34
2.12	0.14	12.57
2.17	0.15	13.29
2.20	0.19	16.23
2.22	0.22	18.92
2.25	0.29	24.49
2.27	0.23	19.29
2.32	0.35	28.86
2.35	0.31	25.98
2.37	0.38	29.88
2.40	0.28	25.21
2.42	0.24	22.26
2.47	0.37	32.82
2.50	0.31	29.25
2.52	0.38	39.27
2.55	0.44	49.69
2.57	0.56	70.96
2.62	0.05	7.65
2.63	0.04	6.27

Appendix C: IP25 data of sediment core PS2837-5 (chapter 6)

depth (m)	IP25 (µg/g sed)	IP25 (µg/g TOC)
2.65	0.04	6.04
2.67	0.23	29.25
2.70	0.37	43.58
2.72	0.29	35.66
2.75	0.32	35.46
2.77	0.39	43.04
2.80	0.35	37.80
2.82	0.40	44.01
2.87	0.43	44.25
2.92	0.38	37.92
3.00	0.38	40.62
3.02	0.38	42.30
3.05	0.22	27.64
3.07	0.35	40.75
3.10	0.28	30.75
3.12	0.24	26.09
3.15	0.19	19.42
3.17	0.28	27.44
3.20	0.26	23.64
3.25	0.29	23.33
3.28	0.38	28.01
3.32	0.41	29.86
3.35	0.42	29.73
3.40	0.45	31.83
3.42	0.43	31.55
3.47	0.00	0.26
3.50	0.00	0.29
3.55	0.00	0.29
3.60	0.00	0.35
3.62	0.21	24.57
3.65	0.16	18.69
3.70	0.25	29.30
3.72	0.24	26.16
3.77	0.22	24.53
3.80	0.22	26.20
3.83	0.15	26.46
3.87	0.03	10.65
3.94	0.00	0.00
3.98	0.00	0.00
4.00	0.00	0.00
4.02	0.04	4.98
4.03	0.04	4.94
4.05	0.10	10.79
4.08	0.72	55.12
4.10	0.86	61.48
4.12	1.15	85.34
4.14	0.65	63.36
4.15	0.19	49.11
4.17	0.06	18.83
4.20	0.05	16.51
4.22	0.00	0.00
4.25	0.00	0.00
4.27	0.00	0.00
4.30	0.98	195.44
4.35	0.00	0.00
4.37	0.00	0.00
4.42	0.07	12.45
4.45	0.26	39.86
4.47	0.10	17.45
4.51	0.44	61.77
4.53	0.47	66.94